Heterogeneous Distribution & Corresponding Mechanical Significance of The Mineral Phase in Fish Scales

Yiming Tan

Thesis submitted to the faculty of the
Virginia Polytechnic Institute and State University
in partial fulfillment of the requirements for the degree of

Master of Science
In
Materials Science and Engineering

Ling Li, Chair
Michael D. Bartlett
Wenjun (Rebecca) Cai

16 February 2023
Blacksburg, Virginia

Keywords: biological materials, fish scales, hierarchal structures, mechanical properties, flexible composite

Heterogeneous Distribution & Corresponding Mechanical Significance of The Mineral Phase in Fish Scales

Yiming Tan

ABSTRACT

Fish scales can be considered as a laminated composite based on collagen fibrils arranged in a cross-plywood structure. This collagen-based composite is often partially mineralized (primarily hydroxyapatite) in the scale exterior in order to resist penetration and hence to enhance protection. Together with the overlapping assembly, the fish scales offer an excellent model system for developing fiber composite materials and flexible armor systems. The primary objective of this thesis is to characterize the distribution of the mineral phase within individual scale and to investigate the corresponding mechanical consequences of the scale as a whole and its different fields through experimental and computational approaches. In this thesis, we chose the scales from the black drum (*Pogonias cromis*) fish as a model system. First of all, the exterior surface morphology of individual scales was systematically studied, from which several distinct structural regions are identified, including focus field (central), lateral field (dorsal and ventral), rostral field (anterior), and caudal field (posterior). In the focus field, the classic two-layer design, i.e., mineralized exterior layer and collagen-based interior layer, was observed, and nanoindentation results revealed that the high mineral exterior layer results in a much higher hardness (800 vs 450 MPa). Moreover, macroscopic tensile tests indicate that the mechanical removal of mineralized layer did not lead to reduction in strength values, whereas acid-treated demineralized scales showed reduced mechanical properties. Finally, we identified a previously unreported mineral distribution pattern in the rostral field, in which the mineral phase is segregated into long strips along the anterior-posterior direction (width, ~300 μm). In addition, towards the interior of the scale, it appears that the mineral deposition is highly correlated with the collagen orientation, resulting a unique mineralized-unmineralized collagen-based composite structure. We built finite element models to compare this unique structure to two other mineral phases in different fields at the individual scale. This unique structure demonstrates a larger deformation displacement when load was applied, indicating that it provides further flexibility in anterior end of an individual scale. The mineralized phases and structures of various fields within a single scale provide different mechanical characteristics and properties. The structural and mechanical analysis of the various regions of the fish scale can further investigate the flexibility and protective capacity of the individual scale.

Heterogeneous Distribution & Corresponding Mechanical Significance of The Mineral Phase in Fish Scales

Yiming Tan

GENERAL AUDIENCE ABSTRACT

There are many protective systems that attracted scientists' attention, and the typical examples include the nacre, crustacean exoskeletons, and teleost fish scales. Fish scales can be considered as the most common flexible bio-inspired armor system, because they consist of mostly collagen fiber and a highly mineralized hydroxyapatite external layer. Due to the need for swimming and effective protection from predators, fish scales need to have excellent flexibility and penetration resistance. In the previous studies on fish scales, researchers usually focused on the entire scale as a multilayered composite, looking at their response against tension and fracture. The primary objective of this thesis is to characterize the distribution of the mineral phase within individual scale and to investigate the corresponding mechanical consequences of the scale as a whole and its different fields through experimental and computational approaches. In this thesis, we chose the scales from the black drum (Pogonias cromis) fish as a model system. First of all, the exterior surface morphology of individual scales was systematically studied, from which several distinct structural regions were identified, including the focus field (central), lateral field (dorsal and ventral), rostral field (anterior), and caudal field (posterior). In the focus field, the classic two-layer design, i.e., mineralized exterior layer and collagen-based interior layer, was observed, and nanoindentation results revealed that the high mineral exterior layer results in a much higher hardness (800 vs 450 MPa). In addition, we identified a previously unreported unique mineralized-unmineralized collagen-based composite structure in the rostral field, in which the mineral phase is segregated into long strips along the anterior-posterior direction (width, ~300 μm). We built finite element models to compare this unique structure to two other mineral phases in different fields at the individual scale. This unique structure demonstrates a larger deformation displacement when load was applied, indicating that it provides further flexibility at the anterior end of an individual scale, implying that the flexibility is more important at the anterior end of scales where the multi-scales overlap and are covered. The structural and mechanical analysis of the various regions of the fish scale can further investigate the flexibility and protective capacity of the individual scale, and provide further design inspiration for flexible armor designs.

Acknowledgments

I would like to acknowledge and give my warmest thanks to my advisor, Professor Ling Li, who made this work possible. His guidance, advice, and endless support carried me through all the stages of writing my project. He is an excellent role model and has taught me the importance of professional success in the balance of life. I would also like to thank my committee members Professor Michael Bartlett, and Professor Wenjun (Rebecca) Cai for letting my defense be an enjoyable moment, and for your brilliant comments and suggestions, thanks to you.

Thanks to the all group members in the Li lab for your help and advice. Special thanks to Dr. Zhifei Deng, Dr. Zian Jia, and Dr. Ting Yang for showing me the ropes and to Liuni Chen, Chenhao Hu, Hongshun Chen, Shahbaz Khan and Yang Geng for being an absolute pleasure to work with. I'm also grateful for my graduate program coordinator Kim Grandstaff and my course professors who always give me kind and academic support and robust advice that assists me throughout the university career.

None of this would have been possible without the support of my family and friends. Thank you to my mom, dad and grandmother for giving me weekly video calls to share the joy and listen to my life so I wouldn't miss them so much, and to remind and support me in the graduation process. Thank you to Ge, Yaning and Cher for meeting me at Tech and for being the best friends as sisters I've never had. Thank you Vanessa, Sixian, and Sirui for your patience and support in my studies and daily life, even though we were unable to see each other from time to time. I am very grateful to be roommates and friends with Haotian, and the time I spent eating and relaxing with you always made me full of joy. And thank you to my adorable cat friend Cola for coming into my life and making everything so much more enjoyable.

Contents

Chapter 1. Introduction

Biological materials, which exhibit complex architectures and hierarchically organized structures, are increasingly serving as models and sources of inspiration for scientists and engineers. The natural protection given by the structure of biological materials is the result of millions of years of biological evolution[1]. As one of the representative biological materials, fish scales can be used as a model for the construction of new technological materials or structures with good mechanical properties (flexibility and a combination of strength and toughness) under various loading conditions.

Our objective is to characterize the distribution of the mineral phase within individual scale and to investigate the mechanical consequences of the scale as a whole and its various fields using experimental and computational approaches. We chose the scales from the black drum (*Pogonias cromis*)[2] fish as a model system in this thesis. Chapter 2 discusses previous researches and studies on fish scales, including an introduction to the main types of fish scales and their various surface and multilayer structural characterizations, the mineralization process and characteristics of fish scales, and a focus on the mechanical properties of elasmoid scales[3]. In addition, this chapter presents the demineralization and applications of elasmoid scale, as well as the motivation and open questions of this thesis. Chapter 3 provides information about the experimental and analytical methods used in this thesis, including the sample preparation, observation experiments, chemical analytical experiments, and mechanical experiments of fish scales. Chapter 4 focuses on the surface and cross-sectional structural characteristics of black drum scales, as well as the chemical analysis of intact and acid demineralized scales. In order to better comprehend the specific mineral phases in fish scales, we analyzed the orientation, shape and size distributions of small mineral particles (Mandl's Corpuscles). The mechanical properties of black drum scales are presented in Chapter 5 in terms of nanoindentation characteristics (hardness) and tensile properties (toughness and stiffness). In addition, Young's modulus of the different mineralized sections of the cross-section of the scale was measured by comparing the stress and strain distribution of the intact and demineralized scales. Chapter 6 focuses on the unreported mineral distribution pattern in the rostral field in terms of structural and nanoindentation characterizations analysis, and displays the comparative analysis by building the finite element simulation models from different fields within individual scale, to investigate the

unique and special mineral pattern at the anterior end of the rostral field provide greater flexibility than the mineral pattern at other fields on the scale. And this thesis concludes with Chapter 7, the conclusion, which summarizes the observations and analysis results of black drum fish scales.

In this thesis, we investigated the exterior surface morphology of individual scales, as well as their classical two-layer structural characteristics and material chemistry. Through macroscopic tensile and nanoindentation tests, we also learnt to analyze the mechanical properties of the various mineralization of fish scales. In addition, we discovered unique mineralized structures along the rostral field margins. As demonstrated by nanoindentation and finite element simulations, the scale structure at the edge of the rostral field provides more flexibility within a single scale, while revealing that flexibility is more significant at the anterior end of scales, where multiple scales overlap and are covered. Next, we can further investigate the mechanical characteristics of the mineralized phases and structures of the various fields within the individual scale and their functions with more precise simulations and studies.

Chapter 2. Background

This chapter will provide a comprehensive overview of previous research on fish scales, including an introduction to the types of fish scales and their various surfaces and the multilayer structure characteristics, biomineralization, and the mechanical properties of elasmoid and ganoid scales. In this chapter, the demineralization and applications of fish scales, as well as the motivation and open questions of this thesis, will be presented.

2.1 Types of Fish Scales

The skin of most fishes is covered with protective scales, which can also provide camouflage through reflection and coloring, as well as hydrodynamic benefits[4,5]. Fish scales develops from the fish's epidermis, and they continue to develop and later become mineralized throughout life. The scales increase in surface area at the periphery and in thickness as newly produced laminae are added to the interior layer's surface. The mineralized tissue is found in the external layer and in a portion of the internal layer that is next to the outer layer[6]. In the more recently formed unmineralized laminae of the internal layer, the small mineral particles, which are also named Mandl's corpuscles[7], are present and independently formed.

There are four major types of fish scales: (i) cycloid, (ii) ctenoid, (iii) ganoid, and (iv) placoid[8]. Fig. 2-1 depicts these fish scale types as well as their overlapping patterns. Cycloid scales contain "ring"-like acellular structures, while ctenoid scales have "comb"-like structures at the protective margins[8]. Similar to tree rings, the concentric rings on a fish symbolize its annual growth. The thin, translucent, collagen-based "plate"-like elasmoid scales[9,10], which comprise cycloid and ctenoid scales, provide enhanced hydrodynamic properties and resistance to penetration[4,8]. The black drum (*Pogonias cromis*) fish scale studied in this thesis is also included in elasmoid scales. The distinguishing feature of ganoid scales is a dense bony structure on the upper side with a ganoine or enamel surface coating[8]. These scales feature a rhomboid structure with "peg-and-socket" joints between adjacent scales[8]. In contrast, placoid scales show "tooth"-like structures known as dermal denticles. Vitrodentine (enamel-like substance) covers the outer layer of placoid scales, which cannot grow in size but increase in number with time[8,11]. Additionally, one more type of scale named "cosmoid"[4] was discovered in the earliest (fossil) fishes[12]. These scales are similar to placoid scales and likely evolved from the fusing of placoid

scales. They consist of two layers of bone at the bone's base: a layer of dentine-like cosmine, and an outer layer of vitrodentine. These fossil fishes were equipped with thick, bony scales that provided them with effective protection from predators[13].

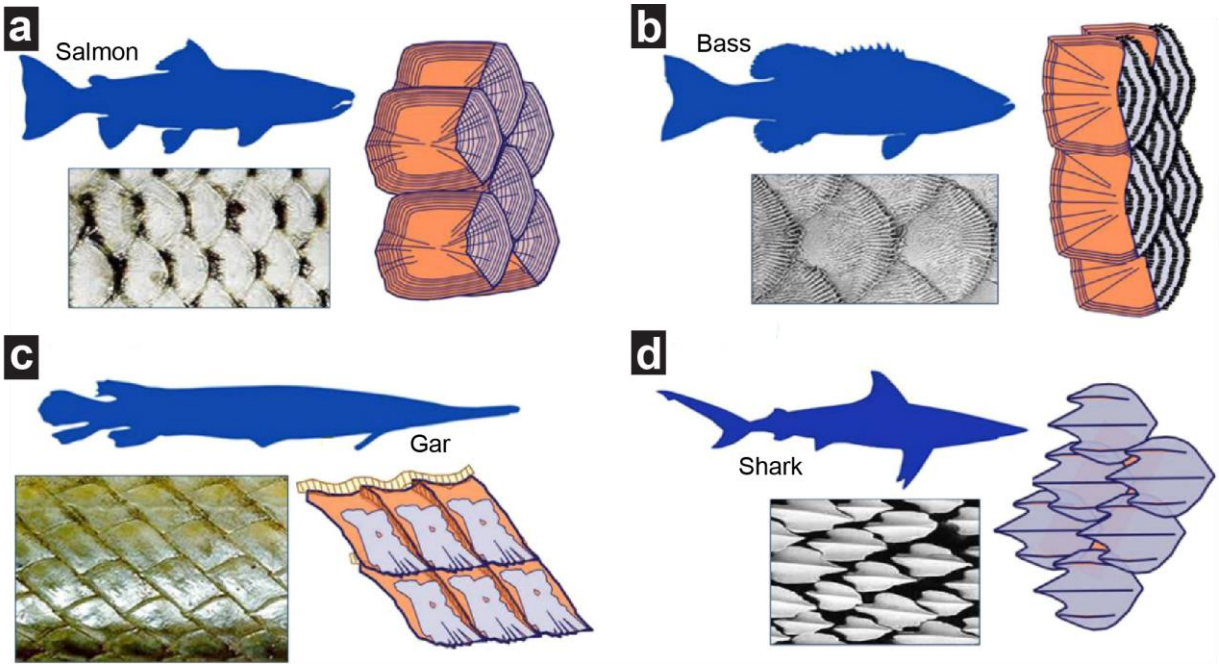

Fig. 2-1. The arrangement and schematics of overlapping scales with examples. (a) Cycloid, **(b)** Ctenoid, **(c)** Ganoid, and **(d)** Placoid fish scales[8].

Four types of fish scales are primarily composed of calcium-deficient hydroxyapatite (HA) and extracellular matrix (type I collagen fibers)[14]. The scales can be generally divided into external and interior layers. Randomly aligned mineralized collagen fibers and mineral deposits constitute the exterior layer[9]. The orientations of the fiber angle depend on the types of fish scales[9]. Fig. 2-2 depicts cross-sections of typical fish scales, illustrating the exterior and internal "collagen" layers of a fish scale. The optical micrograph and SEM image of the internal and external layers of *Arapaima gigas*[15] and *Cyprinus carpio*[16] scales are shown in Fig. 2-2-a and c, respectively. The outermost layers with a corrugated appearance represent the rigid structures of the scale, while the internal layers are composed of soft collagen fibers that are used to protect the fish's skin. In Fig. 2-2-c, for example, the inner collagen layer with collagenous fibers works as a soft buffer for fish scales, protecting the fish skin from the direct impact of the attacker's tooth. Fig. 2-2-b is a SEM image of a transverse section of an *Atractosteus spatula* scale that identifies between the bony layer and the ganoine layer[17]. Four different organic–inorganic

nanocomposite material layers are demonstrated in Fig. 2-2-d of a *P. senegalus* fish scale[18]; the exterior ganoine layer with rich mineral zones protects the fish from predators[18,19].

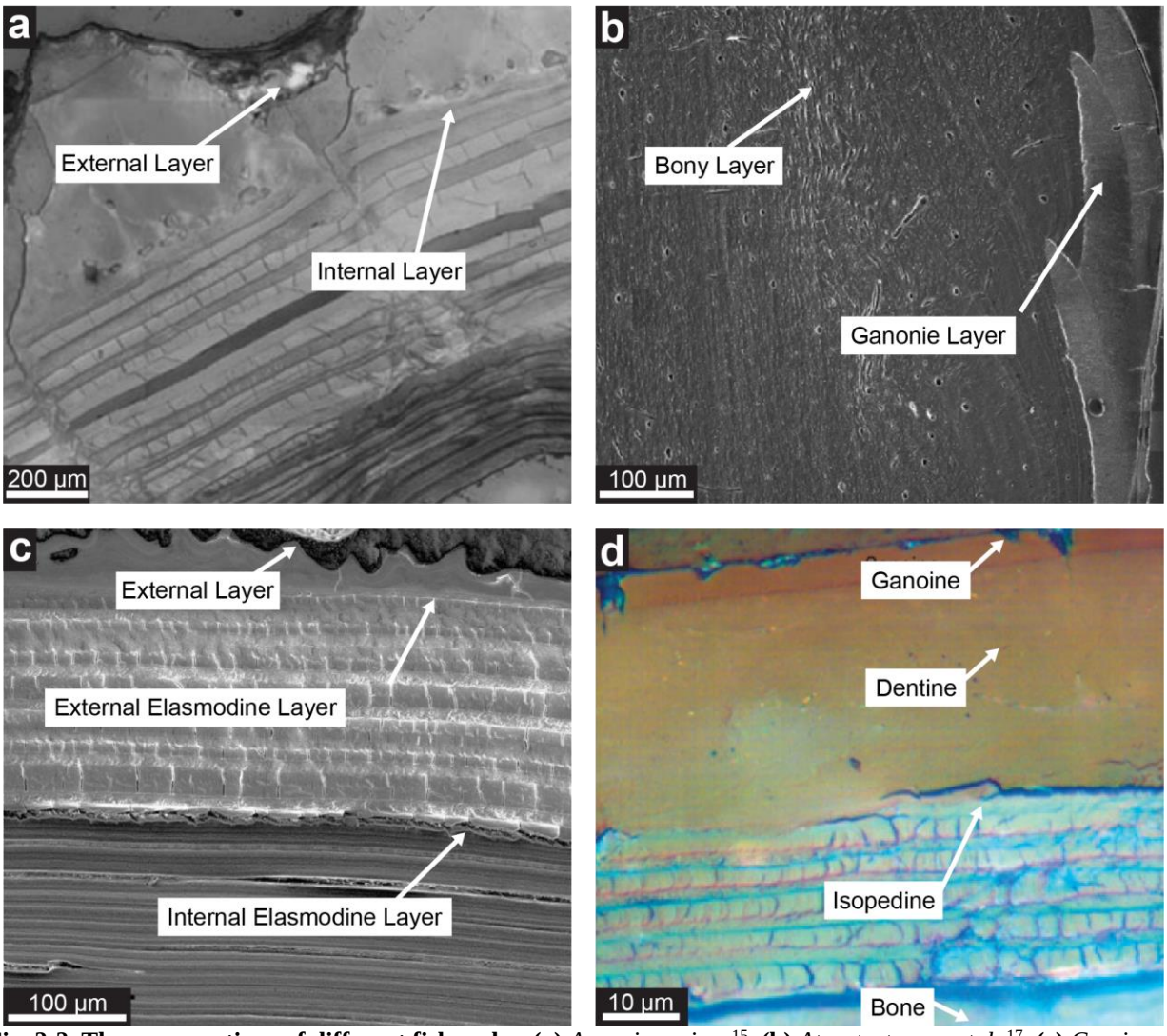

Fig. 2-2. The cross-sections of different fish scales. (a) *Arapaima gigas*[15], **(b)** *Atractosteus spatula*[17], **(c)** *Cyprinus carpio*[16], and **(d)** *Polypterus senegalus*[18].

2.2 Mechanical Properties of Fish Scales

Over the past few decades, mechanical properties of a variety of biological materials such as nacre, wood, teeth, armadillo, and turtle shells have been measured. The Ashby diagram[20] displaying the fracture toughness of a wide range of natural structural materials as a function of their elastic modulus[21,22] is shown in Fig. 2-3, with the red areas representing the properties of inherently brittle building blocks ($CaCO_3$, hydroxyapatite, and alumina), and the green areas representing the properties of biological and bioinspired composites assembled from these brittle

constituents (mollusk shell, bone, dentin, and enamel composite)[20]. A new lightweight bioinspired material with superior mechanical properties can be developed using a combination of engineering materials and fish scales. Tensile properties, indentation properties, and fracture properties can be used to define the mechanical characteristics, which include strength, stiffness, and fracture toughness.

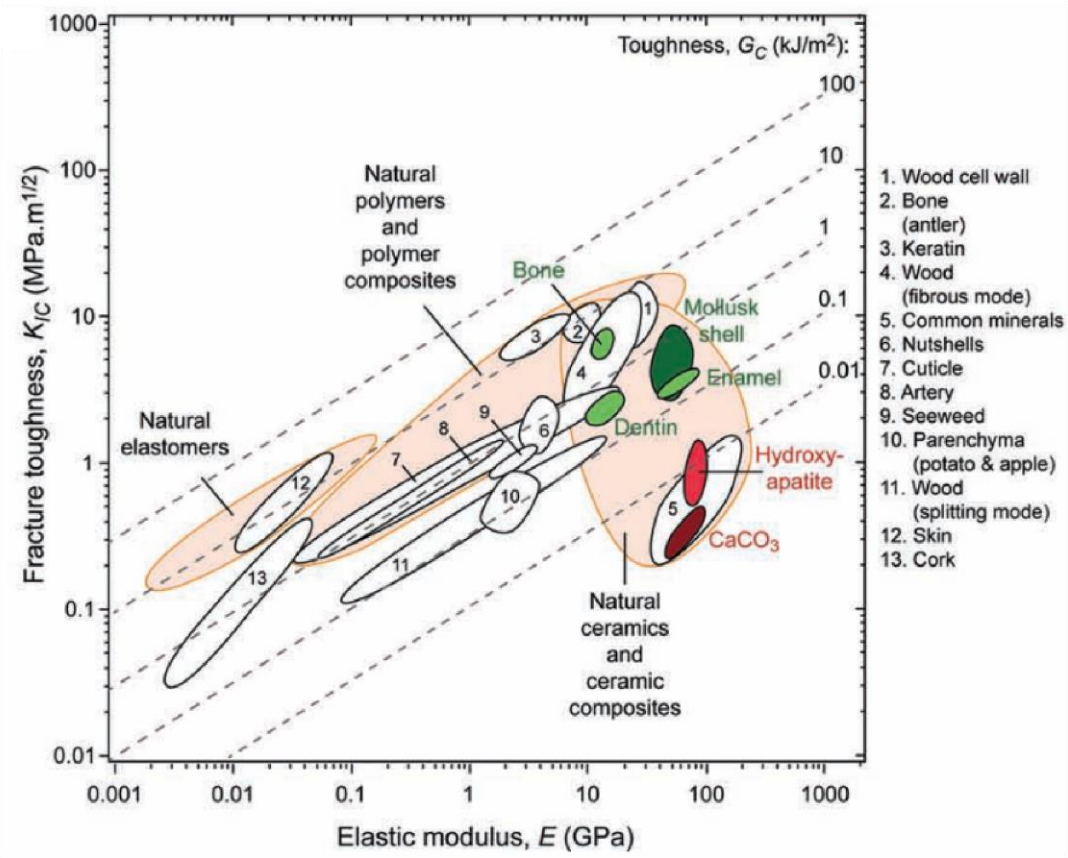

Fig. 2-3. Ashby diagrams displaying the fracture toughness of a wide range of natural structural materials as a function of their elastic modulus[20].

2.2.1 Tensile Properties of Elasmoid Scale

Since the fish scale (black drum fish scale) studied in this thesis is also the elasmoid scale, we wanted to learn more about the structural and mechanical characteristics of this scale type. The tensile test is one of the fundamental mechanical tests used to determine the strength and stiffness (Young's modulus) of materials. One example of tensile testing on *Pagrus major* fish scales by Koma[23] is shown in Fig. 2-4. They demonstrated that the fish scale's behavior in stress was first linear, followed by plastic yielding before breakage[23]. As shown on the right (Fig. 2-4-a), this yielding is the result of collagen fiber sliding and the dissociation of individual fibers[23].

This study inspired the scientists to analyze the mechanical properties of fish scales and their interaction with scale location (over the fish body), mineral contents, fiber orientation, and hydration conditions[8].

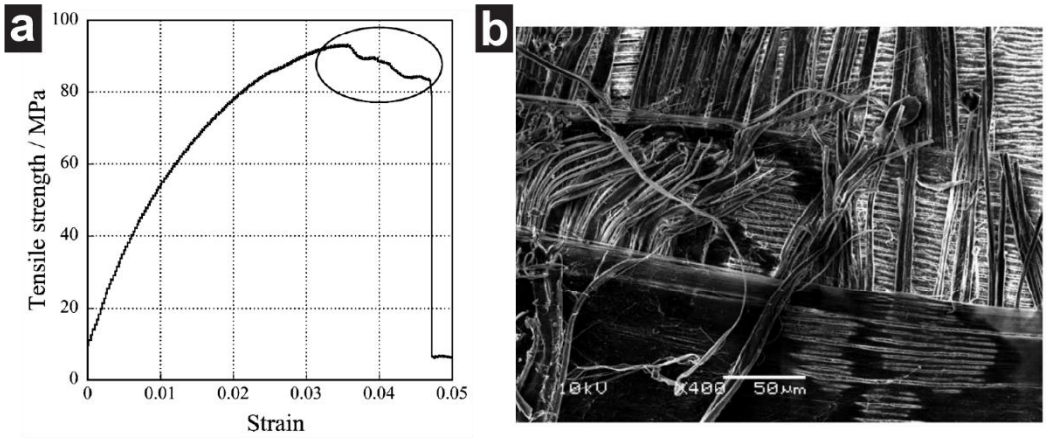

Fig. 2-4. Tensile stress-strain curves and failure of elasmoid scales. (a) Typical tensile stress-strain curve of *Pagrus major* scales and its plastic yielding behavior, and **(b)** SEM image of the fractured sample showing breakage and pullout of collagen fibers[23].

Garrano[24] analyzed the mechanical behavior of fish scales of *Cyprinus carpio* from several anatomical regions (head, body, and tail) as a function of moisture content in scales indicated in Fig 2-5 and 6. They discovered that the mechanical behavior of fish scales is highly location-dependent. When not dehydrated, the strength and elastic modulus of head scales were nearly double those of tail scales[24]. The amount of moisture lost during dehydration is dependent on the drying duration[24]. Interestingly, for the dehydrated samples, there was no discernible variation in mechanical strength across scales obtained from any position (i.e., from head to tail)[8].

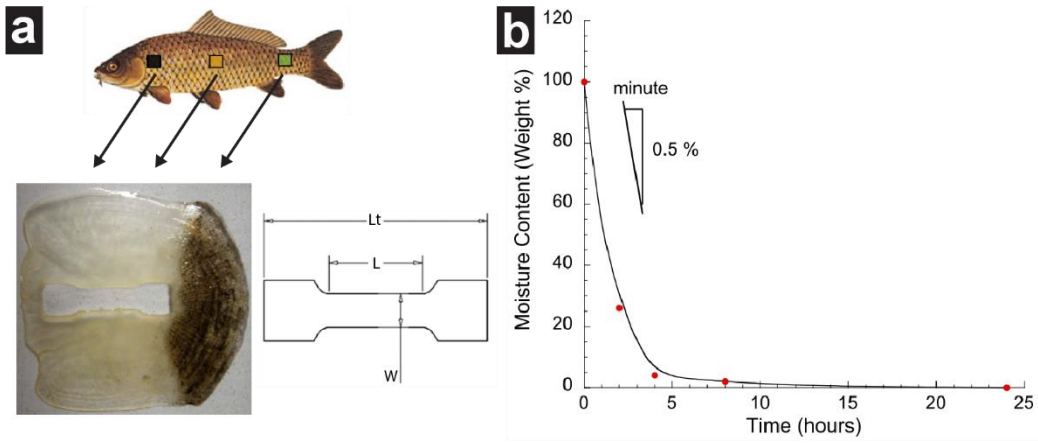

Fig. 2-5. Tensile stress-strain curves and failure of elasmoid scales. (a) Anatomical positions (head, middle, and tail) of the sample preparation and specifications of the fish (*Cyprinus carpio*) scales (Lt = 16 mm, L = 7 mm, and w = 3 mm), and **(b)** Moisture content versus drying time[24].

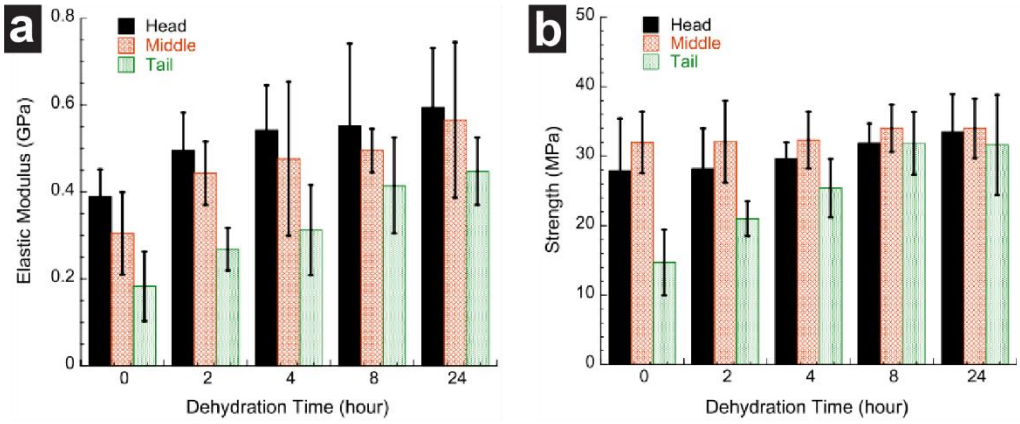

Fig. 2-6. Dependence of the fish (Cyprinus carpio) scale mechanical properties on the degree of dehydration and on the anatomic position, **(a)** elastic modulus and **(b)** tensile strength[24].

Zhu[13] analyzed the arrangement of collagen fibrils and tensile strength of the scale of the striped bass *(Morone saxatilis)* in Fig. 2-7. They discovered that angular differences affect mechanical properties. The tensile strength and Young's modulus vary between 30 and 50 MPa and 600 and 850 MPa along 0 degrees, 45 degrees, and 90 degrees from the longitudinal axis of the fish[13], respectively. The ultimate stress is same for samples with and without the bone layer (mainly collagen fibers)[13]. This study suggested that the behavior of collagen fiber is mostly influenced by the stretching of individual, straight collagen fibers.

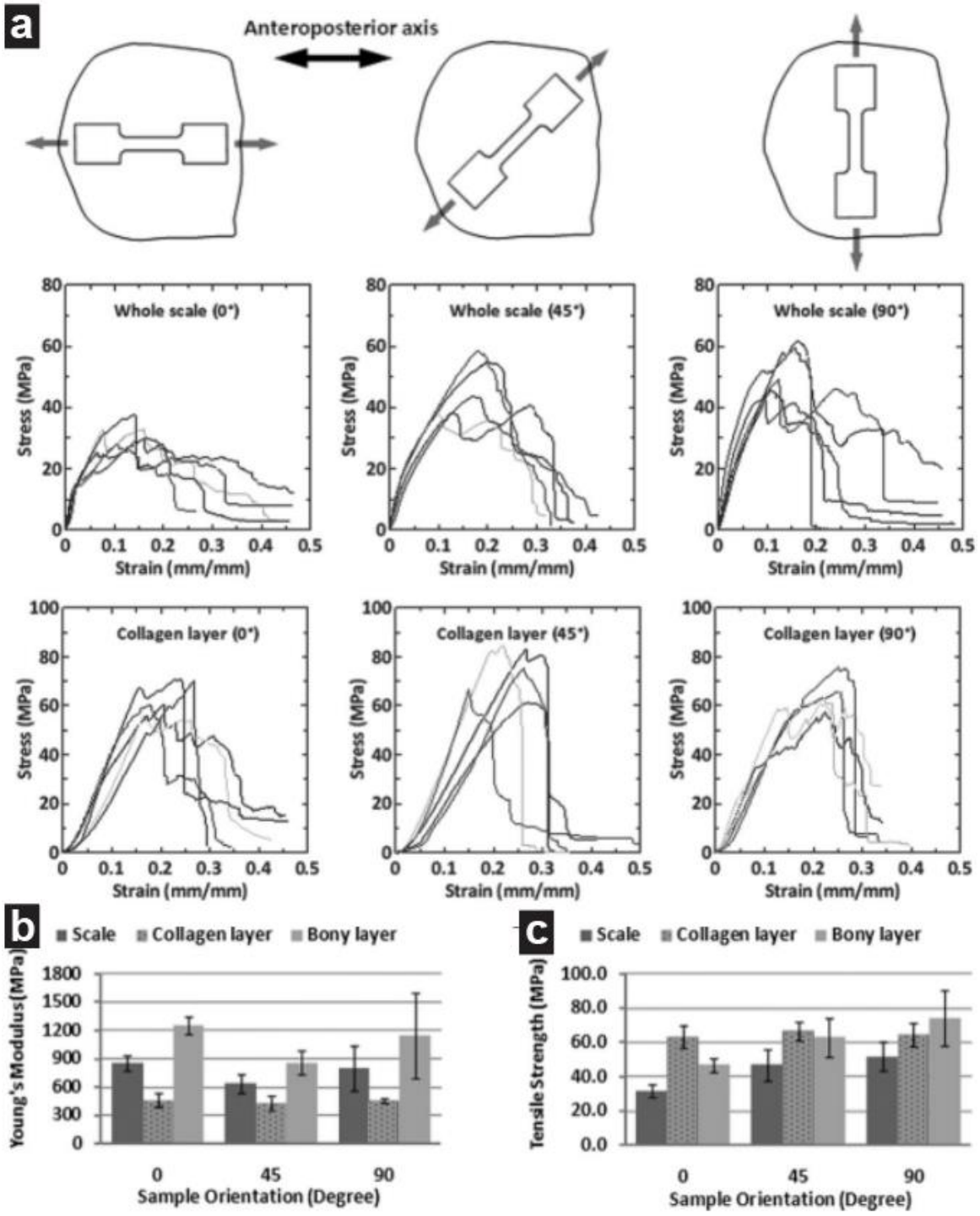

Fig. 2-7. Tensile properties for fish scales along 0°, 45°, and 90° from the longitudinal axis of the fish (*M. saxatilis*)[13]**. (a)** Tensile sample preparation and stress–strain curves. **(b)** Young's modulus. **(c)** Tensile strength. The error bars indicate standard deviations.[13]

Fig. 2-8 displays the structural and mechanical characteristics of *arapaima (Arapaima gigas)* scales[25]. According to the study, elasmoid scales are composed of HA and type-I collagen fibers, and the aspect ratio of HA and type-I collagen fibers is approximately 50[25]. The outermost layer is highly mineralized, whereas the interior layer has a low mineral concentration. As shown in Fig 2-8-b and c, Young's modulus and tensile strength (for the entire scale and collagen layer) of longitudinally oriented samples were greater than those of transversely oriented samples. As demonstrated in Fig. 2-8-d to f, the major failure modes of scales are as follows: total fracture of the outer layer, delamination of lamellae, and fracture of collagen fibers near the bone layer[25].

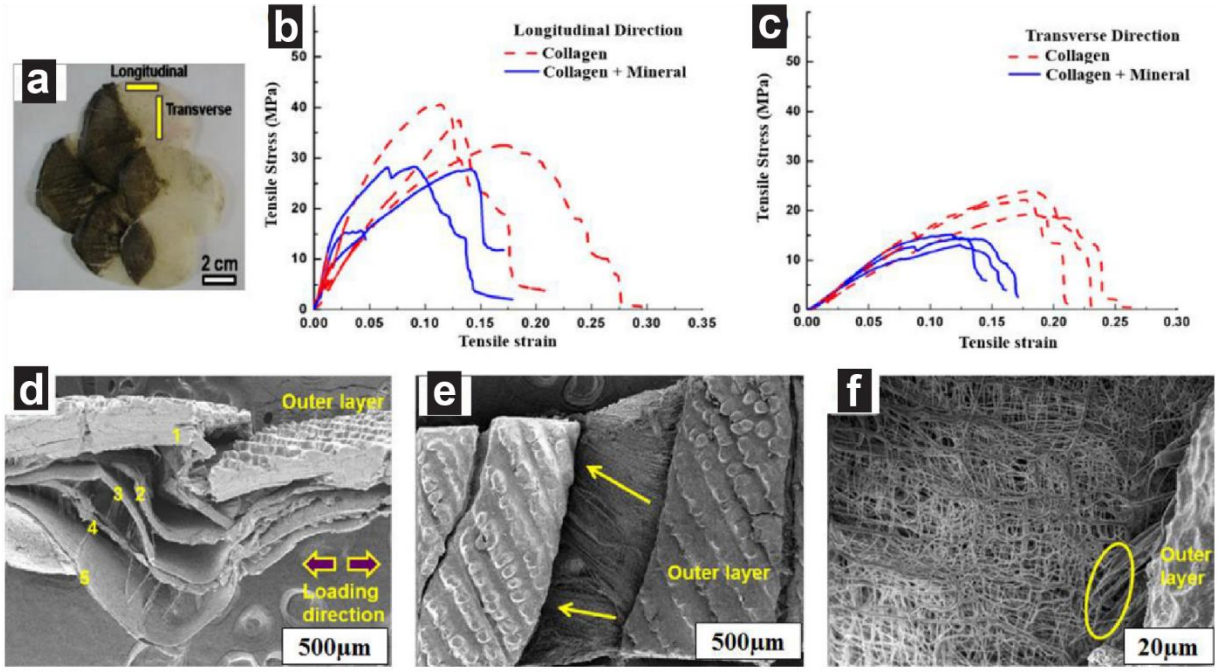

Fig. 2-8. Tensile properties and failure mechanisms of *arapaima* (*Arapaima gigas*) scales[25]. (a) Overlapped scales of *arapaima* fish showing longitudinal and transverse directions selected for mechanical testing. **(b,c)** Tensile stress-strain curves in longitudinal and transverse directions for collagen and collagen + mineral layers, respectively. **(d)** side view of fractured scale showing delamination of different layers, **(e)** top view of the fractured surface showing complete fracture of bony (mineral) layer and exposed collagen fibers, and **(f)** the fracture of outer layer after tensile testing and the separation of collagen layers from the outer layer.[25]

Table 2-1 (constructed by Li Group's member, Zhifei Deng) summarizes the tensile results of several types of fish scales, where the 0° and 90° samples are specified as being cut along and perpendicular to the long axis of the fish in order to study the in-plane anisotropy[13,25]. Rate-dependent behavior is also observed[26].

Table 2-1. Tensile results of different types of fish scales

Sample	Scale type	Conditions	Directions	Strength (MPa)	Modulus (GPa)
Arapaima Gigas[27,28]	Cycloid	Dry	—	46.7~53.85	1.2~1.38
		Wet	—	22.26~25.2	0.1~0.83
Pagrus major[23]	Elasmoid	Wet	—	93±1.8	2.2±0.3
Megalops Atlanticus[29]	Ctenoid	Wet	0°	22.6±5.1	0.22±0.03
Morone saxatilis[13,30]	Ctenoid	Wet	0°	~32[a]	~0.85[a]
		Wet	45°	~48[a]	~0.62[a]
		Wet	90°	~52[a]	~0.8[a]
Cyprinus carpio[24]	Cycloid	Wet	0°	33.4~34.0	0.45~0.59
Atractosteus spatula[31]	Ganoid	Wet	Longest diagonal	96~125[a]	1.75~3.3[a]
Latimeria chalumnae[32]	Elasmoid or Cosmid	—	0°	~50	~0.21
		—	90°	~50	~0.25

[a]Note that some values in the table are estimated from the stress-strain curve.

2.2.2 Fracture Resistance of Elasmoid and Ganoid Scales

The external layer of fish scale exhibits strong stiffness, but undesirable brittleness results in a lack of toughness[33]. However, the exceptional fracture toughness of the entire scale is primarily due to the unique combination of the exterior hard and rigid layer with the interior soft layer[13,33]. Below are images of a new fracture test technique[34] presented for the fracture toughness analysis of the entire scale, as well as the removed bony (high mineral) and collagen layers from striped bass *(M. saxatilis)* fish. During the testing, small steel plates were clamped to the sample to transfer uniform loading and control crack growth. The sensitivity of the bony layer to the notch demonstrates the high toughness of the scale. As shown in Fig. 2-9-b and c, the pre-crack positions over the scales had a significant effect on the fracture characteristics of the whole scale[34]. Moreover, the fiber orientations in the sublayers had a major influence on the directions of crack propagation. The optical image of fracture testing findings in Fig. 2-9d and e were examined to reveal the defibrillated structure, thereby illuminating the fracture mechanisms[34]. And Fig. 2-9f and g indicate the interlaminar fracture toughness test and experimental results of individual scales[34].

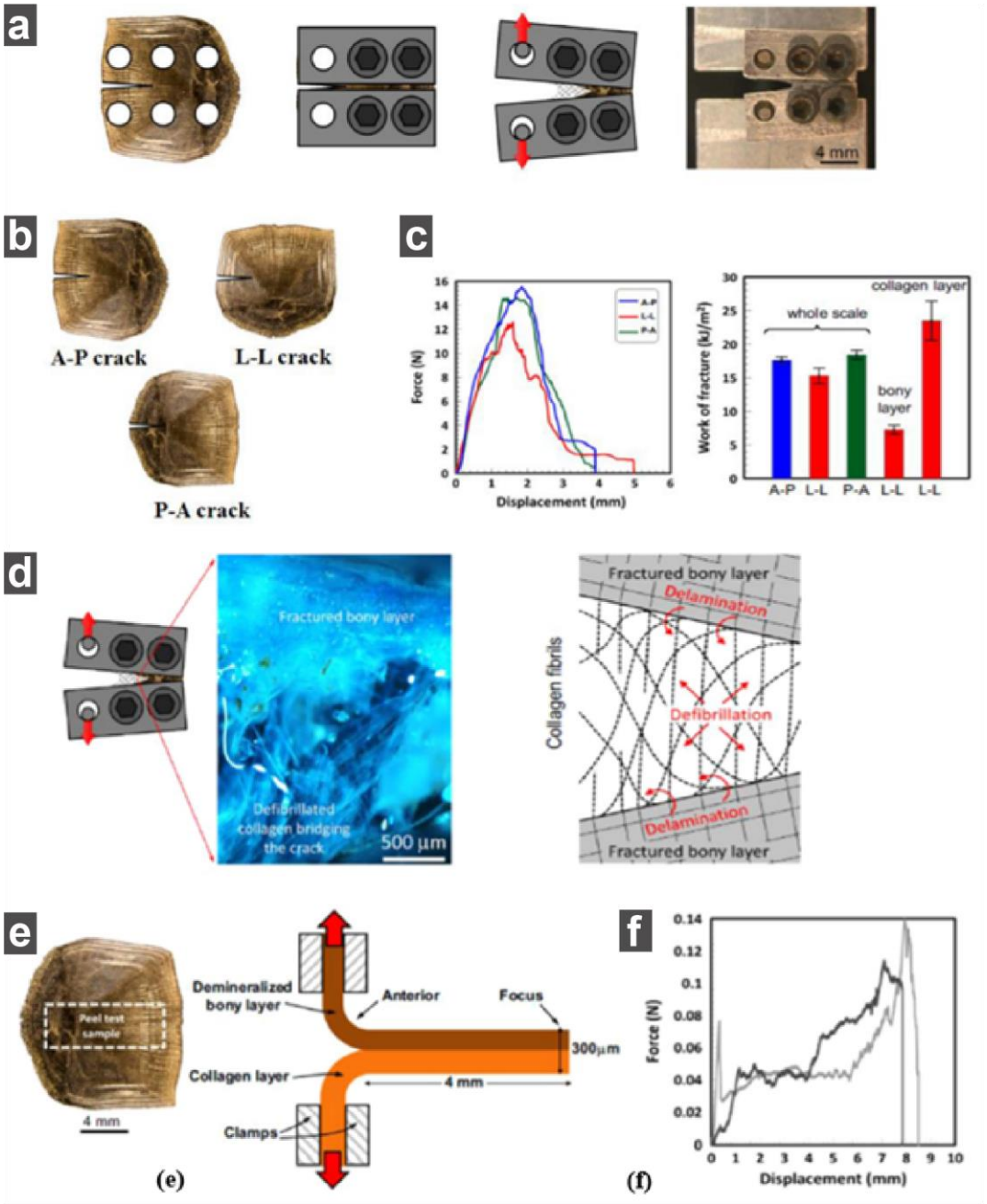

Fig. 2-9. Fracture resistance of striped bass (*M. saxatilis*) fish scales. (a) Miniature fixtures of stainless steel for fracture testing. **(b)** types of pre-cracks in preparing samples. **(c)** load-carrying capacity, and work of fracture with different samples. **(d)** optical image and schematic diagram of the softening region for fractured bony (mineral) layer and defibrillated crack bridging of collagen fibers. **(e)** sample preparation and schematic diagram for peel test of a scale. **(f)** force versus displacement curves obtained by peel test[34].

Yang[31] investigated the fracture toughness of alligator gar *(Atractosteus spatula)* scales that used three-point bending tests to determine R-curves (crack-resistance curves) as a function of crack initiation and propagation, as well as three different orientations under dry and wet conditions (Fig. 2-10). Due to the orientation of collagen fibers in relation to the formation of

cracks, orientation 3 exhibited the highest slope (in R-curves)[31]. For orientations 1 and 2, tubule and collagen fibers were oriented slightly with the direction of fracture propagation[31].

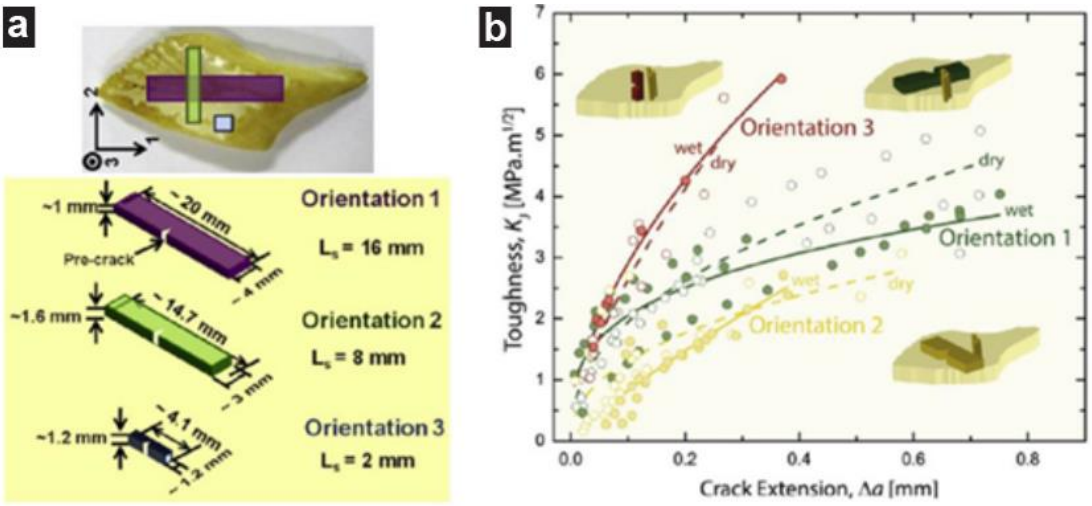

Fig. 2-10. Fracture resistance of Alligator gar(*A. spatula*) fish scales[31]. (a) R-curve testing orientations with specimen dimensions, and **(b)** toughness versus crack extension for selected orientations under dry and wet conditions.

2.2.3 Flexural Properties of Elasmoid and Ganoid Scales

For multifunctional and competitive performance, identifying bio-inspired fish scale composites requires flexibility and protection (penetration resistance). Rudykh[35] presented a competitive and multifunctional design for protection, which he named "protecto-flexibility," or protection with flexibility. This model was built using 3D printing technique. These microstructural configurations (Fig. 2-11) are determined by the volume fraction and inclination angle of the scales, and the behavior of the materials can be tailored to achieve the desired performance. The bi-layered scale with a volume fraction of 1 has the stiffest reaction, and the indentation force decreases as the inclination angle increases[35]. Thus, while the composite can resist penetration, it is also flexible due to the various deformation mechanisms of each loading condition, such as inter-plate matrix shear, plate rotation, and plate bending[35,36].

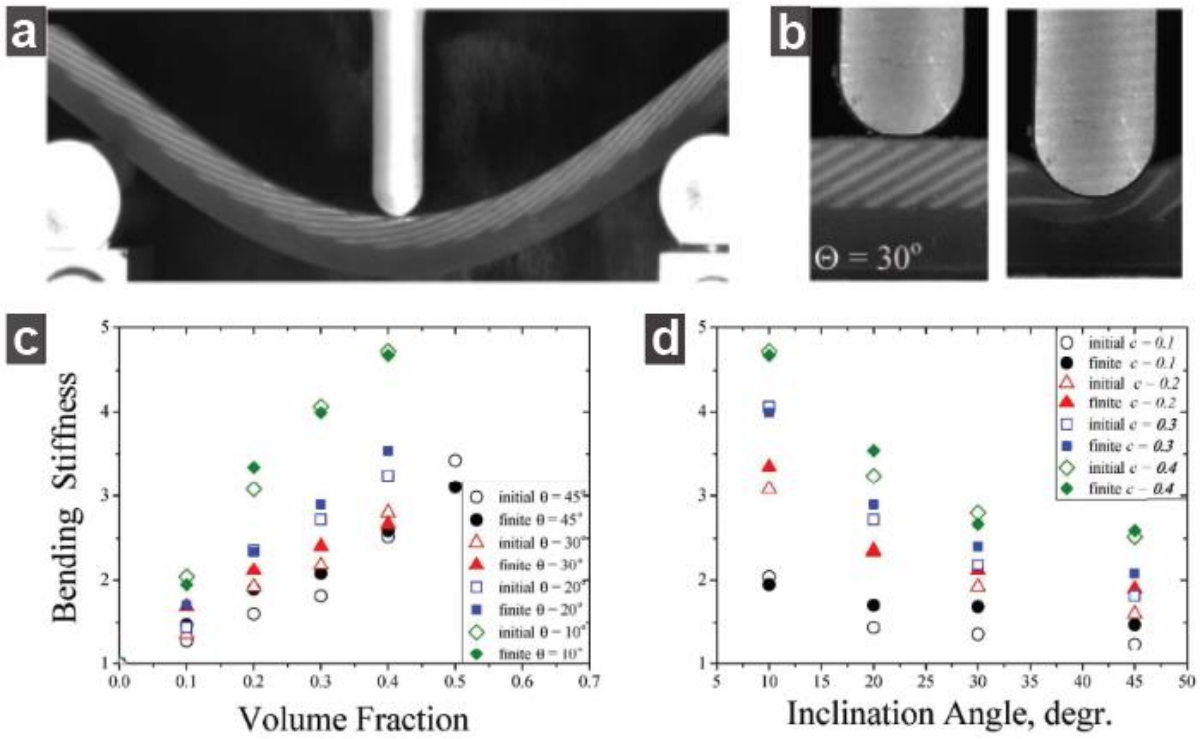

Fig. 2-11. Bio-inspired armor designs of micro-structured elasmoid scale armor. (a) The three-point bending tests for optimising the angle of scale, **(b)** illustration of deformation mechanisms in laminates at the inclination angles of 30°, and the relative bending stiffness vs **(c)** volume fraction and **(d)** inclination angle[35].

To investigate how scale form affects local inter-scale mobility mechanisms and produces anisotropic mechanical behavior, Zolotovsky[37] evaluated bioinspired flexible composite prototypes under active loading (bending). Using bio-inspired, multi-material 3D-printed prototypes, the team also demonstrated how scale shape, articulation, and composite architecture induce anisotropic mechanics[37]. Flexible connections between the scales lead to mechanical anisotropy, as demonstrated by passive loading (draping)[37]. Active loading (bending) simulations and experiments reveal orientation-dependent stiffness involving multiple orders of magnitude. The results demonstrated how morphometry is a powerful tool for adjusting flexibility in composite structures independent of the composition of the constituent materials[37].

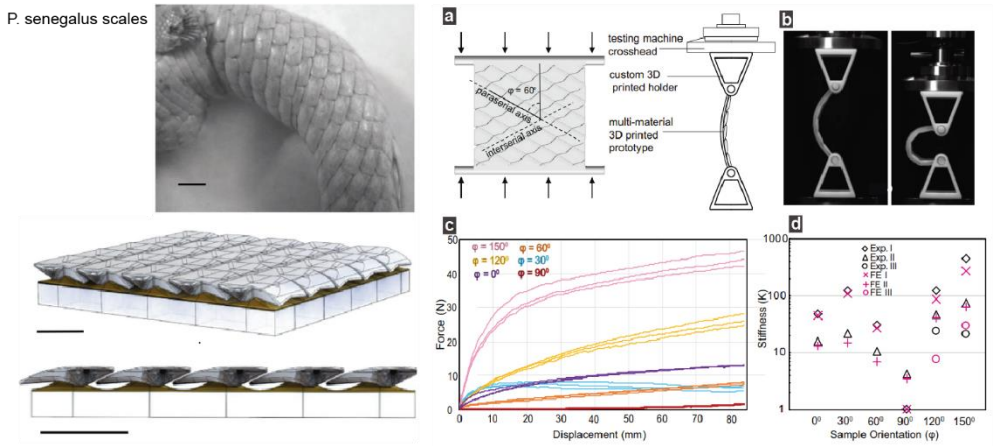

Fig. 2-12. Anisotropic bending stiffness of the flexible composite prototypes design inspired by *P. senegalus*. (a) Rendered front view of the prototype designed for bending with rigid rods at the top and bottom and with the paraserial axis oriented at an angle (φ) = 60° away from the loading direction. **(b)** Side view of the φ= 60° sample loaded in bending at various vertical displacement. **(c)** Force–displacement curves for prototypes with φ= 0°, 30°, 60°, 90°, 120°, and 150°. **(d)** Normalized stiffness (K) of each phase of each prototype's loading curve (experiments and finite element simulations). Error bars represent standard deviation with N= 3 samples per prototype orientation[37].

2.3 Biomineralization in Elasmoid Scales

For the calcification process, the external layer of the scale is the first to be mineralized and can be classified as the initial calcifying structure of the scale[6]. Initial calcification loci are always recognized as matrix vesicles of cellular origin during the formation of this layer[6] (Fig. 2-13). After the formation of the outermost layer, the outer limiting and interior layers of the scale evolve. While subsequent mineralization indicates a mineral substance deposited in these two layers without the mediation of matrix vesicles, it is in contact with the previously mineralized outermost layer[6]. The mineralization of the outer limiting layer closely follows the secretion of a collagen-free organic matrix, unlike the mineralization of the interior layer, where the mineralization front remains distant from the collagen matrix surface and corresponds to a delayed mineralization process[6]. The isolated calcifications are Mandl's corpuscles that grow in the unmineralized laminae of the interior layer and are mineralized in the absence of matrix vesicles and without getting in contact with a pre-calcified tissue (Fig. 2-14), most possibly by a heterogeneous nucleation of collagen fibrils[7].

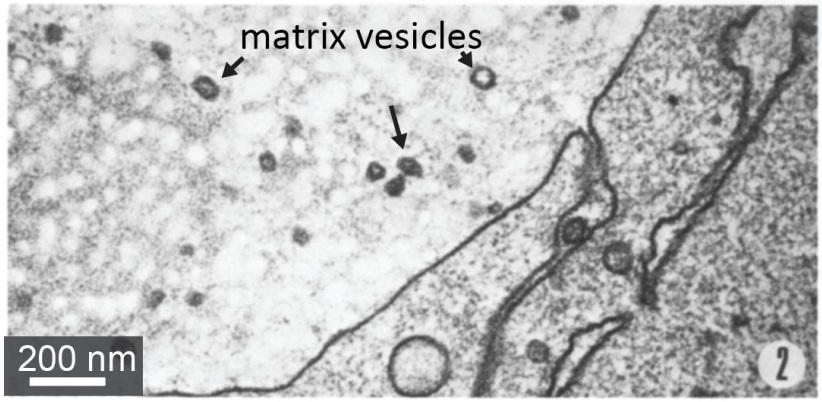

Fig. 2-13. In the osteoid tissue, matrix vesicles bound by a trilaminar membrane are observed among collagen fibrils[6].

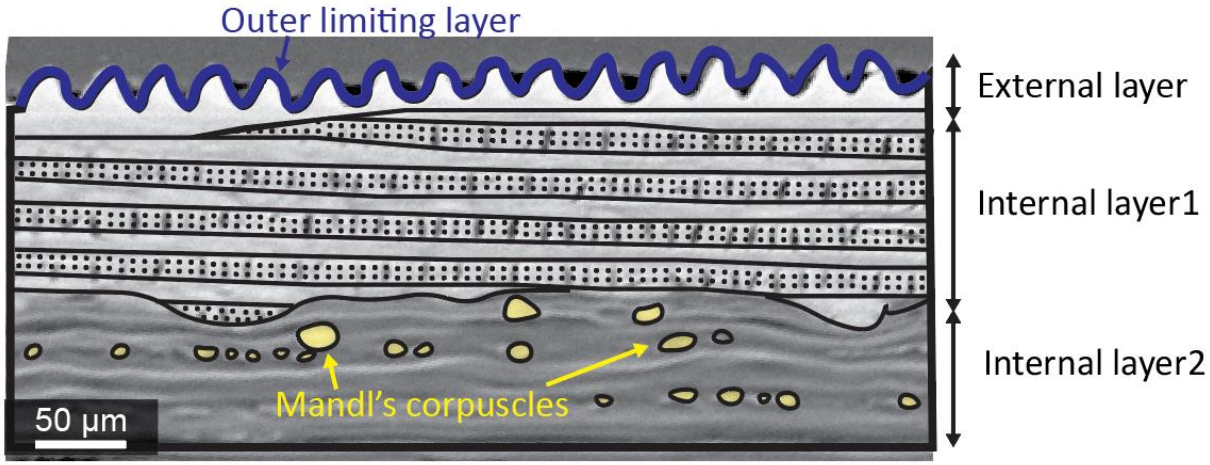

Fig. 2-14. Mineralization process of black drum fish scale from SEM image.

The mechanical properties performed by the Meyers's group on the scales and teeth demonstrated that the *Arapaimas* scales[38] are impermeable to the piranha tooth's ability to cut and puncture them. They demonstrated how the higher corrugations, which provide channels with a thinner thickness, reduce the tensile strains in the mineralized layer when measured across the section of the scale. Additionally, they contend that the mineralized layer's corrugations have an important structural function. The tension is concentrated at their bottoms because of the corrugations (circled in A area in Fig. 2-15). However, in the analysis section, the team employed the transformed beam, which is the homogeneous collagen section, instead of the specified model to investigate the puncture properties[39].

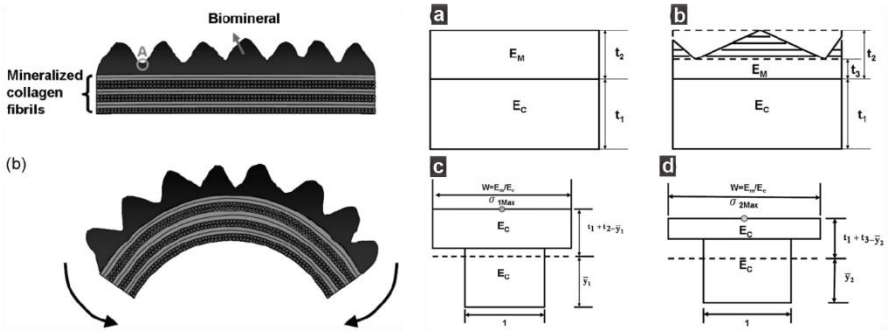

Fig. 2-15. Schematic representation of the flexing of the *Arapaimas* scale[39]. Circled region A undergoes minimum strain by virtue of geometry. **(a)** The fully mineralized surface layer, and **(b)** corrugated mineral layer of longitudinal section of the *Arapaima* scale[39]. Cross-section of transformed beams for **(c)** smooth and **(d)** corrugated mineral layers; neutral axis marked by $\bar{y}$[39].

2.4 Scale Demineralization and Applications

Natural protective layers, such as shells, fish scales and turtle nails, have a layered structure that exhibits superior performance and complicated mechanisms to avoid failure[40]. And they are excellent lightweight and ductile structural materials. Skin protection for animals varies from rigid to flexible. Flexibility allows movement, while rigidity enhances protection. And fish scales combine these two characteristics[41]. Most of fish scales are composed of calcium-deficient hydroxyapatite (HA) and type I collagen fibrils[33]. The fibrils of mineralized collagen produce various architectures, such as plywood structures[28,42]. In addition, scales typically exhibit a composite or graded structure, with decreasing hardness from the exterior to the interior[17].

According to previous research and observations, black drum scales consist of an outer layer with a highly mineralized, rough exterior surface and an interior base of collagen layers[9]. It has a Bouligand-type[43,44] structure with lamellae of parallel collagen fibers arranged in vary orientations. In this thesis, we will analyze the deformation of scales before and after demineralization as tested by the tensile test, the strength and toughness of different scale fields as evaluated by the nanoindentation test, and the unique characteristics of mineralized-unmineralized collagen-based composite structure in rostral field.

There are many mechanical and chemical demineralization methods for removing the mineralized layers of fish scales. In this study, the acid demineralization and polish demineralization methods were applied to dogbone samples. The samples for acid demineralization must be immersed in saltwater solution for more than 24 hours before being

immersed for 90 minutes in a 0.4 mol/liter hydrochloric acid solution[45]. Fig. 2-13 displays the demineralization of fish scales by hydrochloric acid solution. The demineralized scale samples were compared to the original scale samples in both directions. It is evident that the demineralized samples differ from the original scales in a transparent way. In addition, the sample becomes softer and more flexible after demineralization.

Fig. 2-15. Demineralization of black drum fish scales with hydrochloric acid solution.

2.5 Open Questions & Motivation

The natural protection afforded to living beings is the consequence of millions of years of biological evolution, as evidenced by the fish scale[46,47]. Unique hierarchical patterns design offer fish, armadillos, and turtles with the protection they need to live in their environments[11].

The scales of fish can serve as a model for the construction of new technical materials or structures with great mechanical performance under a variety of loading conditions. The scale arrangement on fish skin is hierarchical, making it harder for a predator to penetrate[39]. The current form of fish skin offers remarkable combinations of various components. The building blocks or constituents of these hierarchical structures (fish, bone, and nacre) exhibit distinctive and desirable mechanical strength and toughness combinations[47]. The objective of this study on fish scales can be summarized in three sections. First, identify the composition of the fiber composites (mineralization, chemical components, etc.) and characterize the structure of black drum fish scale. The second objective is to investigate the influence of mineralization in the protection and deformation mechanisms of intact fish scale composites. The third is to study the influence of mineralization on the protection and deformation mechanisms of different fields within the individual scale, in order to determine the relationship between the mineralization phases and their mechanical properties in different regions of the scale, and to gain insight into

the biomechanical consequences of the mineralized structural design and bio-inspired application of different fields of individual fish scale.

Chapter 3. Materials and Methods

3.1 Materials

The black drum fish scales were obtained from Fruge Seafood Companies, Texas, USA. These scales were preserved with ice and kept in fresh condition upon arrival. After separating cleaning up the remaining flesh/tissues, these scales were kept in frozen condition before further sample preparation.

3.2 Fish Scales Observation Experiments

Sample cross-section polishing: After thawing, cleaned by sonicating in deionized water, and completely dried, the selected scales were embedded in epoxy (Epo-Fix, Electron Microscopy Sciences). After cured at room temperature, the scale samples were cut along the longitudinal (anterior-to-posterior) and transversal (dorsal-to-ventral) directions to reveal the cross-sections. Sequential polishing was applied to the scale cross-sections using an automatic polishing machine (MultiPrep TM System, Allied HighTech Products, Inc.) with diamond lapping films (15 μm, 9 μm, 6 μm, 3 μm, and 1 μm). The final procedure of surface finish involve cloth polishing with 40 nm colloidal silica suspension. Later, the samples were sonicated again in DI water to remove the remaining colloidal particles.

Scanning electron microscopy (SEM): The polished and fractured scale samples were dried and then coated with a 10 nm Pd/Pt layer before to electron microscope imaging to reduce charging effects. SEM images were then acquired with a FEI Quanta 600 FEG environmental SEM with acceleration voltage of 15 kV and working distance of ~12 mm.

3.3 Fish Scales Chemical Experiments

Energy-dispersive X-ray spectroscopy (EDS): SEM-EDS data were obtained using the FEI Quanta 600 FEG environmental SEM. The acceleration voltage was set at 20 kV. The backscattered electron (BSE) images were acquired with a Bruker QUANTAX 400 with XFlash 4010 ($10mm^2$) silicon drift detector, which achieves an energy resolution Mn K – 125eV at over 100,000 cps. The elemental composition is quantified using the Bruker Esprit 2.1 Software with PB Linemarker-ZAF correction.

Scale demineralization process: The acid demineralization and polish demineralization methods were applied to scales that cut in custom shape steel cutting die that designed in dogbone shape (WhiskyTime, Etsy, Inc.). The scale samples for acid demineralization was immersed in saltwater solution for more than 24 hours and then immersed for 90 minutes in a 0.4 mol/liter hydrochloric acid solution for 90 minutes[45]. The polish demineralization method is to manually polish the scale thickness from 0.5 to 0.3 mm based on the high mineralization thickness results of the scale from the EDS and nanoindentation tests.

3.4 Fish Scales Mechanical Experiments

Synchrotron-based micro-computed X-ray tomography (μCT): The μCT measurements was conducted using the synchrotron X-ray at beamline 2-BM of the Advanced Photon Source, Argonne National Laboratory, Chicago. The beam energy used was 27.4 keV, and the camera imaging resolution was 1.30 μm/pixel and the field of view (FOV) of 2560×2560 pixel^2, corresponding to ~3.33 mm in width and height. Tomographic reconstructions were performed using TomoPy and rendered with Avizo (Thermo Fisher Scientific, USA).

Uni-axial tensile test: The macroscopic tensile test was mainly focused on the conditions in terms of wet dogbone and rectangular shapes (prepared by custom steel cutting die from WhiskyTime, Etsy, Inc.), and intact and demineralized scales. Uni-axial tensile tests were carried out on an Instron 6800 mechanical testing machine in Virginia Tech, Blacksburg, with a load cell of 5 kN at a strain rate of 0.01 s-1. The testing area is 10 mm long and 4 mm wide. The mechanical tests were performed at room temperature at a displacement rate of 0.20 mm/min, on hydrated samples maintained through the use of the glass spray bottle. The tensile results were expressed in terms of engineering stress–strain curves. The ultimate tensile stress, uniform elongation (strain at maximum stress) and the toughness, as measured by the area beneath the stress–strain curves, were established.

Digital imaging correlation (DIC): The DIC test was conducted on fish scale samples by tensile testing. The speckle pattern was prepared by spray black paint, videos were recorded by optical microscopy at 20 frames per second. The video was converted to pictures using customized MATLAB code and analyzed using the Vic 2D software by correlated solutions, based on which the stress and strain fields were obtained.

Finite element (FE) simulation: Based on the characteristics of rostral and focal fields structures, black drum scale FE simulation beam models for various external surfaces and multilayer structures were created using Abaqus/CAE 6.14. The scale models for black drum fish were made of type I collagen fiber and hydroxyapatite (HA). The average slopes of the stress and strain curves of intact and acid demineralized scales were used to calculate Young's modulus of HA and collagen fibers, which were approximately 697 MPa and 184 MPa, respectively. The average failure stresses in tension experiments of demineralized scales were used to calculate the collagen fibers' yield stress, which was 20 MPa. Poisson's ratios of the collage fibers and HA were defined as 0.3[48,49]. The 8-node linear brick, decreased integration, and hourglass control elements (C3D8R) were used in finite element beam simulations. Each finite element beam model has 1 million quadrilateral mesh elements. A three-point bending load was applied, considering the symmetry only half of the beam model was simulated. The supporting locations in each model were simply fixed with a 100 N loading force applied to either the top or bottom of the beams' edge at zero coordinates.

3.4.1 Nanoindentation Experiment preparation

The dried scales are epoxy embedded and serially polished as part of the sample preparation for nanoindentation described in **Section 3.1**. The polished fish scales were subjected to nanoindentation using a Micro-Materials instrumented nanoindentation system (NanoTest Vantage platform 4). Line mapping over the scale thickness was accomplished using a Berkovich tip to examine the hardness and reduced modulus gradients. The spacing between adjacent indentation was 2 μm, and the maximum load was 2 mN with a loading profile of loading (15 s), holding (10 s), and unloading (15 s). Thermal drifting was monitored for 30 s at the unloading stage when the load was unloaded to 10% of the maximum force (0.2 mN). For each sample, 3 lines are drawn near the central region of the sample for statistical purposes.

To compare the influence of humidity, nanoindentation was performed in both dry and wet conditions. In the sealed chamber where the indentation was conducted, the humidity level was monitored and controlled by a humidity sensor (hygrometer) (Fig. 3-1). For dry condition, the measured relative humidity was *ca*. 36%, while for wet condition, the target humidity level was 90%, where the supplemented humidified air was guided to the humidity cell. The system was set to equilibrate for at least three hours prior to performing nanoindentation.

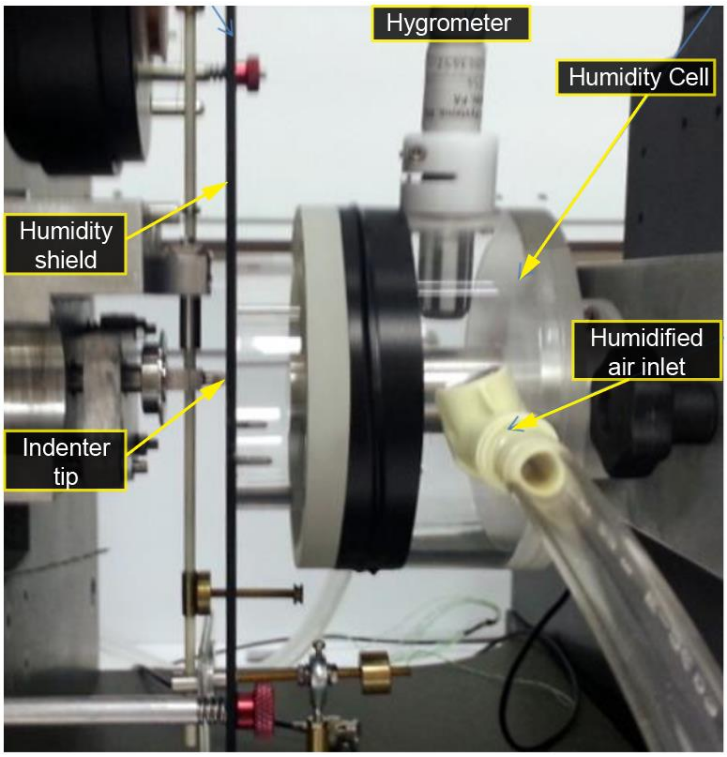

Fig. 3-1. Nanoindentation conducted under wet condition with humidity cell and shield installed on the nanoindentation system.

3.4.2 Tensile Experiment preparation

Fig. 3-2 shows the general dimension of the cutting dies that are used to prepare the tensile samples and the cutting locations of the tensile samples in longitudinal and transverse directions. The testing area of the samples in both directions are from the focus field, rostral field and the lateral fields. The overall testing area of the testing is 40 mm^2. The original size of the fish scales and the average thickness of the test area after cutting the sample were measured in Table 3-1 and 3-2 respectively, with the test area thickness difference being no greater than 0.05mm.

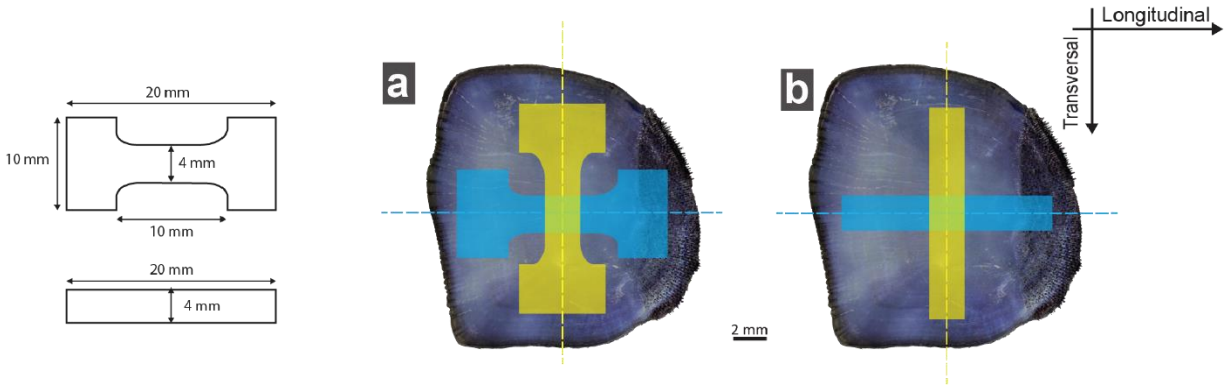

Fig. 3-2. Tensile experiment preparation with cutting dimensions and fracture locations. The dimension of tensile cutting dies in **(a)** dog-bone shape and **(b)** rectangular.

Table. 3-1 The average thickness of the testing area of the unnotched samples.

Transverse direction cut samples										
	R_S1	**R_S2**	**R_S3**	**R_S4**	**R_S5**	**D_S6**	**D_S7**	**D_S8**	**D_S9**	**D_S10**
Thickness	0.407	0.507	0.503	0.537	0.553	0.327	0.617	0.55	0.52	0.623
Longitudinal direction cut samples										
	D_S1	**D_S2**	**D_S3**	**D_S4**	**D_S5**	**R_S6**	**R_S7**	**R_S8**	**R_S9**	**R_S10**
Thickness	0.507	0.38	0.517	0.437	0.567	0.487	0.52	0.523	0.497	0.473
Where the thickness is calculated by three different positions on the test area, and the unit is mm. R means rectangular samples, and D means dogbone shape samples.										

Table. 3-2 The average thickness of the testing area of the notched samples.

Transverse direction cut samples										
	D_S1	**D_S2**	**D_S3**	**D_S4**	**D_S5**	**R_S1**	**R_S2**	**R_S3**	**R_S4**	**R_S5**
Thickness #1	0.21	0.26	0.30	0.37	0.36	0.25	0.21	0.17	0.17	0.22
Thickness #2	0.37	0.35	0.43	0.43	0.42	0.50	0.37	0.37	0.35	0.35
Thickness #3	0.34	0.27	0.42	0.38	0.35	0.24	0.20	0.22	0.22	0.26
Notch length	1.06	1.31	1.31	1.33	1.35	1.06	1.73	1.25	1.29	1.35
Longitudinal direction cut samples										
	D_S1	**D_S2**	**D_S3**	**D_S4**	**D_S5**	**R_S1**	**R_S2**	**R_S3**	**R_S4**	**R_S5**
Thickness #1	0.36	0.32	0.32	0.34	0.31	0.32	0.32	0.36	0.36	0.39
Thickness #2	0.42	0.51	0.46	0.44	0.36	0.42	0.39	0.49	0.47	0.42
Thickness #3	0.33	0.43	0.36	0.32	0.28	0.33	0.26	0.41	0.30	0.37
Notch length	1.31	1.35	1.28	1.30	1.30	1.30	1.36	1.31	1.29	1.32
Where the thickness is calculated by three different positions on the test area, and the unit is mm(also shown in Fig. 3-2). The notch area of the first three transverse direction samples of the dogbone and square sizes are located at the right and the rest of the samples are located at the left. The notch area of the first three longitudinal direction samples of the dogbone and square sizes are located at the top and the rest of the samples are located at the bottom.										

3.4.3 Digital Imaging Correlation Experiment preparation

The sample was prepared using two different techniques: 1) used waterproof paint to print the DIC pattern, and 2) used waterproof pen to draw the dots on the collagen-side surface of the fish scales. The scale must first be dried in the air, then it needs to be inked or painted on the surface before being rehydrated in the seawater solution. On dry fish scales, paint dried rapidly

whereas pen ink took longer to dry. When placed in seawater, it was clear that neither paint nor ink had blurred or lost its color. The results of the DIC analysis are better for the samples that are generated by paint, even though the hand-drawn dots samples have larger and clearer pattern surfaces than the paint printed samples.

Chapter 4. Structural and Chemical Characterization of Black Drum Fish Scales

The structure characterization of fish scale in micron scale can be divided into surface structure analysis and cross-sectional structure analysis. The surface morphology was mainly presented by SEM images to explain the structural distributions in different fields of the scale. The structural characterization of local areas of fish scales was restored through the segmentation of micro-CT scan images of the scales. Additionally, by comparing SEM images, the focal, rostral, lateral, and caudal fields' surface features were identified. Besides, the curvature distribution results of primary and secondary radii on external layer surface were obtained from CT images. In order to examine the chemical composition and characteristics of the materials, EDS tests were also performed on several fields of fish scale structures. The optical images and SEM images were mostly used to illustrate the cross-section structure characterization of fish scales. We can comprehend the interior stratification and mineralization of black drum scales by looking at their cross-sectional structure. The mineralization of the scales can be compared to that of other scales in order to identify differences and to investigate the effects of laminar angles and layer thickness on the structure of the scales.

4.1 Introduction of Black Drum Fish

The black drum is a saltwater fish that may reach lengths of 40 to 60 inches and weighs between 50 and 100 pounds[2]. It has a dark, silvery-gray body with a brassy sheen. The black drum can commonly be found in an estuary close to oyster beds or other abundant food sources. Another interesting fact about black drum fish is that they receive their name from a huge, elaborate swim bladder that can resonance and make croaking or drumming noises when particular muscles are used. And in our group's fascinating research areas, we also concentrate on the teeth of black drum fish[50] since it exhibits as one of the highest bite forces among extant animals with an exclusive diet of hard-shelled mollusks.

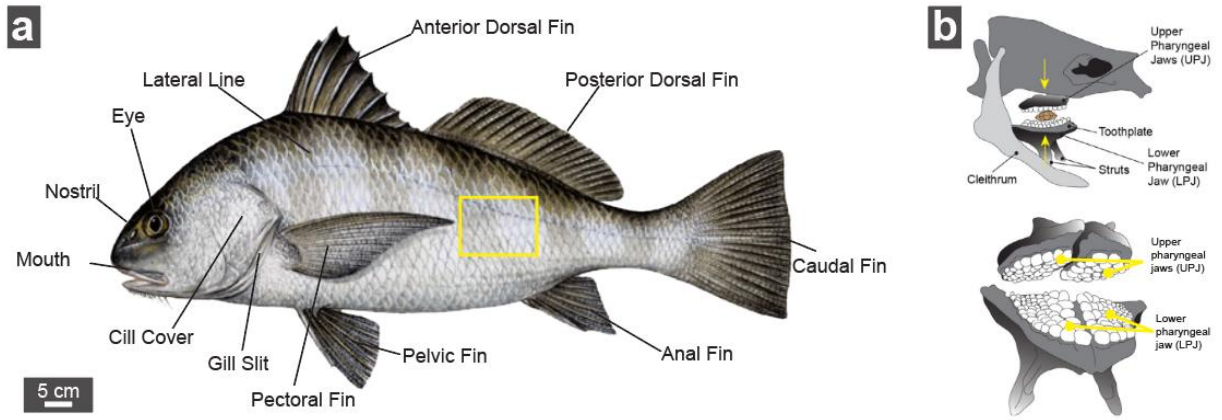

Fig. 4-1. Overview of black drum fish (*Pogonias cromis*), including **(a)** schematic showing the anatomic structures[51] of black drum fish and **(b)** pharyngeal jaws and teeth[50].

The schematic structural overview of the black drum fish scales can be found below. The anatomical structures of black drum fish are shown in Fig. 4-2a. The schematic diagram of an individual scale is shown in Fig. 4-2b. The scale can typically be divided into four fields: the focus field at the center, which is the first part of the scale to appear in growth; the lateral field on the dorsal and ventral sides with circuli that show the develop circular growth rings around the focus; the rostral field on the anterior end, which is frequently embedded under the preceding scale of the fish, with radii which are grooves that radiate from the focus to the projection, which is the margin of scale; and finally, the posterior field of the scale with the tubercles facing the tail is known as the caudal field[8].

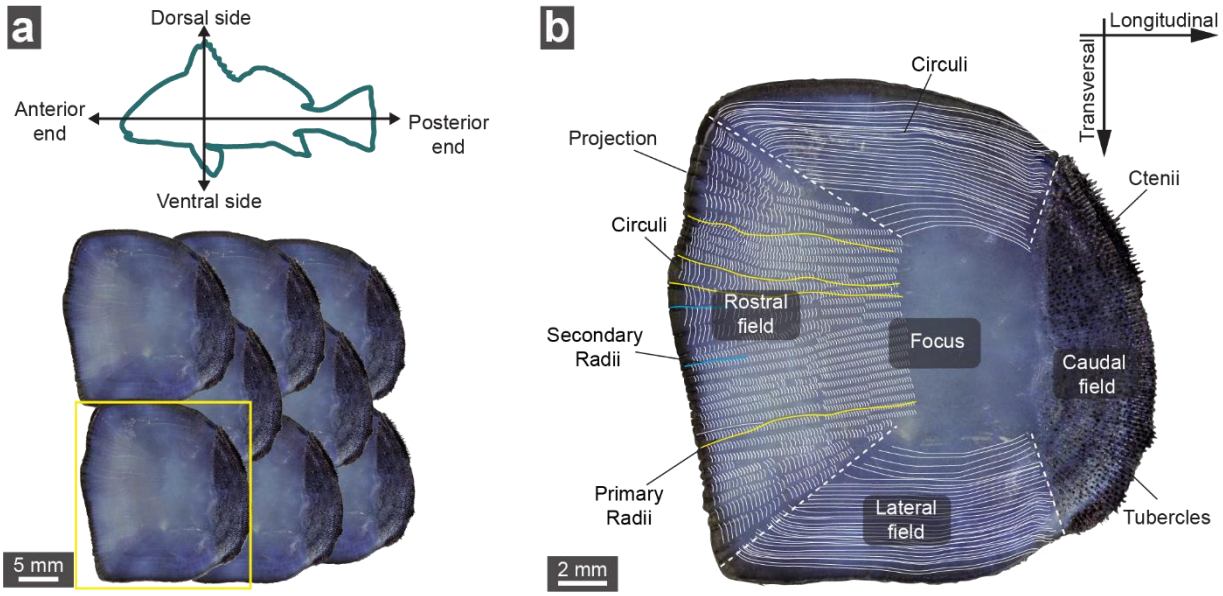

Fig. 4-2. Overview of black drum fish scales. (a) The staggered multiple scales in correspondence to the anatomical directions of black drum fish, and **(b)** the definition of structural features on an individual scale.

4.2 Characterization of Surface Structure

The surface morphology of the black drum fish scale reveals the intricate surface structure of the different regions of the fish scale. From it, we can conclude that the structure of the different fields of the fish scale differs significantly, and the process by which the various regions transition is apparent. Different radii types can be used to distinguish by the regular and directional radii arrangement on the surface of the rostral and lateral fields. Tubercles at caudal field have special structure characteristics. The caudal section of *Carassius auratus*[52] scales, which are the same sort of scale as black drum scales, are arranged, however, in a disorganized and irregular manner. The tubercles arrangement of the black drum scales may offer unique properties or functions. These can be researched in this subject further. Furthermore, hydroxyapatite crystals constitute the majority of the surface structure of fish scales[42]. The consistency of the composition in various surface areas can be assessed by EDS analysis. The relationship between compositional variation and structure distributions will need to be addressed if the composition of different locations changes.

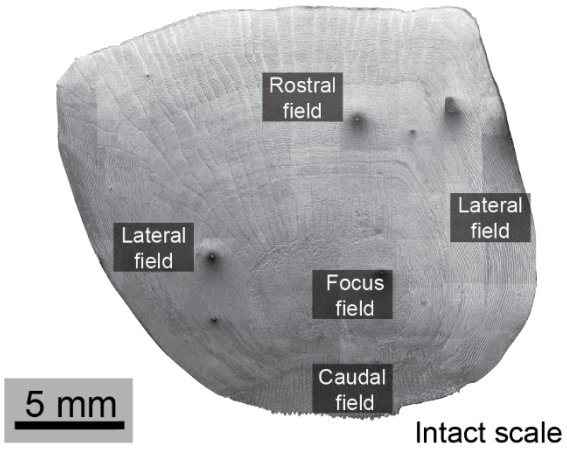

Fig. 4-3. Overview of surface structure on the black drum fish scales.

The exterior view of the detailed SEM surface morphology is shown below (Fig. 4-4). Fish scale surface morphology diagrams in longitudinal and transverse directions are presented in Fig. 4-4a and b, respectively, while detailed magnified diagrams of different surface fields on the scale are displayed in Fig. 4-4c, d, e, f, and g. Fig. 4-4c and d are the transition regions of the focus and rostral field. Protrusions with irregular shapes are depicted in both diagrams. In contrast to continuous mineralized circuli, the posterior region typically has protrusions that have no discernible pattern. Diagrams of the radii sections at the rostral field are presented in detail in

Fig. 4-4e. In the lateral field, the continuous mineralized bridges known as criculi are seen in Fig. 4-4f. Radii and criculi have prominences similar in shape but different in orientations. Fig. 4-4g shows an array of tubercles that resemble regular teeth and cover the scale's exposed area.

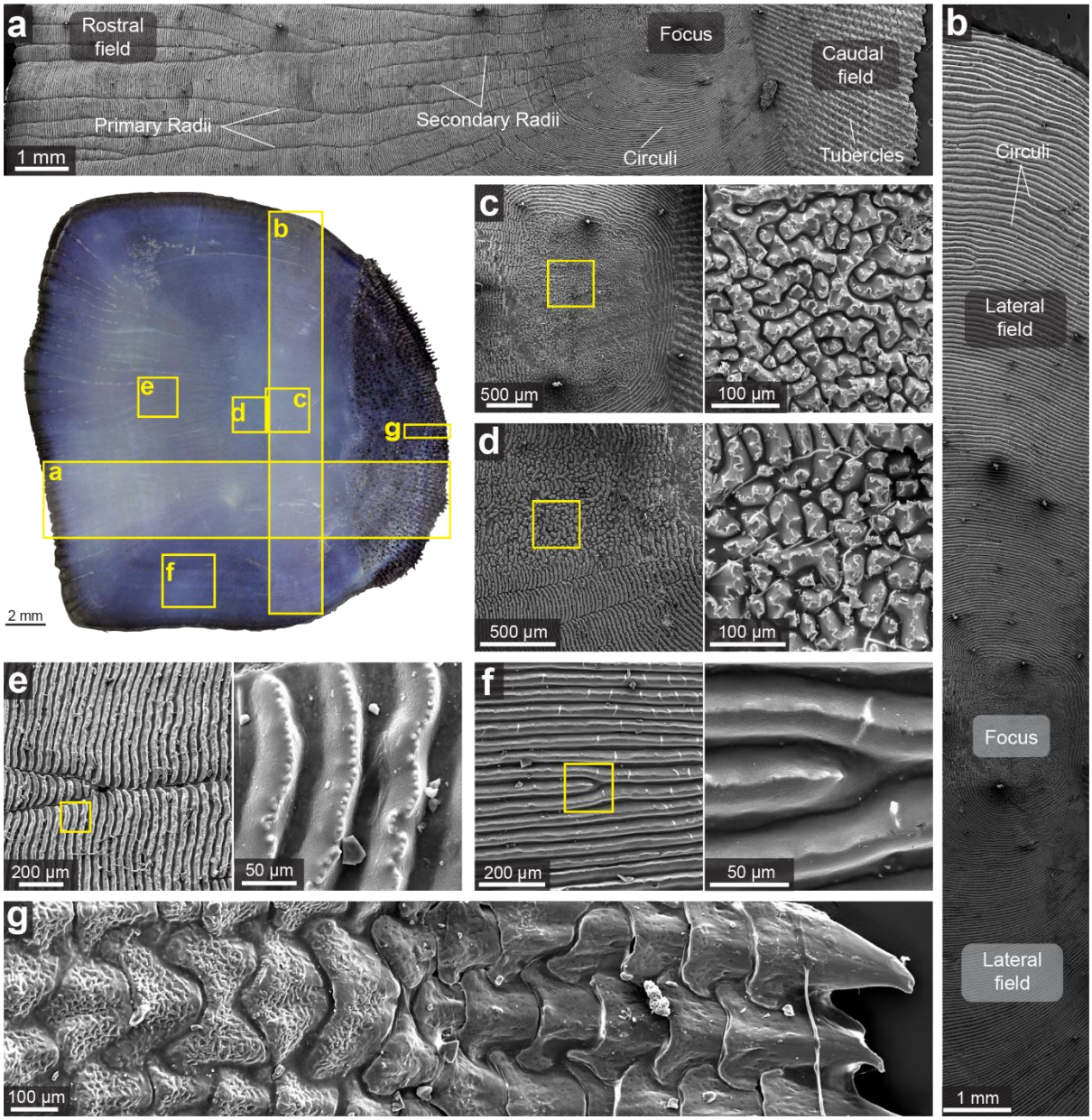

Fig. 4-4. Detailed surface structure on the black drum fish scales at different regions, including **(a)** a selected row along the longitudinal direction, **(b)** a selected column along the transversal direction, **(c)** focus, **(d)** near-focus, **(e)** rostral field, **(f)** lateral field, and **(g)** caudal field.

It is corroborated by the micro-CT scanning results that the samples in Fig. 4-5 originate from the lateral field and focus transition area. Primary radii and secondary radii have different orientations, as is evident from the figure. Furthermore, the surface structure of the exterior layer, which is composed of numerous irregular bumps and depressions, is also shown by the micro-CT segmentation result. Since there is no air in the different layers of fish scales, variations of the mineralization of external layer should be the main responsible for the surface structure. The cross-sectional structure was investigated to provide a detailed explanation. The surface curvature analysis result for the external layer is presented in Fig. 4-5c. As can be seen, the same radii have a uniform in curvature change. Additionally, secondary radii have a larger curvature than primary radii.

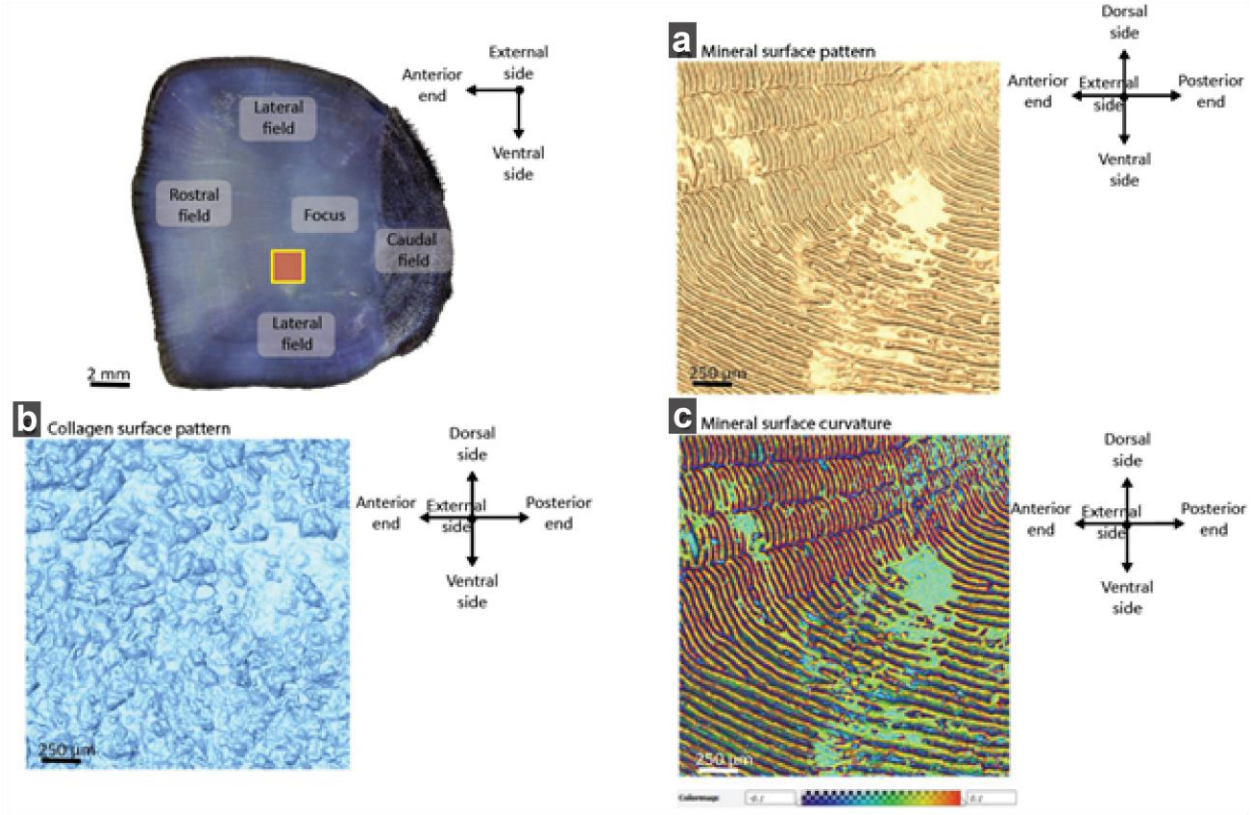

Fig. 4-5. Surface morphology of black drum scales based on synchrotron-based µCT measurements.

The samples in fig. 4-6 were prepared by using a micro blade along the same trajectory notch on the external and internal sides of the wet fish scale and tearing the fish scale along the trajectory notch. The three SEM images illustrated the fiber orientations in different regions of the scales with "U-shaped" fiber orientations at local regions, overall perpendicular arrangement of the fibers between adjacent layers and mineralization difference between the rostral field and

caudal field. We can conclude that the directions of fish scale fibers can be roughly divided into two directions by combining the findings from the orthogonal arrangement of the fibers in structural characterization: one direction is similar to the circuli direction, and the other is orthogonal to the fiber direction of the previous direction and points to the focus field. This conclusion is primarily confirmed in the fiber orientations near the focus and lateral fields. Additionally, we discovered that the fiber on the fracture margins of each layer had a "U-shaped" orientation in the tearing regions close to the margins of fish scales at the anterior and posterior end. We haven't come across a structure like this in previous works of literature. The "U-shape" oriented fiber is a combination of fibers pointing to the focus region and fibers in the circuli direction, as seen in Fig. 4-6f. Furthermore, the fractures in the lateral field lacked U-oriented fibers; they were only present at the anterior and posterior ends. This could be the primary cause of the difference in fish scale longitudinal and transverse tensile results. Our future research will focus on whether this "U-shaped" fiber arrangement has unique advantages and functions compared to orthogonal fibers.

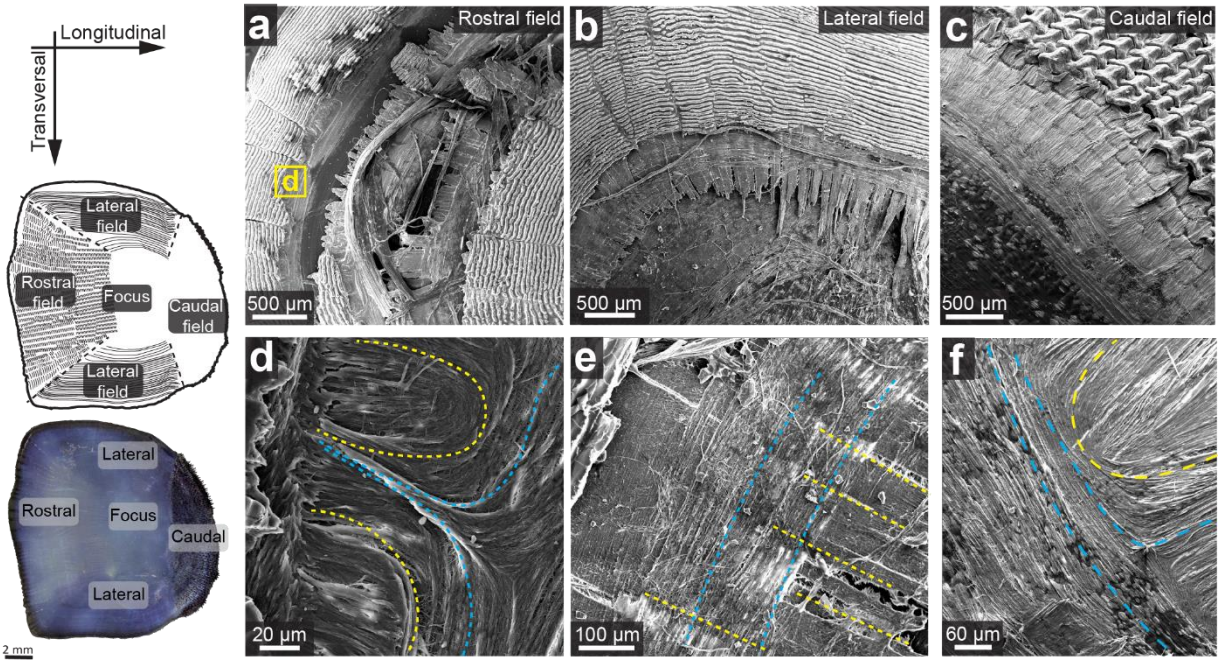

Fig. 4-6. Fractured surface of black drum fish scales at different regions, including **(a,d)** rostral field, **(b,e)** lateral field, and **(c)** caudal field. Yellow and blue dot lines indicate different fiber orientations.

4.3 Characterization of Cross-sectional Structure and Chemistry

The goal of studying the cross-section of fish scales is to learn more about how fish scales are layered and how each layer is structured in relation to the others. First, the overall stratification of fish scales was constructed by the mineralization process, and SEM and optical images were used to study the arrangement, thickness, and laminate angles of the laminae layers in each structural layer of the scale. Further, the cross-sectional structure arrangement of various surface regions was used to investigate how fish scales form, and EDS analysis was used to corroborate the compositions of fish scales. We can further analyze the connections between the laminae layers and how they end up at the margins of the scale. In order to further understand the degree of mineralization of fish scales, fish scales were divided into different components for analysis using micro-CT data segmentation. Mandl's corpuscles, which are small mineral particles, were arranged according to sizes and positions in the collagen layer.

The black drum fish scales are constructed of hydroxyapatite (HA) and type I collagen fibers, which together form the elsmoid scales' composition. In addition, the figures below demonstrate the multilayered structure of the black drum scales from both longitudinal and transverse cutting directions. The SEM images of the transversal cut scale are shown in Fig. 4-7. The scale contains multiple layers in both directions, including an exterior layer, an external elasmodine layer (higher mineralized collagen), and an internal elasmodine layer (less/no mineralized inner collagen). In the detailed cross section (Fig. 4-7b), the exterior mineral layer's corrugated shape is obvious. Moreover, we can more clearly see that the mineral phases of the exterior and internal elasmodine layers in the SEM images of the longitudinal cut scale, demonstrating that the external elasmodine layer is more mineralized than the interior elasmodine layer. The thickness of several layers in various orientations and alternating fiber orientations (0° /90°) were also indicated in the SEM images (Fig. 4-7b and c).

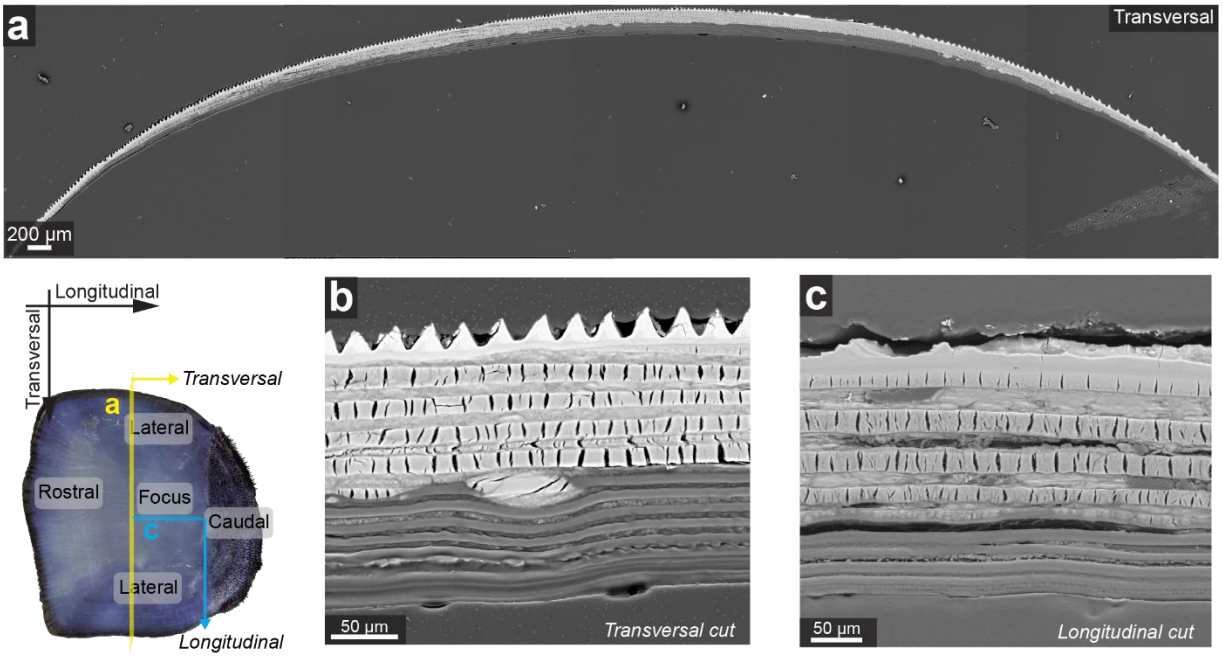

Fig. 4-7. Polished cross-sections of black drum fish scales, including **(a)** entire transversal cross-section, **(b)** magnified near-focus region on the transversal cross-section, and **(c)** magnified near focus region on the longitudinal cross-section.

Another cutting direction sample's multilayered structure can be seen in Fig. 4-8 as a result of SEM images taken from polished cross-sections; Fig 4-7 is from a transverse cut, while Fig. 4-8 is from a longitudinal cut across the thickness at the focus area. We can more easily distinguish between the external and internal elasmodine layers in these two figures. The internal elasmodine layer has an uncertain microstructure and a thickness of roughly 90 µm, whereas the external elasmodine layer has a plywood structure with vertical fiber direction between adjacent layers with thickness of about 125 µm. Thus, there are three distinct layers in a fish scale. The first layer's degree of mineralization is higher than the second layer's degree of mineralization in the inner layer, which also varies between the first and second layers (brightness similar to that of the epoxy matrix). The organization of the laminate sheet and the direction of the collagen fibers of the external and internal elasmodine layers are included in Fig. 4-8b and c, which are magnified views of the ventral side. The direction of the fibers in each laminate sheet, which is the perpendicular fiber orientations of adjacent lamellae in the exterior elasmodine layer, was confirmed by the blue arrow and dot in the magnified regions of Fig. 4-8c. The internal elasmodine layer has a lamellae thickness of 4 to 5 µm, whereas the external elasmodine layer has a lamellae thickness of 15 to 16 µm.

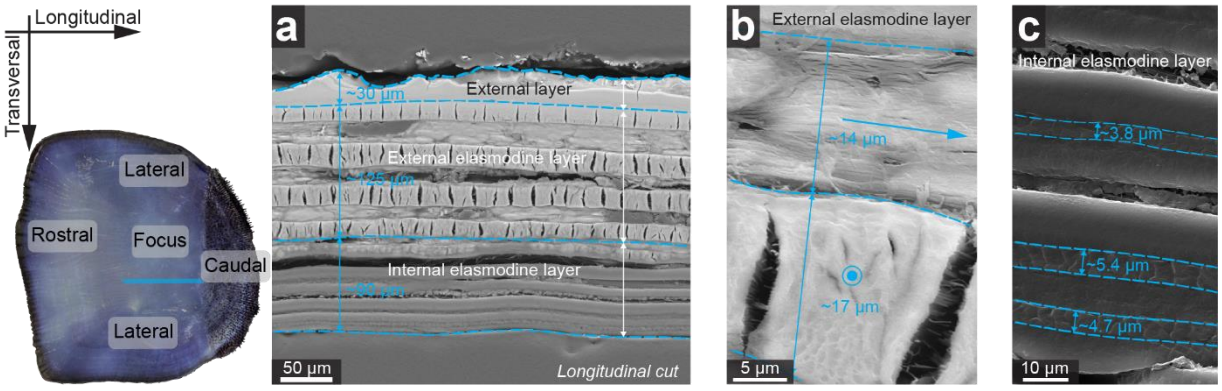

Fig. 4-8. Detailed structural features on the longitudinal cross-section of black drum fish scales, including **(a)** near-focus structure, **(b)** magnified region in the external elasmodine layer, and **(c)** magnified region in the internal elasmodine layer.

After learned the surface morphology and mineral phase multilayer structure of the black drum fish scale, the material properties that we want to know more about the chemical characterization of the mineral phase. First, we investigated the cross-section of the scale in focus field using EDS point spectra (Fig. 4-11). According to literature, the main elements present in fish scales include phosphorus (P), calcium (Ca), carbon (C), oxygen (O), silicon (Si), sulfur (S), and chloride (Cl). It is because the type I collagen fiber and hydroxyapatite constitute the majority of fish scales.

According to the EDS area (Fig. 4-9) and line (Fig. 4-10c) profiles, the internal layers of fish scales are mainly comprised of collagen, whereas the external layer is made primarily up of HA (hydroxyapatite that includes largely O/P/Ca). When we get closer to the interior elasmodine layer, calcium and phosphorus nearly disappear and are substituted by an almost linear increase in carbon element.

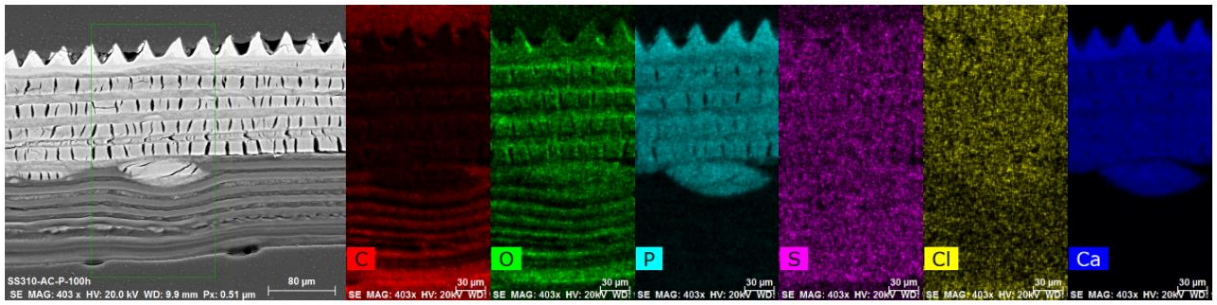

Fig. 4-9. EDS maps on a selected region of polished transversal cross-section of fish scale. **(a)** Secondary electron image of the transversal cross-section near the focus region of fish scale. The box indicates the region for EDS maps. **(b-g)** Element maps, including **(b)** carbon (C), **(c)** oxygen (O), **(d)** phosphorus (P), **(e)** sulfur (S), **(f)** chloride (Cl), and **(g)** calcium (Ca).

The detailed trend of elements across the thickness of the fish scale could be seen in Fig. 4-10, along with layered distributions for the three layers; oscillations of the trends within sub-layers correspond to alternate orientations, especially C in the internal elasmodine layer. The results of the quantitative characterization of the point spectra on the scale cross-section at different locations were shown in Fig. 4-11 and Table 4-1.

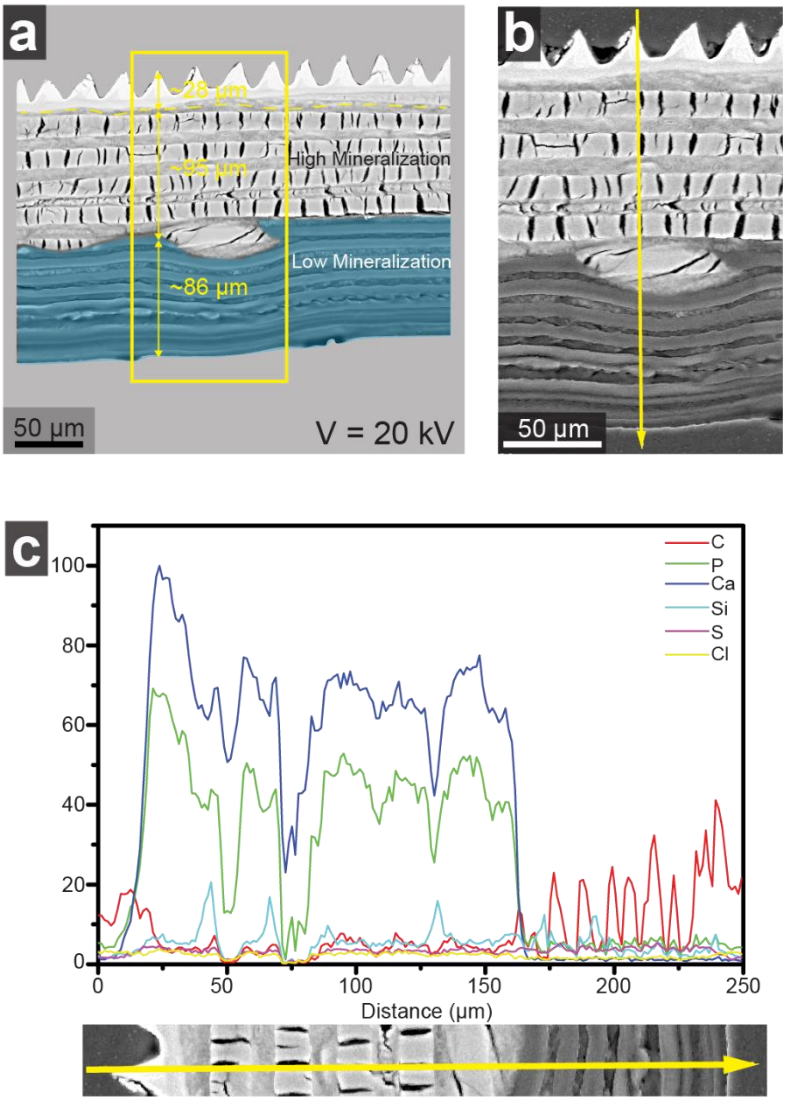

Fig. 4-10. EDS line map across the fish scale thickness.

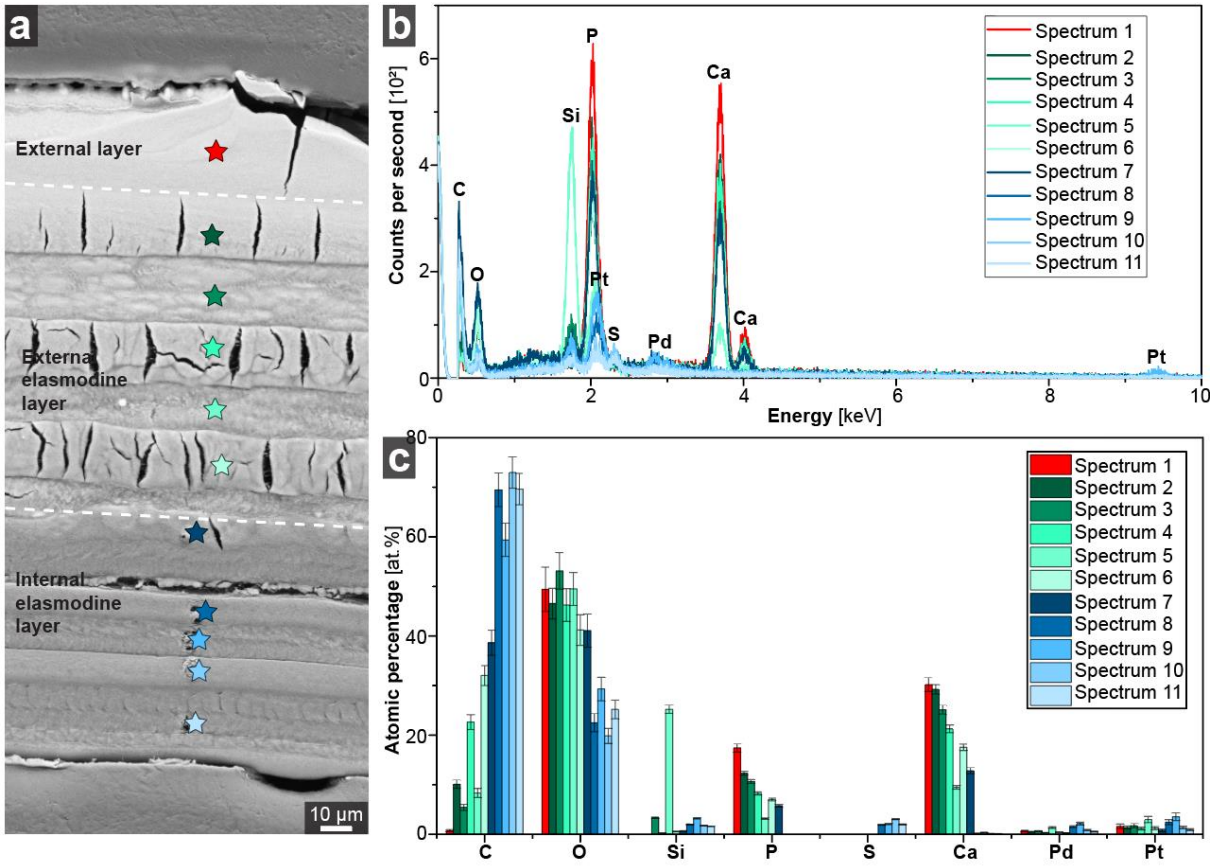

Fig. 4-11. Quantitative characterization of EDS results based on point spectra. **(a)** Secondary electron image of the longitudinal cross-section near the focus region of fish scale. The stars indicate the spots for EDS point spectra. **(b)** EDS spectra with characteristic peaks of elements, including C, O, P, S, Ca, etc. **(c)** Atomic percentage of the selected elements.

Table 4-1. Atomic percentage of the major elements in fish scales at different points.

Elements	C (*at.*%)	O (*at.*%)	Si (*at.*%)	P (*at.*%)	S (*at.*%)	Ca (*at.*%)	Pd (*at.*%)	Pt (*at.*%)
Point 1	0.71 ± 0.23	49.42 ± 4.49	0	17.40 ± 0.78	0	30.20 ± 1.35	0.67 ± 0.14	1.61 ± 0.49
Point 2	10.07 ± 0.82	46.55 ± 3.10	0	12.31 ± 0.40	0	29.23 ± 0.93	0.48 ± 0.09	1.35 ± 0.30
Point 3	5.41 ± 0.61	53.14 ± 3.69	3.36 ± 0.14	10.64 ± 0.38	0	25.10 ± 0.86	0.62 ± 0.11	1.73 ± 0.40
Point 4	22.63 ± 1.51	46.24 ± 3.31	0.21 ± 0.041	8.24 ± 0.32	0	21.26 ± 0.78	0.29 ± 0.07	1.12 ± 0.29
Point 5	8.33 ± 0.90	49.48 ± 3.34	25.19 ± 0.80	3.17 ± 0.14	0	9.47 ± 0.36	1.36 ± 0.18	2.99 ± 0.64
Point 6	32.03 ± 2.00	41.20 ± 3.08	0.56 ± 0.05	7.03 ± 0.28	0	17.54 ± 0.66	0.42 ± 0.09	1.22 ± 0.31
Point 7	38.64 ± 2.52	41.09 ± 3.36	0.65 ± 0.06	5.77 ± 0.27	0	12.80 ± 0.57	0.25 ± 0.07	0.80 ± 0.25
Point 8	69.47 ± 3.38	22.49 ± 1.82	1.97 ± 0.10	0	1.89 ± 0.10	0.19 ± 0.05	1.53 ± 0.19	2.45 ± 0.51
Point 9	59.38 ± 3.32	29.30 ± 2.38	3.22 ± 0.15	0	2.04 ± 0.11	0.34 ± 0.06	2.19 ± 0.27	3.53 ± 0.77
Point 10	72.97 ± 3.15	19.85 ± 1.51	1.74 ± 0.08	0	3.05 ± 0.12	0.19 ± 0.04	0.86 ± 0.12	1.34 ± 0.27
Point 11	69.62 ± 3.16	25.19 ± 1.87	1.62 ± 0.08	0	1.99 ± 0.10	0.11 ± 0.04	0.55 ± 0.10	0.93 ± 0.22

4.4 Analysis of Mineralized Particles (Mandl's Corpuscles)

According to the previous structural investigation, the external layer and elasmodine layer constitute the majority of the black drum fish scales. The internal and external elasmodine layers, which are sub-layers of the elasmodine layer and the internal elasmodine layer contains small mineral particles, are separated by no air or other materials. The distribution of the mineral ridges, which are the primary radii, is typically perpendicular to the transverse direction based on the surface pattern of the external layer. We can also identify the small mineral particles from the dorsal direction surface figure of the mineral layer (Fig. 4-6c).

In Figure 4-12, synchrotron CT results (side view) demonstrate that in addition to the mineralized outer and elastic layers, the internal elasmodine layer contains some isolated mineral particles (Mandl's corpuscles) . These Mandl's corpuscles varied in size from large to small with special arrangement distribution according to Fig. 4-13. It exhibits the scanning results of micro-CT data on fish scale cross-section. As the position of the CT scan shifts, corpuscles appear and disappear as depicted by the transparency of the shadows. Mandl's corpuscles can be observed to

appear and disappear in the same direction, indicating that they are situated in the same layer of the lamellae. Additionally, the orientation of the long axis of the corpuscles directly corresponded to the collagen fibrils in each lamella was where the mineralization of Mandl's corpuscles extended further. The various fibril directions in the corpuscles in Fig. 4-14 correlate to the order of traversing lamellae. In the same layer of the laminae, there is only one orientation of the corpuscles.

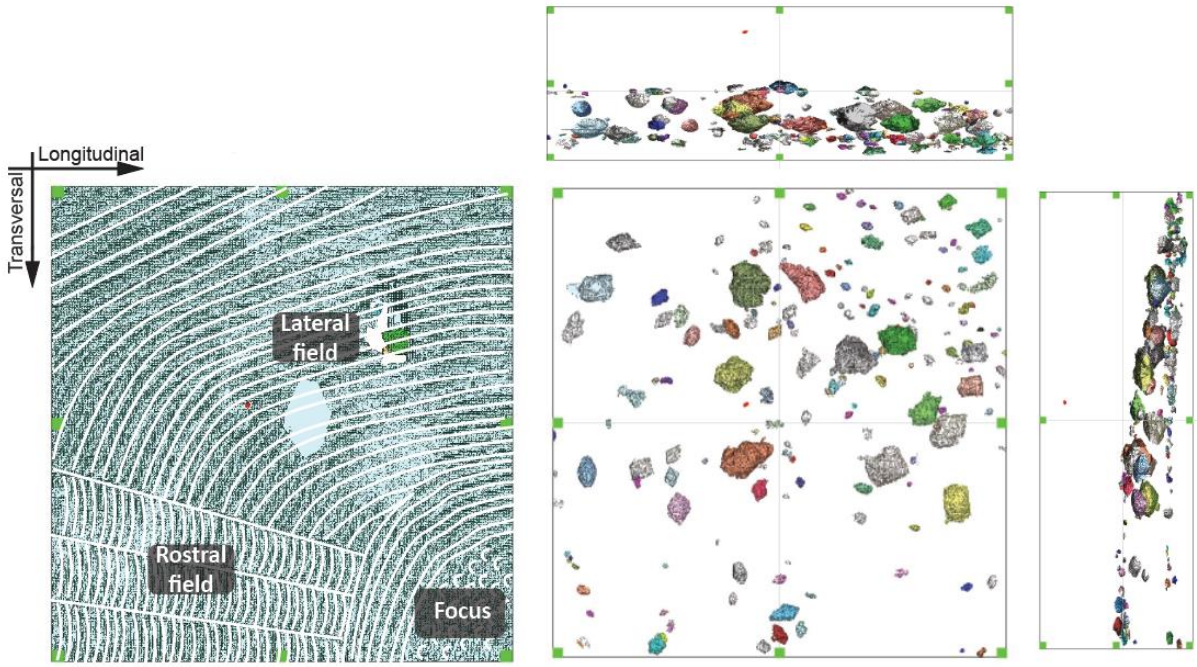

Fig. 4-12. The distribution of small mineral particles (Mandl's corpuscles) in black drum scale. The whole scale cross-sectional pattern that located at transition area of focus and lateral field from external surface view, the distribution of the Mandl's Corpuscles from three sides of view.

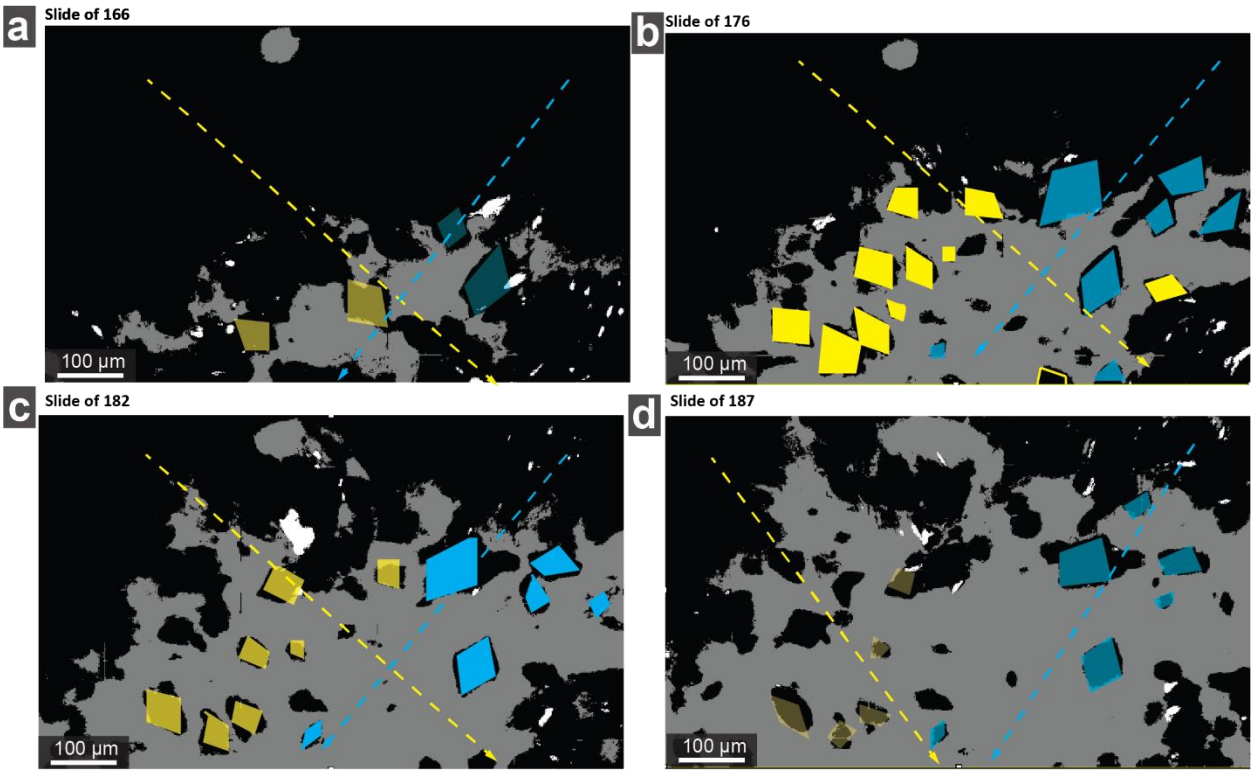

Fig. 4-13. Orientation distribution of Mandl's corpuscles by CT scanning. (a-d) The yellow and blue diamond shadows transparency process from slide 166 to 187.

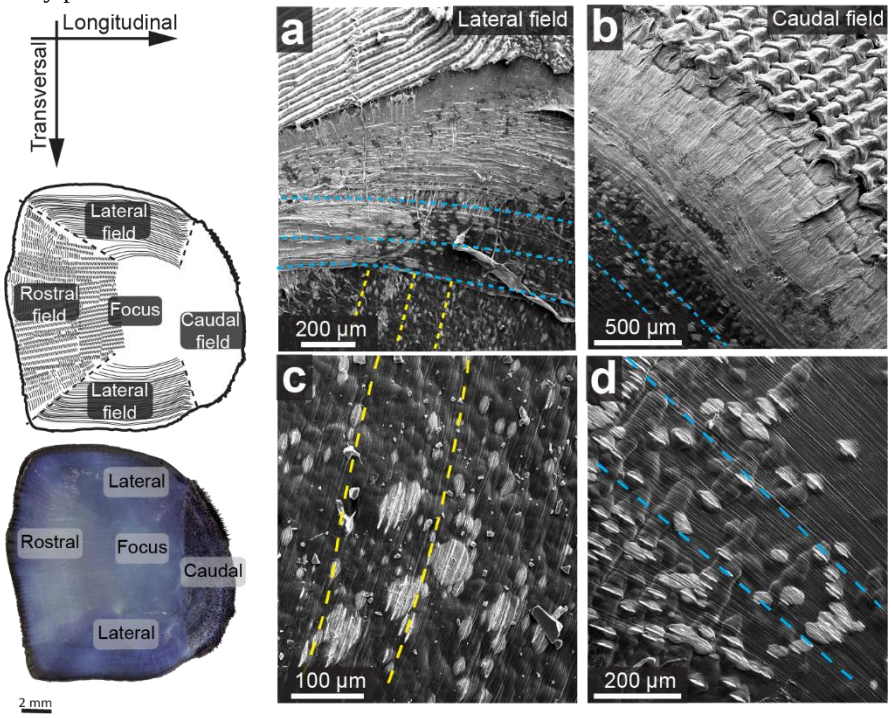

Fig. 4-14. Mineral particles (Mandl's corpuscles) exposed on the fractured fish scales. Schematic representation of the black drum scale distributed within the fields on the left. SEM images of fractured fish scales, exposing the rhombus-like Mandl's corpuscles. **(a)** Lateral field. **(b)** Caudal field, and **(c-d)** detailed images of Mandl's corpuscles from different fields. Yellow and blue dot lines represent the orientation of collagen fibers.

Based on the synchrotron CT data, a systematic characterization of the particle geometries and orientations was conducted out. A total of 100 Mandl's corpuscles were selected at random from Fig. 4-15 and given labels for further analysis using the synchrotron CT scan's Scale 140 data. Large mineral particles are distributed in the top portion of the internal elasmodine layer in fish scales, whereas small particles are arranged in the bottom, as can be seen from the organization of size of mineral particles. The size of the Mandl's corpuscles varied irregularly in the scale. Moreover, the size of the particle has an impact on how smooth its surface is. The surface is smoother the smaller the particle is.

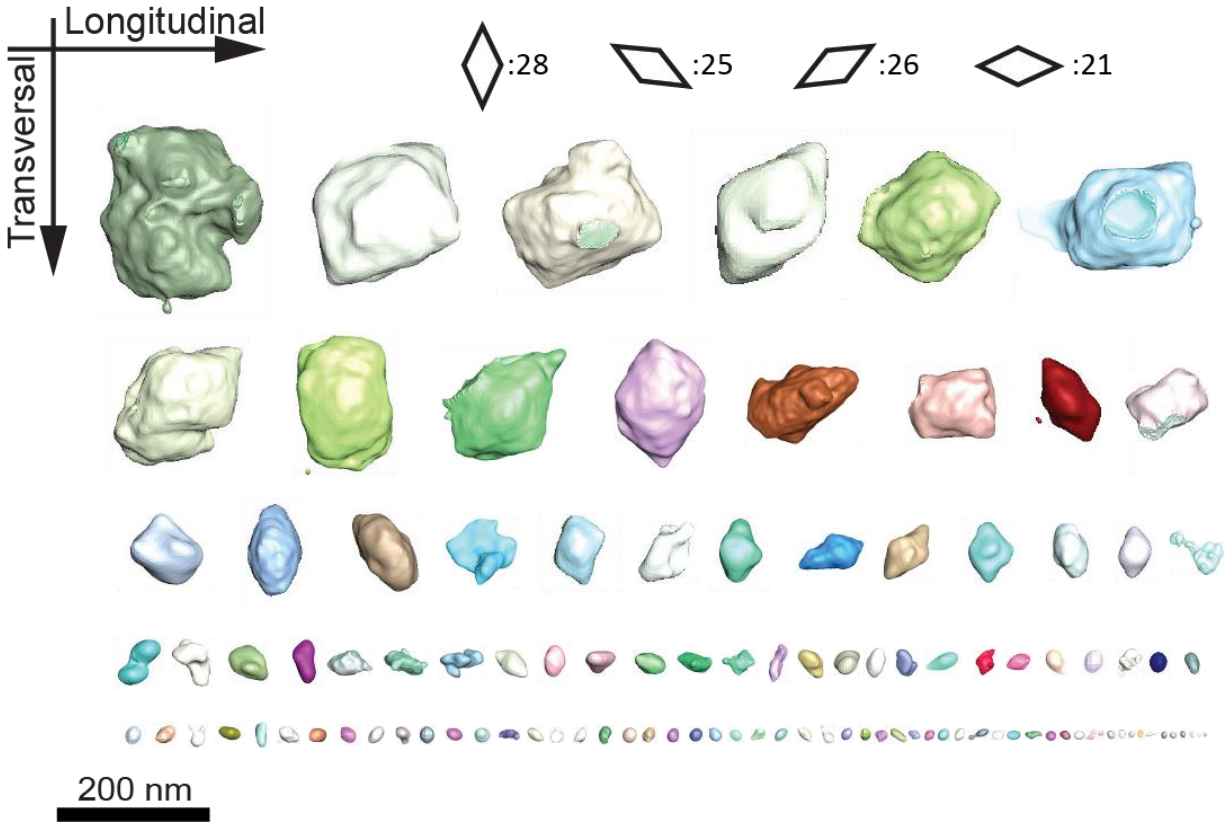

Fig. 4-15. Synchrotron-based micro-computed X-ray tomography of the fish scales. The arrangement and distribution of 100 Mandl's corpuscles from *μCT* data Scale 140.

These bar charts are the calculated results of three-dimensional volume distributions of Mandl's corpuscles from different fields that selected and presented in Fig. 4-15 by Avizo. After distinguished the different fields' locations from *μCT* data Scale 140, we separated the Mandl's corpuscles collected from rostral and focus fields for further different fields mineral phase distribution analysis. The size distribution and longest axis orientation of Mandl's corpuscles in rostral and focus fields were displayed in Fig. 4-16b. Microns cubed is the units for 3D volume.

There are 29 corpuscles that were selected in the rostral field and 12 corpuscles were selected in focus field. In rostral field, the number of Mandl's corpuscles (10) is largest in the range of 3D volume from 10000 to 50000 microns cubed. We may better comprehend the correlation between the mineralization process of Mandl's corpuscles and different surface fields of the black drum scales by separately extracting and re-segmenting the sizes and locations of Mandl's corpuscles using APS CT data from Argonne laboratory.

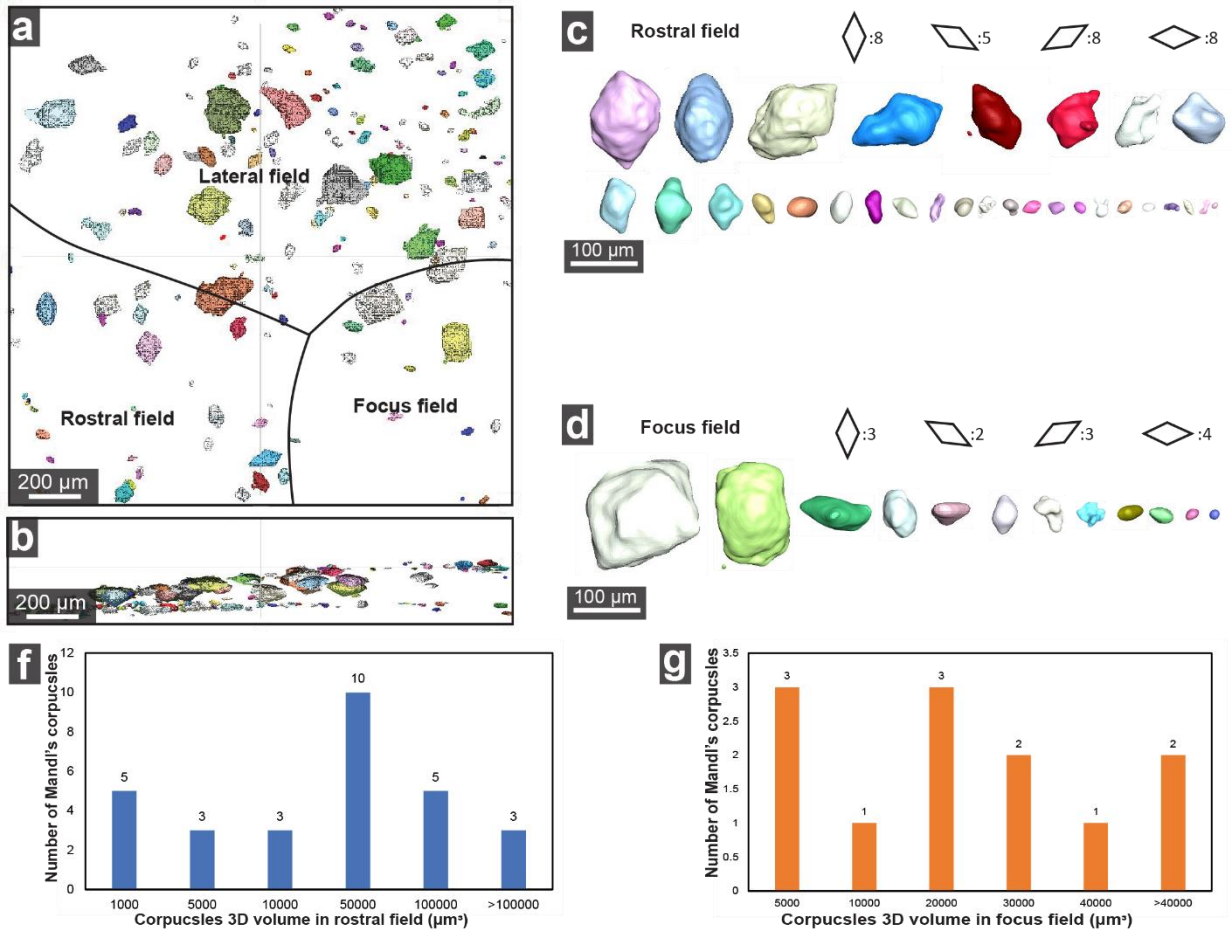

Fig. 4-16. Quantifications of particle geometries and sizes. Size and location distributions of small mineral particles (Mandl's corpuscles) in black drum scale. **(a)** Mandl's corpuscles' location distribution within rostral and focus fields. **(b)** The size distribution and longest axis orientation of Mandl's corpuscles in rostral and focus fields from µCT data Scale 140. The bar charts of volume distribution of Mandl's corpuscles in **(c)** rostral and **(d)** focus field.

4.5 Comparative Structural and Chemical Analysis of Acid Demineralized Scales

Fig. 4-17 is SEM surface characterization results of acid demineralized scale. It can be found that the radii structure (high mineralized external layer) of the demineralized scale cannot

be seen while the circuli distribution is still shown on the external surface, which also verifies that this method can completely demineralize the fish scale. Interestingly, the natural bending direction of acid demineralized scale during drying process is opposite to that of intact scale. This may be due to the high mineral crystals having the function of grouping fiber boundaries and fixation.

In the detailed SEM external surface morphology of acid demineralized fish scales (Fig. 4-17a,b,c,d), NaCl crystals were found at the edges of rostral field and lateral field, which was caused by the fish scales being placed in seawater solution before air drying and the smaller thickness of the edge of fish scales. But no NaCl crystals were found on the intact scale, which had been dried in the same way.

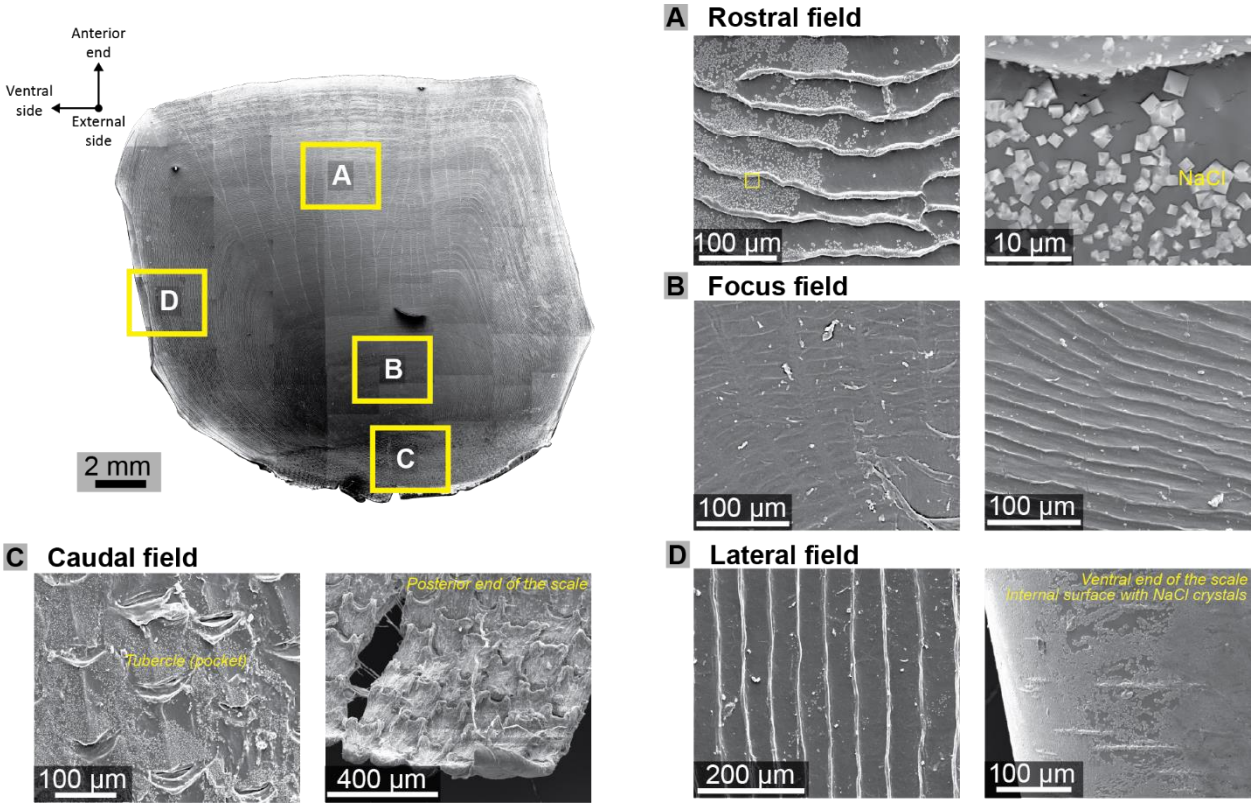

Fig. 4-17. SEM results of external surface fields morphology of acid demineralized scale. Schematic representation of the acid demineralized black drum scale surface. The detailed SEM images of fish scales from **(a)** rostral field, **(b)** focus field, **(c)** caudal field, and **(d)** lateral field.

First, based on previous measurements of the thickness of the acid demineralized scales, we can conclude that the thickness does not change significantly between before and after acid demineralization, or that the thickness of fish scales after demineralization is greater than that of

intact fish scales (tensile test measurements). In the investigation of the EDS cross-sectional structure of acid demineralized fish scale, it is possible to determine that the scale is entirely demineralized, but its cross-sectional distribution may still be separated into two distinct zones. As depicted in Fig. 4-18c, the formerly highly mineralized region now has evident gaps, and only the distribution of in-plane horizontal fibers (yellow area) is visible, therefore the gaps should be out-of-plane fibers based on the orthogonal fiber orientations. This also shows that high mineral crystals may serve the purpose of gathering and fixing fiber boundaries.

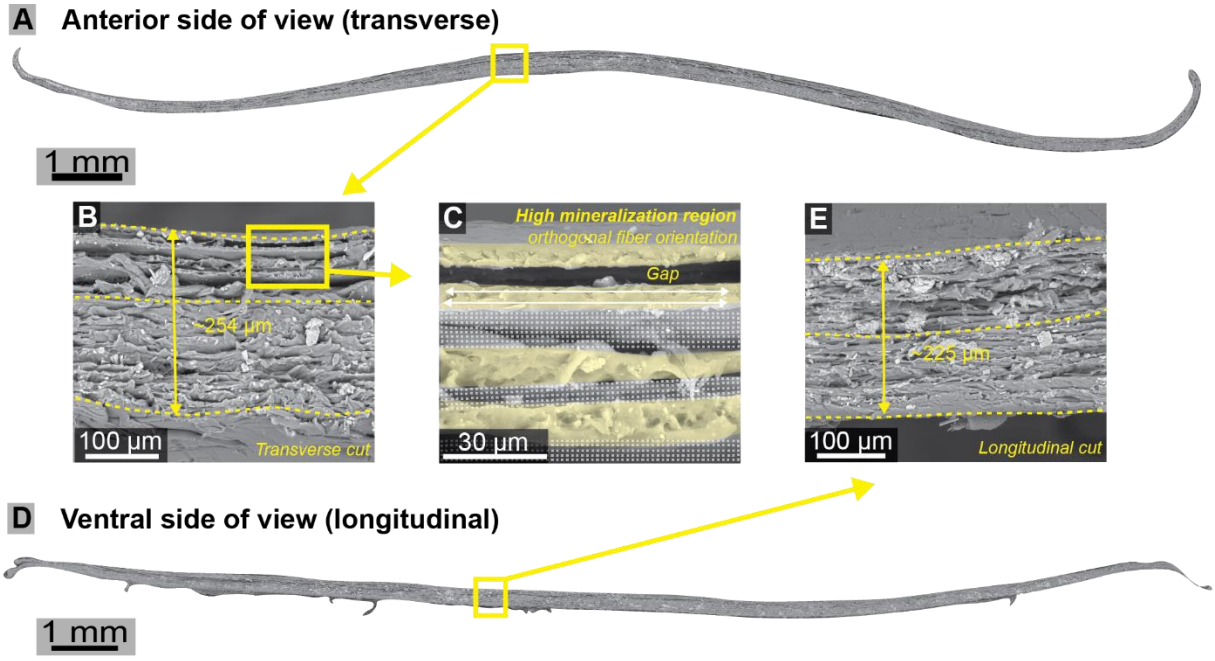

Fig. 4-18. Cross-sectional structure of acid demineralized scales from (a) transversal and (b) longitudinal cutting directions. **(b-e)** The detailed SEM images of the transversal and longitudinal cutting samples. There is the observed gap at the high mineralization region.

EDS line profile analysis in Fig. 4-19 shows that the external layer of fish scales is mainly composed of HA and the internal layers are mainly composed of collagen. The middle layers (upper layers of internal layers) are a mixture of HA and collagen. Along the thickness, we see an almost linear decrease in Ca and P (blue and green lines, HA mineral content), disappearing as we approach to internal layer and a corresponding increase in C (red line). It is worth noting that the line profile results of sample # 1 and sample # 2 of rostral fields are significantly different due to the different trend of the variation of the two samples. The distribution of elements in the internal layer of sample # 2 (Fig. 4-19b) indicates the distribution of high and low mineralization in the sublayer, and the thickness of the sublayer decreases

gradually. In addition, EDS area profile results (Fig. 4-20) clearly show that Ca and P mainly occur in high mineralized regions.

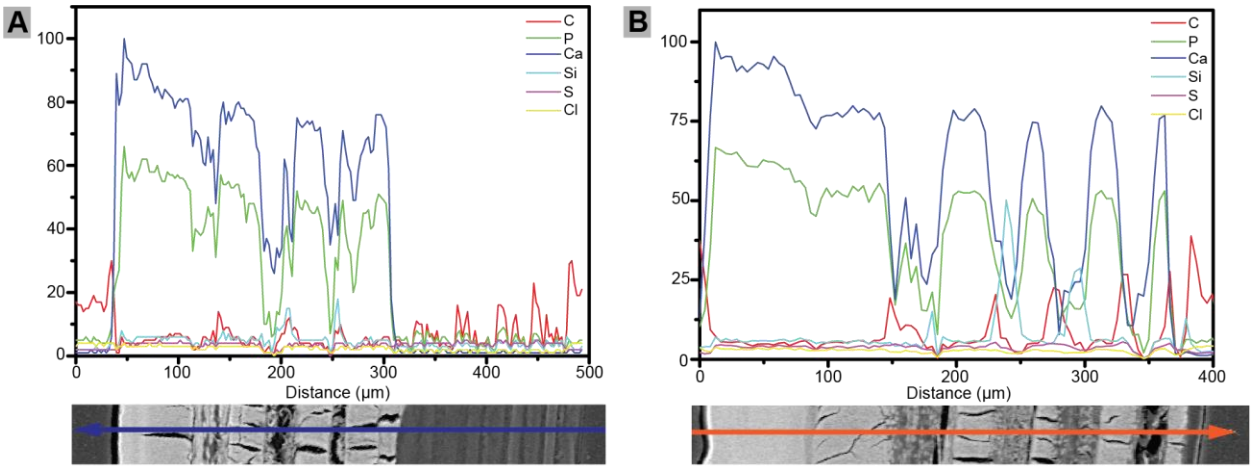

Fig. 4-19. EDS line profile analysis of (a) sample #1 and (a) #2 in Rostral field.

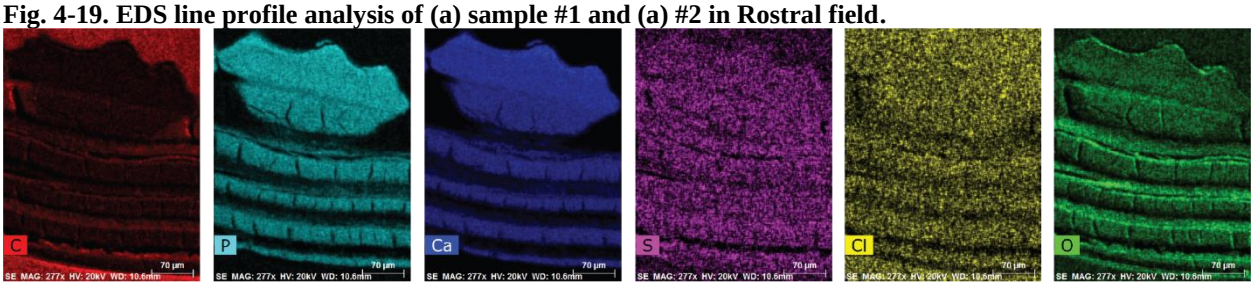

Fig. 4-20. EDS area profile analysis of elements distribution of Rostral field sample.

Chapter 5. Mechanical Properties of Fish Scale

After characterizing the distribution of the mineral phase within individual black drum fish scale, we aim to use experimental and computational methods to explore the mechanical properties effects. The significance of comprehending the mechanical properties of fish scales, including bulk (millimeter) scale tensile qualities and microscopic level nanoindentation.

5.1 Nanoindentation Properties of Focus Field

5.1.1 Nanoindentation Results

In transverse and longitudinal cross-sections, the reduced modulus and hardness of black drum scales in dry and wet conditions are shown. In various cross-sections and humidity levels, the fundamental distribution tendency of the mechanical characteristics gradually decreases from the external layer to the internal layers. Likewise, this table displays the average reduce modulus and hardness under varying situations.

The nanoindentation results of longitudinally cut samples in dry and wet nanoindentation conditions are summarized in Fig. 5-1. First of all, hydration "softens" fish scales by reducing the indentation modulus of the inner layer and treating, while there is no significant change in the properties of the mineralized outer layer. Second, physical properties decrease from the exterior to the interior layers, which may be associated with a reduction in mineralization. In addition, both the outer and inner layers of plywood have significant characteristic oscillations. The oscillating layer of external elasmodine is thicker than that of internal elasmodine, which may be related to the thickness of the fiber layer of plywood.

Table 5-1. Average mechanical characteristics in different layers of various cutting directions and humidity.

	Transversal cut				**Longitudinal cut**			
	Dry		***Wet***		***Dry***		***Wet***	
	Er (GPa)	Hardness (GPa)	Er (GPa)	Hardness (GPa)	Er (GPa)	Hardness (GPa)	Er (GPa)	Hardness (GPa)
External layer	22.1	0.8	35.4	1.5	23.8	1.1	29.6	1.3
External elasmodine layer	16.1	0.5	5.7	0.2	17.3	0.6	6.3	0.3
Internal elasmodine layer	7.4	0.4	2.1	0.1	6.5	0.3	4.9	0.2

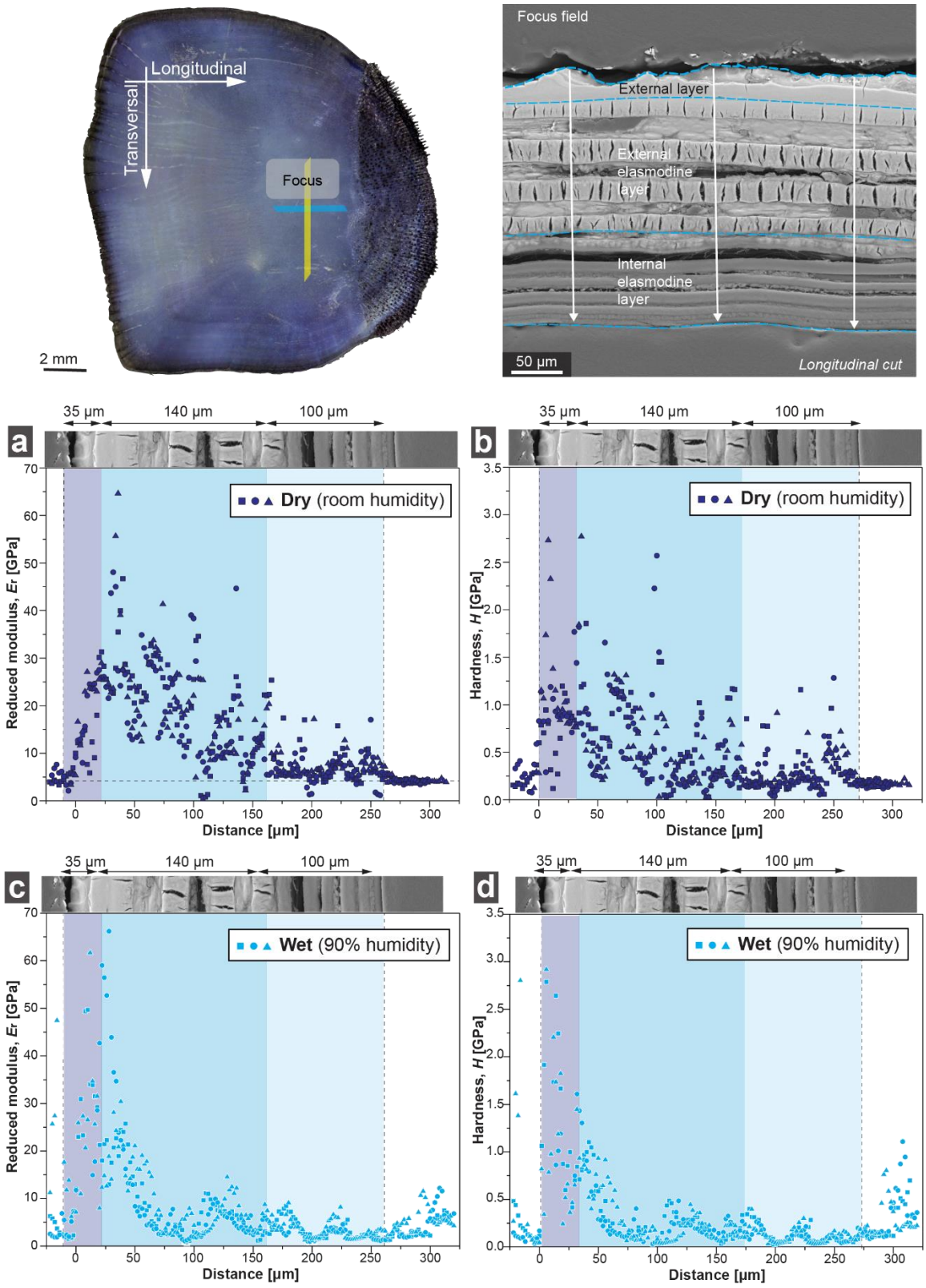

Fig. 5-1. Nanoindentation results on the longitudinal cross-section of scale near the focus region. Shematic image of a scale shows the longitudinal cut orientation. SEM image of the post-indented sample. **(c-f)** Nanoindentation results across the scale thickness under **(a-b)** dry and **(c-d)** wet conditions, including **(a,c)** reduced modulus and **(b,d)** hardness.

In Fig. 5-2, the consequences of dry and wet indentation on transverse cutting samples were contrasted. It's important to understand that dry and wet indentation are performed on different samples which explaining thickness variations. Degradation was observed in the inner layer of the scales. However, the inner layer does not oscillate like the longitudinal cut sample does. Nonetheless, it is unknown what structural factors related to this trend.

We can find that the average modulus and hardness of transversal and longitudinal cut samples are about the same by comparing the modulus and hardness from different cross-sections. Moreover, longitudinal cross-section mechanical property distributions exhibit definite oscillatory tendencies. However, when comparing mechanical characteristics between wet and dry conditions, moist conditions often have bigger mechanical properties in each layer. Furthermore, the average modulus and hardness of the wet condition samples in external layer are signification larger than that of internal layers.

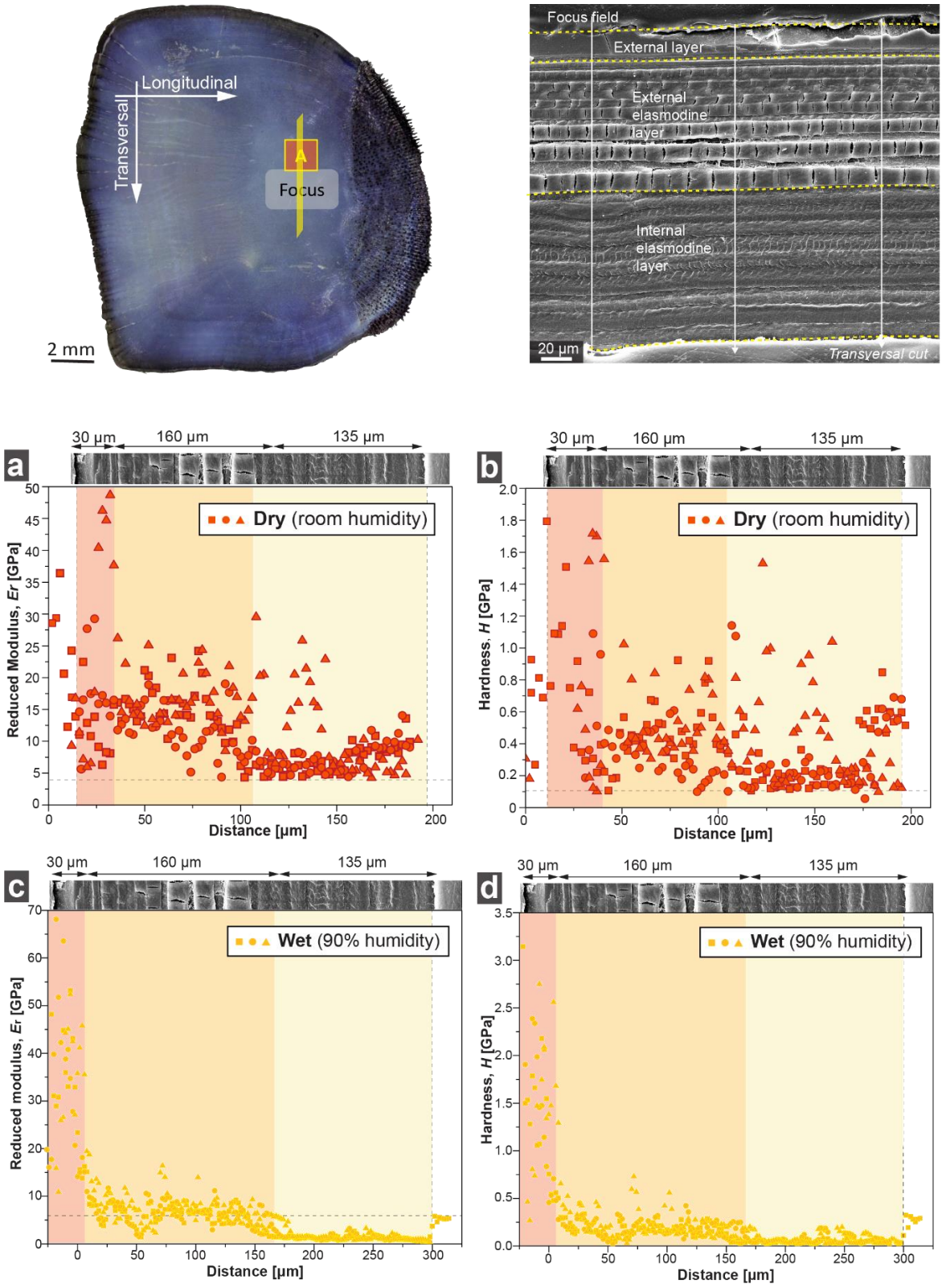

Fig. 5-2. Nanoindentation results on the transversal cross-section of scale near the focus region. Schematic image of a scale shows the transversal cut orientation. SEM image of the post-indented sample. Nanoindentation results across the scale thickness under **(a-b)** dry and **(c-d)** wet conditions, including **(a,c)** reduced modulus and **(b,d)** hardness.

5.2 Tensile Properties

5.2.1 Tensile Results on Intact Scale

5.2.1.1 Longitudinal vs. Transversal samples

The stress and strain curves of the dogbone and rectangular shape samples are shown in Fig. 4-5 in two different cutting directions. In Fig. 4-5a, the blue curves were characterized as longitudinal dogbone shaped samples, while the yellow curves were transverse dogbone shaped samples. For the 10 samples in two directions, the overall distribution of force and displacement curves is comparable. The average ultimate load of dogbone-shaped samples is around 60 MPa, which is higher than that of rectangular-shaped samples, which is about 35 MPa, according to the stress and strain curves. In addition, based on the slopes of the curves that are shown in the black dot lines, Young's modulus of dogbone shape samples (410 MPa) and rectangular shape samples (400 MPa) are roughly equivalent. As a result, we can say that the stiffness in the various cutting orientations is not significantly different. Besides this, the tensile strength of the longitudinal samples and the strength of the transverse samples with the same shape and distribution and peak show no significant difference. Along these, there are some small load drops noticed in the curves in each plot, which are attributable to the laminate's partial failure or to layer separation or sliding.

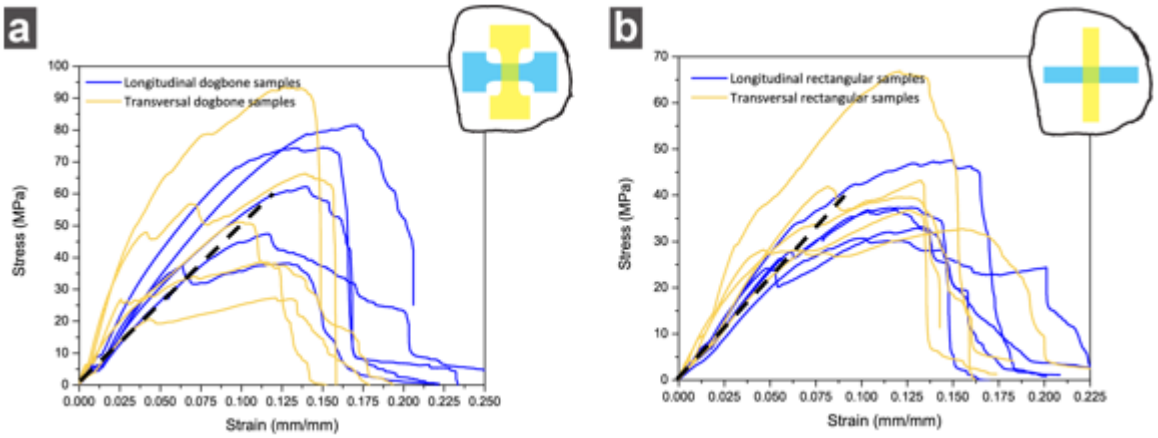

Fig. 5-3. The stress-strain curves of dogbone and rectangular shape unnotched wet scale samples that cut in transverse direction(a) and longitudinal direction(b).

The fracture results of the tensile analysis are shown in Fig. 4-6 below. According to the schematic schematics provided, the transverse cut samples fractured close to the grips section's two ends in the lateral field. Meanwhile, the ends of the longitudinally cut samples fractured

close to the rostral field. The fracture may have occurred because the thickness of the fish scales is inconsistent throughout, with the anterior end being thinner than the posterior end. Moreover, radii on the surface of Rostral field can also be regarded as many tiny notches. As a result, the mineral layer of the longitudinal cut samples will first fracture close to the rostral field. The location of each fracture in transversal cut samples is not defined since the surfaces of lateral fields at the dorsal and ventral ends are constructed of criculi of uniform sizes. The stratified mineral and collagen layers found in longitudinal cut samples are another interesting observation. These layers may be correlated to the mineralization of fish scales and the arrangement of laminate sheets.

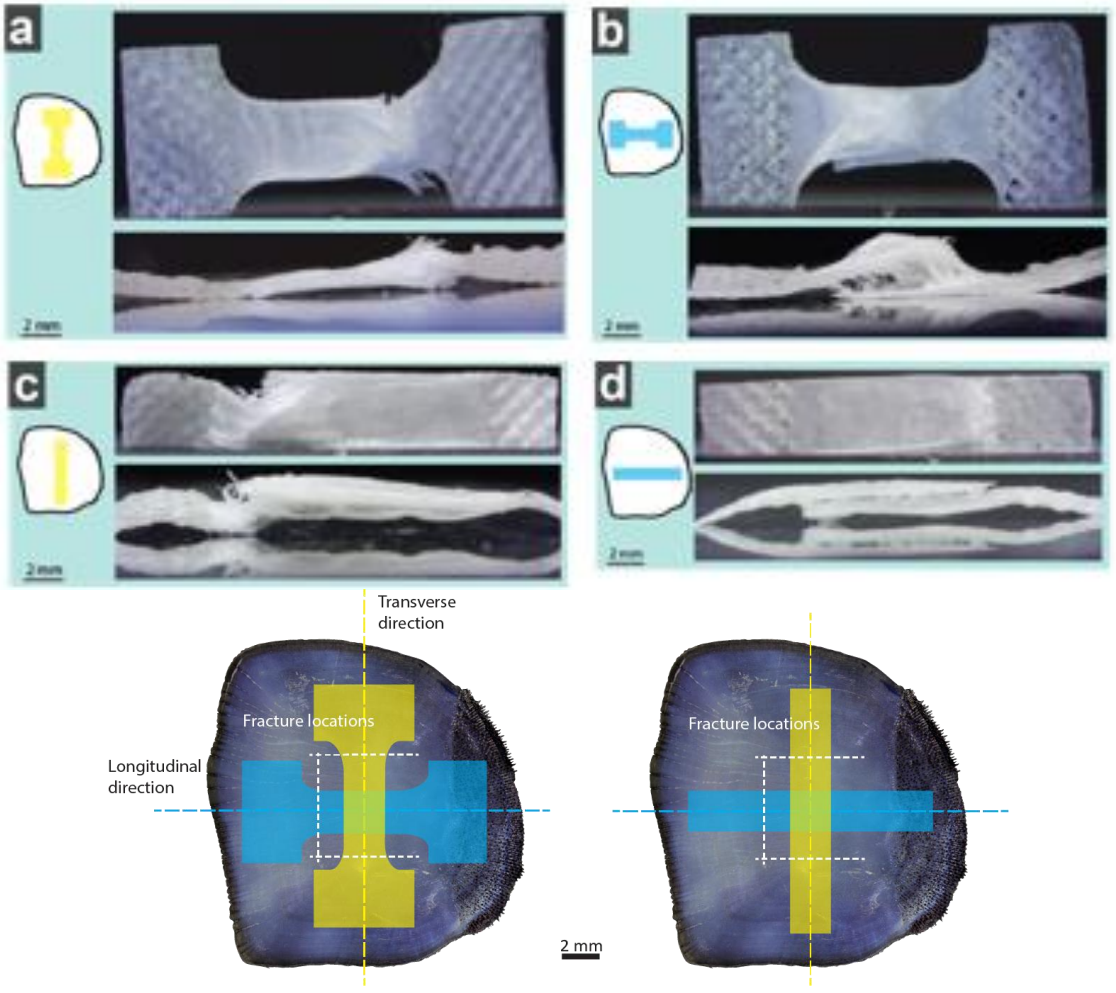

Fig. 4-6. The fracture locations of the rectangular (a) and dog bones (c) shape samples that cut in longitudinal direction were all at the test area near the anterior end. The transverse cut samples were broken at either the dorsal and ventral sides **(b)(d)**. The fracture of the tensile results were displayed at the bottom with white dot lines.

5.2.1.2 DIC analysis on the tension tests

In contrast to manually generated samples, wet DIC samples prepared by paint printing that were observed under a microscope showed a considerable reduction in pattern loss of undetected spots and fracture areas. By cutting the DIC samples using a new cutting die that allowed the test region to be completely captured under the microscope, we also substantially enhanced overall test results. The true (log) strain and von Mises strain trends in the longitudinal and transverse directions of the samples are described in Fig. 4-7 and 4-8. These strain variation distribution plots allow us to certainly observe how the strain variation varies depending on the thickness of the fish scales and characteristic distributions of the fish scale surface. It's interesting to note from Fig. 4-7 that the longitudinal fish scale samples have inclined strain variation and fracture locations, which are not reflected in the tensile test results. This may be caused by the fact that the lamellar angle of the fish scales is not perfectly vertical in the longitudinal direction.

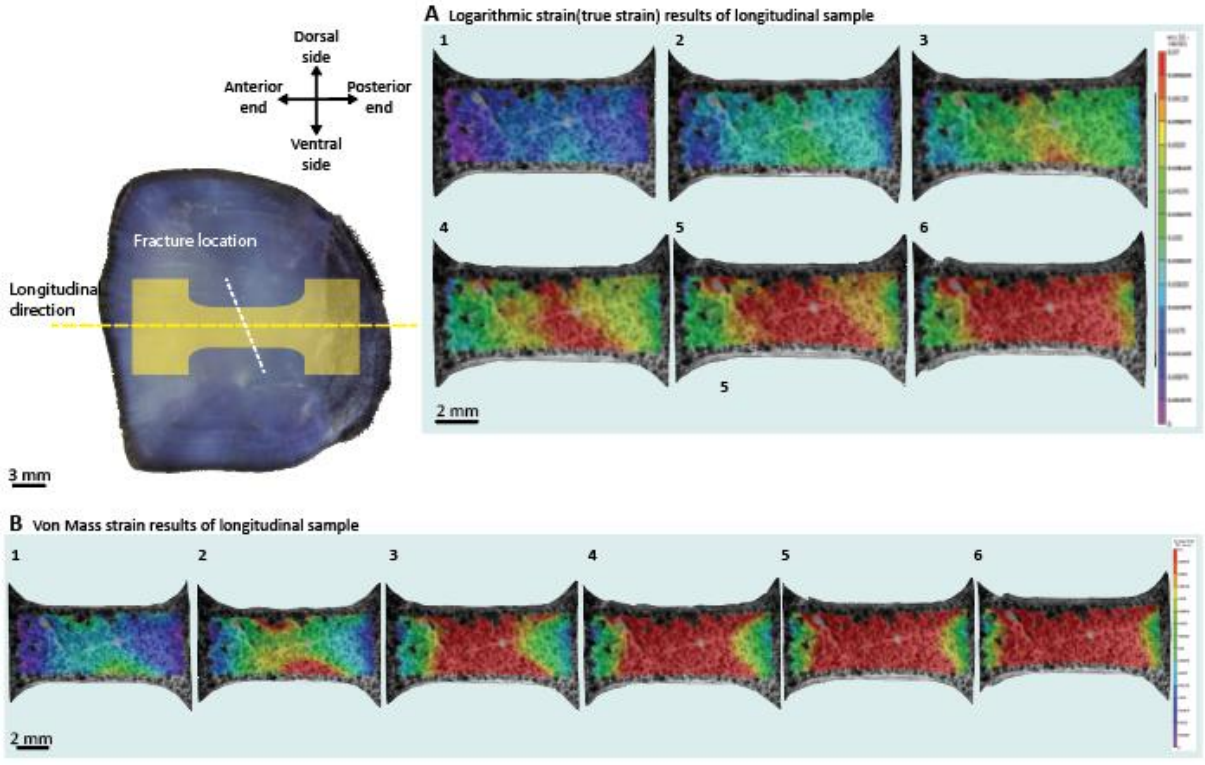

Fig. 4-7. Variation trend maps of true(logarithmic) strain and von Mises strain of the wet un-notched samples from longitudinal direction.

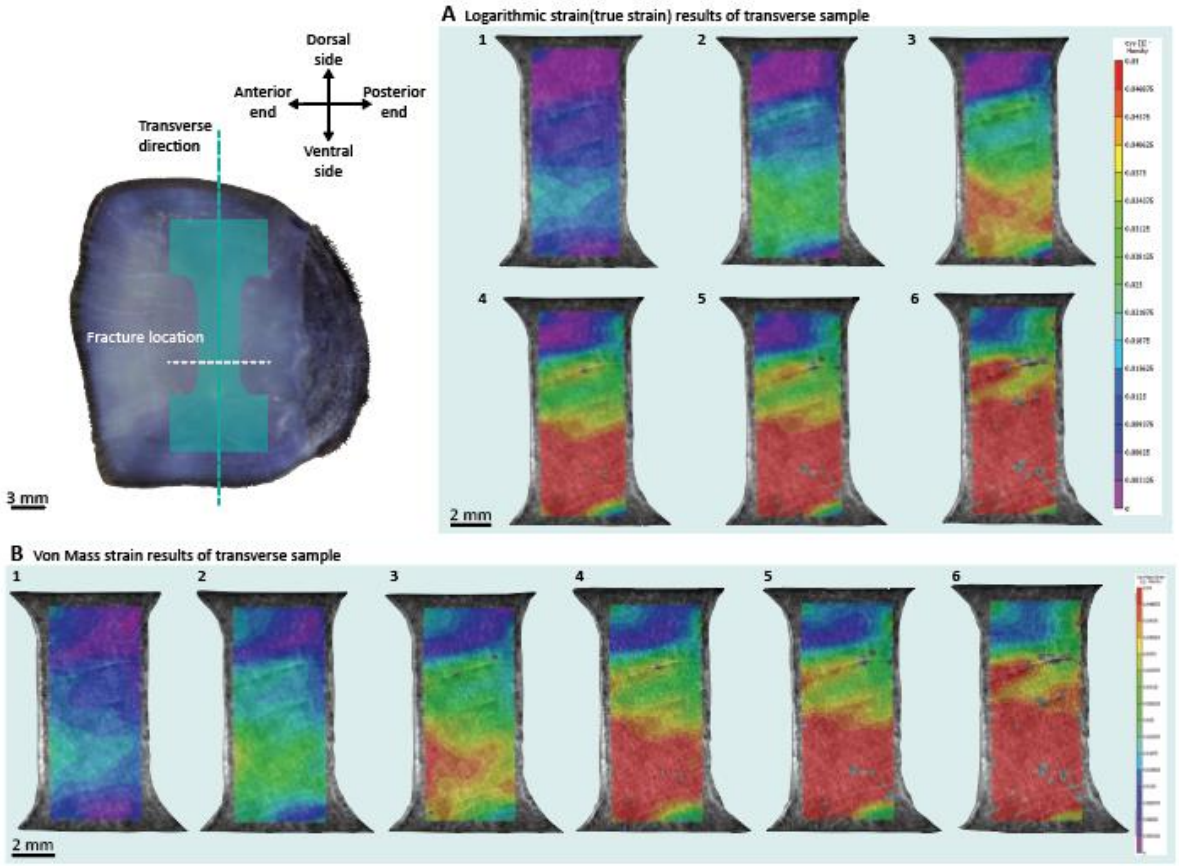

Fig. 4-8. Variation trend maps of true(logarithmic) strain and von Mises strain of the wet un-notched samples from transverse direction.

5.2.2 Tensile Results on Demineralized Scale

Furthermore, we will compare and analyze the tensile properties of intact and demineralized scales. There are many mechanical and chemical demineralization methods for removing the mineralized layer of fish scales. Here, dog bone-shaped scale samples were subjected to acid demineralization and polished demineralization, respectively. For the acid demineralization method, samples must be soaked in saltwater solution for more than 24 hours, followed by 90 minutes of demineralization in 0.4 mol/l hydrochloric acid solution[45]. The polished demineralization approach comprises manually polishing the scale thickness from 0.5 to 0.3 mm based on the results of EDS and nanoindentation tests indicating high mineralization layers of the scale were removed.

Figure 4-12 reveals the stress and strain curves of a comparison between intact and acid or polish demineralized scales. In addition, the tension process figures of the different

demineralized scales were shown at the bottom of each method of plots. It is evident from comparing the stiffness of intact and acid demineralized scales that the stiffness of acid demineralized scales is less than that of intact scales. While there is no substantial change in stiffness between intact and polished demineralized scales, according to the stress and strain curves. Therefore, the tensile test indicates that the removal of the mineralized layer via polishing did not result in a decrease in strength values, however the mechanical characteristics of acid demineralized scales treated with acid were reduced. The acid-demineralized scales produced more useful findings.

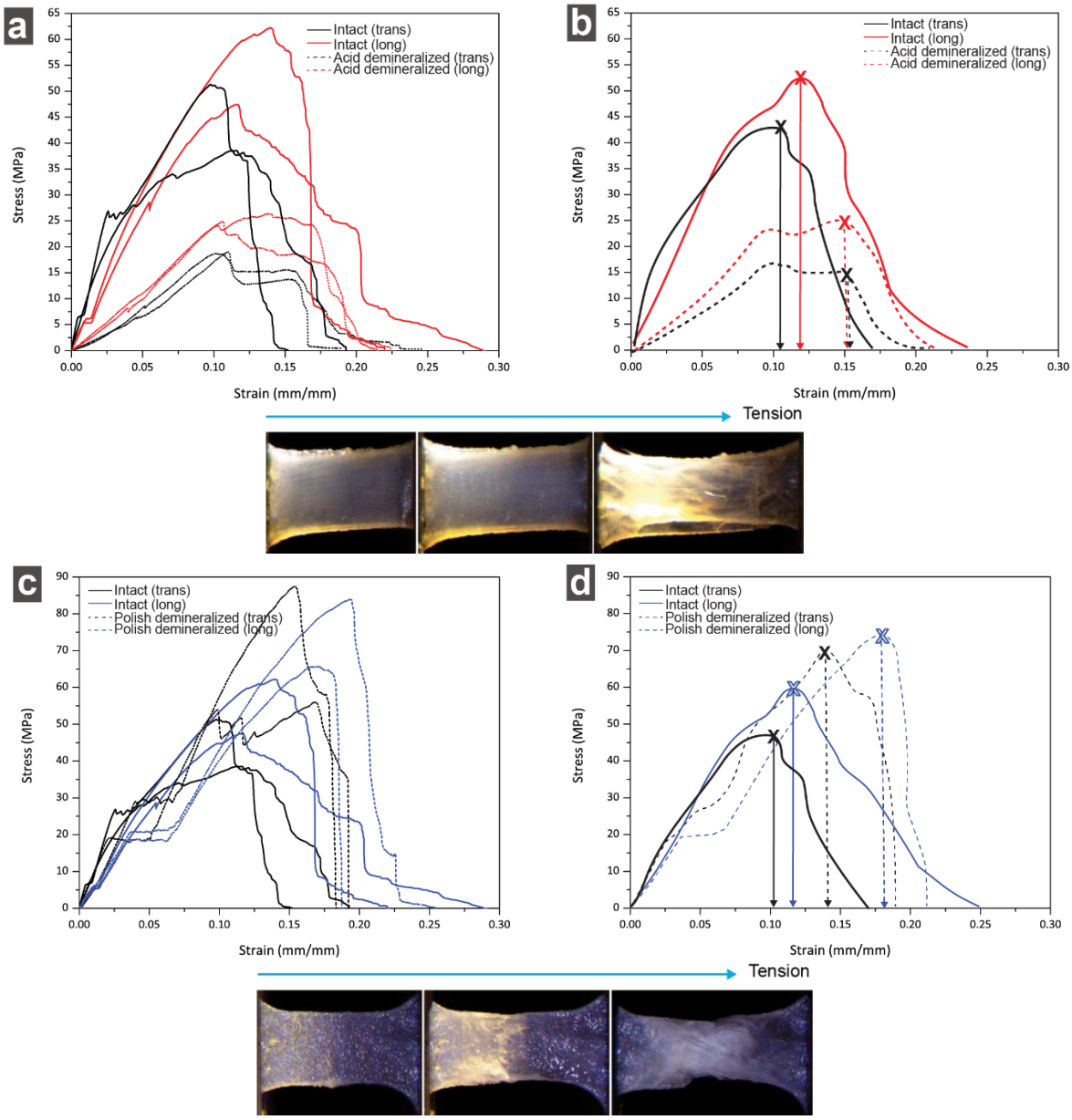

Fig. 4-12. The stress-strain curves of the different demineralization method dogbone samples in two

orientations. (a,b) the HCl demineralized dogbone samples, (c,d) the polish demineralized dogbone samples tensile test results.

As a conclusion, comparing the stress and strain curves of intact scales with those of acid or polished demineralized scales, and comparing intact and acid demineralized scales, it is evident that acid demineralized scales are less stiff than intact scales. In addition, there is no significant difference between the stiffness of the stress and strain curves of demineralized intact and polished scales. Tensile experiments revealed that polishing to remove the mineralized layer did not result in a fall in strength values, however acid-treated demineralized scales demonstrated a decrease in mechanical properties.

Chapter 6. Mineral distribution pattern analysis of Rostral Field

While previous research has focused on microscale characterization of the entire scale thickness (near the focal region, nanoindentation map) or bulk scale properties using tension tests, this section examines the internal structural variations between the rostral and focal regions of fish scales. When we used SEM analysis studies to explore the distribution of mineral phases within individual scales, we discovered an unreported mineral distribution pattern in which the mineral phases are distributed in long strips along the anterior-posterior axis with a unique mineralized-unmineralized collagen-based composite structure.

6.1 Structural Characterization of the Rostral Field

6.1.1 Comparative Structural Analysis of Rostral Field and Focus Field Scales

First of all, according to Fig. 6-1, it can be found that the mineralization of different fish scales in the rostral field is different. R1 structure can be roughly divided into two sections, the radii section that located in the external layers and the upper layer of the internal layers close to the radii section (about half in size) are high mineralization sections; And the bottom layers are the low mineralization section, although there are some high mineral particles (Mandl's corpuscles). While R2 structure is more complicated compared with R1. From the BDS image in Fig. 6-1b, there was no obvious difference in mineral content in radii section, but fiber orientation changed. However, the difference of mineral content in internal layers shows that the part near the top of each sub layer is highly mineralized, and the part near the bottom is low mineralized. Mineral differences in each sub layer may be controlled by the fractions of the two regions. Compared with F0 structure in focus field (Fig. 6-1c), the number of sub-layers in the multi-layer structure of rostral field is significantly smaller than that of focus field. The external layer of focus field is also significantly smaller than that of rostral field. However, the mineralization distribution of F0 and R1 are roughly the same.

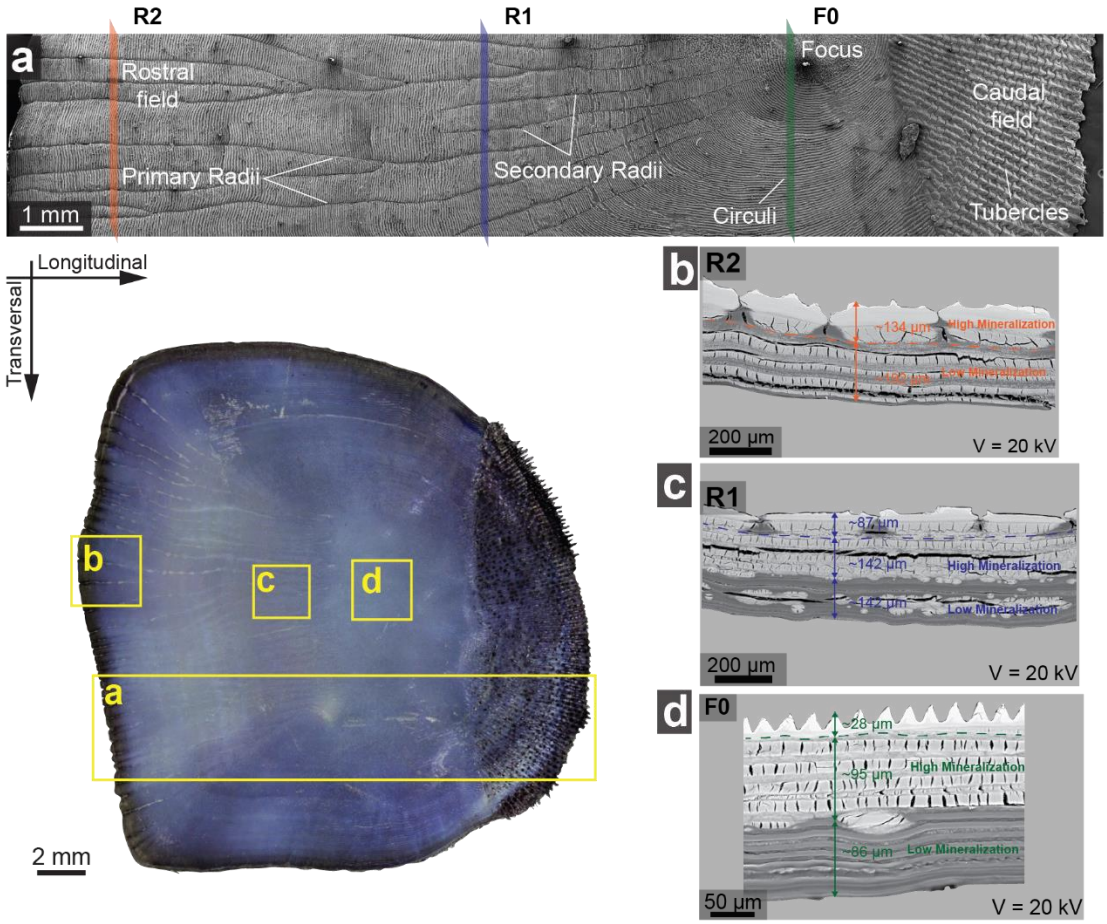

Fig. 6-1. Structural characterization of black drum fish scale. (a) The overview surface morphology of black drum scale with specific analysis locations R2, R1, and F0. The cross-sectional structures of **(b)** R2, **(c)** R1, and **(d)** F0 regions.

6.1.2 Comparative Structural and Chemical Analysis of Intact and Acid Demineralized Scales

Fig. 6-2 is SEM surface characterization results of acid demineralized scale. It can be found that the radii structure (hig(Hh mineralized external layer) of the demineralized scale can not be seen while the circuli distribution is still shown on the external surface, which also verifies that this method can completely demineralize the fish scale. Interestingly, the natural bending direction of acid demineralized scale during drying process is opposite to that of intact scale. This may be due to the high mineral crystals having the function of grouping fiber boundaries and fixation.

In the detailed SEM external surface morphology of acid demineralized fish scales (Fig. 6-3,b,c,d), NaCl crystals were found at the edges of rostral field and lateral field, which was caused by the fish scales being placed in seawater solution before air drying and the smaller

thickness of the edge of fish scales. But no NaCl crystals were found on the intact scale, which had been dried in the same way.

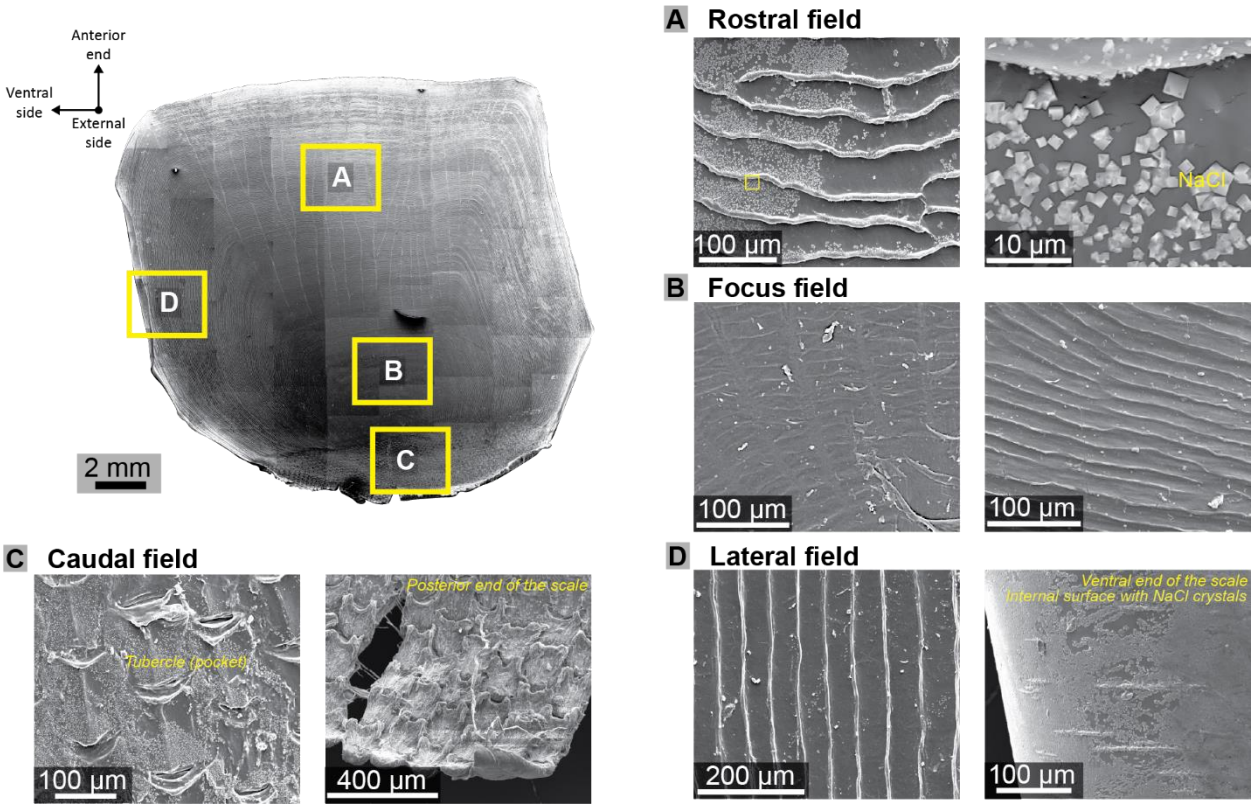

Fig. 6-2. SEM results of external surface fields morphology of acid demineralized scale. Schematic representation of the acid demineralized black drum scale surface. The detailed SEM images of fish scales from **(a)** rostral field, **(b)** focus field, **(c)** caudal field, and **(d)** lateral field.

First, based on previous measurements of the thickness of the acid demineralized scales, we can conclude that the thickness does not change significantly between before and after acid demineralization, or that the thickness of fish scales after demineralization is greater than that of intact fish scales (tensile test measurements). In the investigation of the EDS cross-sectional structure of acid demineralized fish scale, it is possible to determine that the scale is entirely demineralized, but its cross-sectional distribution may still be separated into two distinct zones. As depicted in Fig. 6-3c, the formerly highly mineralized region now has evident gaps, and only the distribution of in-plane horizontal fibers (yellow area) is visible, therefore the gaps should be out-of-plane fibers based on the orthogonal fiber orientations. This also shows that high mineral crystals may serve the purpose of gathering and fixing fiber boundaries.

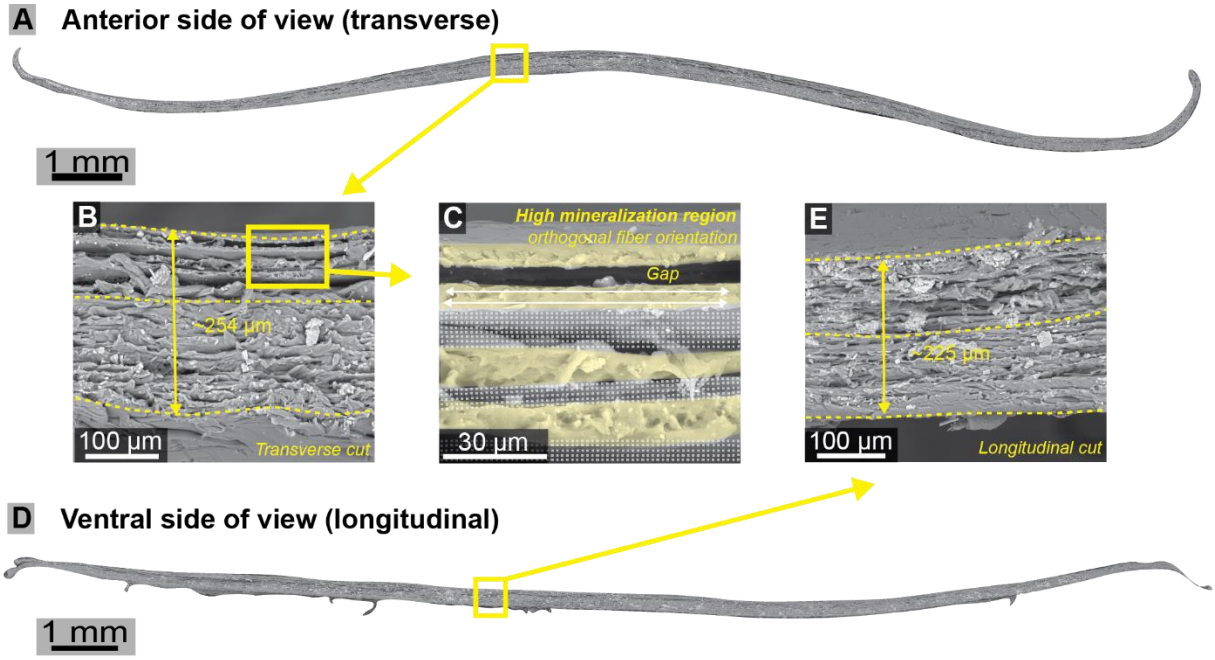

Fig. 6-3. Cross-sectional structure of acid demineralized scales from (a) transversal and (b) longitudinal cutting directions. **(b-e)** The detailed SEM images of the transversal and longitudinal cutting samples. There is the observed gap at the high mineralization region.

EDS line profile analysis in Fig. 6-4 shows that the external layer of fish scales is mainly composed of HA and the internal layers are mainly composed of collagen. The middle layers (upper layers of internal layers) are a mixture of HA and collagen. Along the thickness, we see an almost linear decrease in Ca and P (blue and green lines, HA mineral content), disappearing as we approach to internal layer and a corresponding increase in C (red line). It is worth noting that the line profile results of R1 and R2 of rostral fields are significantly different due to the different trend of the variation of the two samples. The distribution of elements in the internal layer of R2(Fig. 6-4b) indicates the distribution of high and low mineralization in the sublayer, and the thickness of the sublayer decreases gradually. In addition, EDS area profile results (Fig. 6-6) clearly show that Ca and P mainly occur in high mineralized regions.

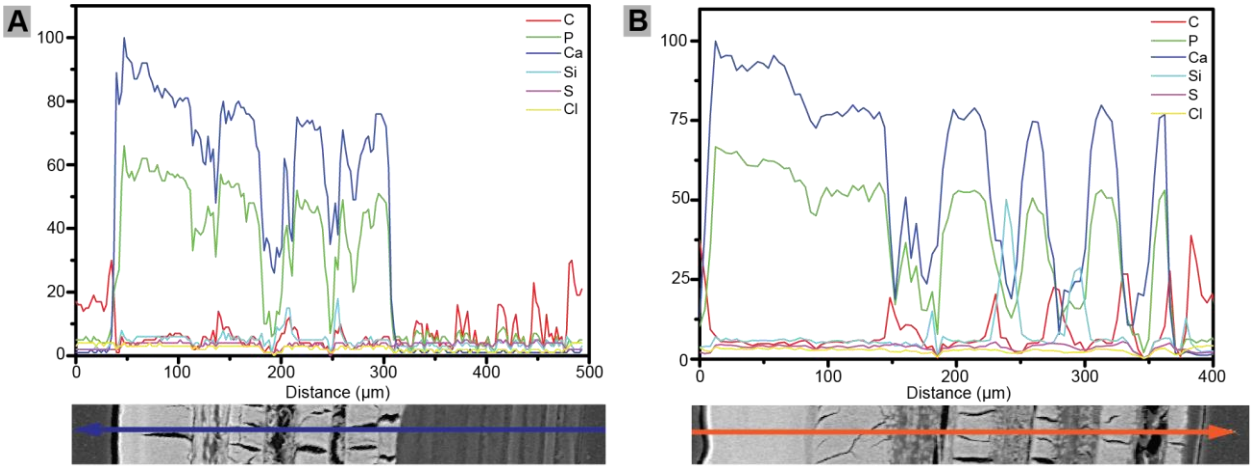

Fig. 6-4. EDS line profile analysis of (a) R1 and (b) R2 in rostral field.

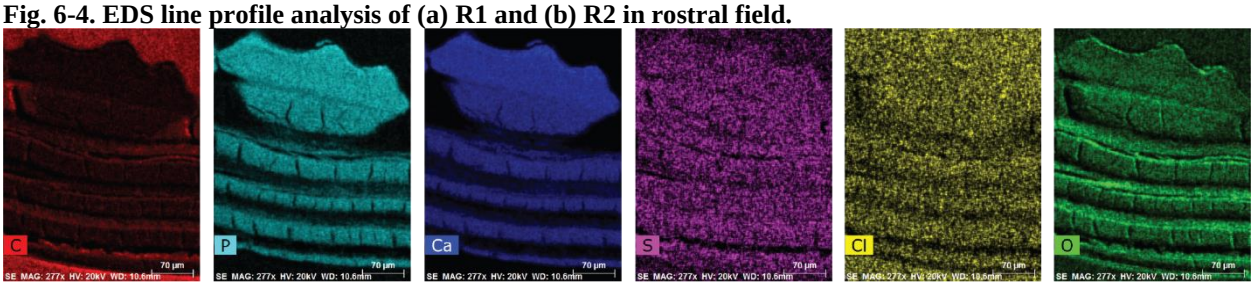

Fig. 6-5. EDS area profile analysis of elements distribution of Rostral field sample R2.

6.2 Nanoindentation Analysis of Rostral Field of Black Drum Scale

By nanoindentation line mapping (Fig. 6-6), it can be seen that the distributions and difference of mechanical properties (reduce modulus Er and hardness H) in the rostral region and the focus region mainly according to the multi-layer structure of fish scales, showing an oscillating trend. The distribution trend of the mechanical characteristics of fish scales is decreasing from the external layer to the internal layers, this trend is more obvious in the Focal field F0. Moreover, the external layer of the scales has greater modulus and hardness compared with the inner layers, due to the high mineralization of the region.

In addition, we also completed the external layer area mapping with one complete radii section in Rostral field, as can be seen from Fig. 6-7. The mean modulus and hardness of the region are Er = 40 ~ 50 GPa and H = 0.5 ~ 2.0 GPa, respectively. It should be noted that the modulus of radii section does not change significantly with fiber orientation (the sublayers), but the hardness is obviously higher at regions with in-plane horizontal fibers (H = 1.0 GPa) than out-of-plane fibers (H = 0.5 GPa). And in general, the area mapping also shows that the external layer has larger modulus and hardness than the internal layers.

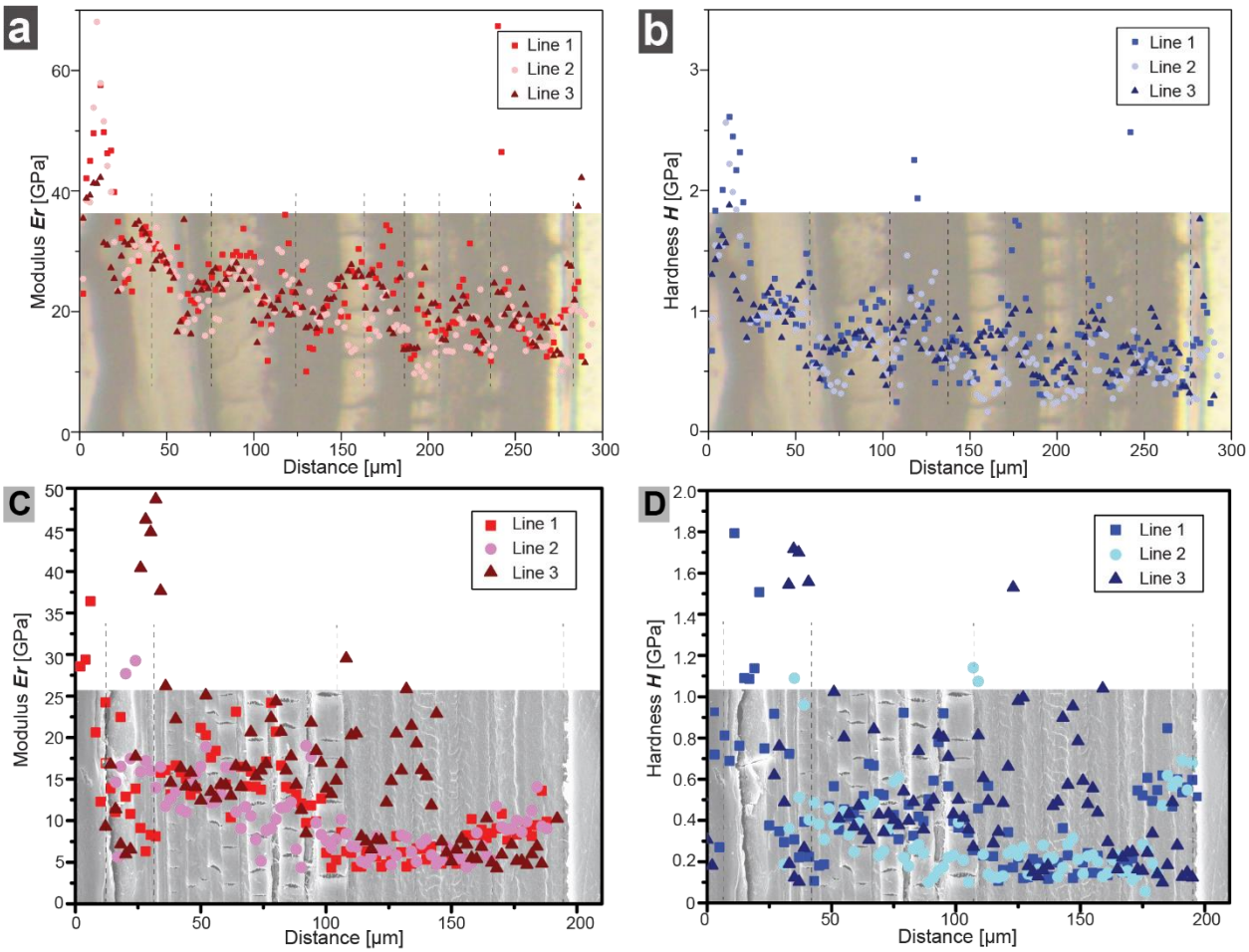

Fig. 6-6. Comparison of nanoindentation line mapping of (a) (b) R2 in rostral field and (c) (d) F0 in focus field, including **(a) (c)** reduced modulus Er and **(b) (d)** hardness H in GPa.

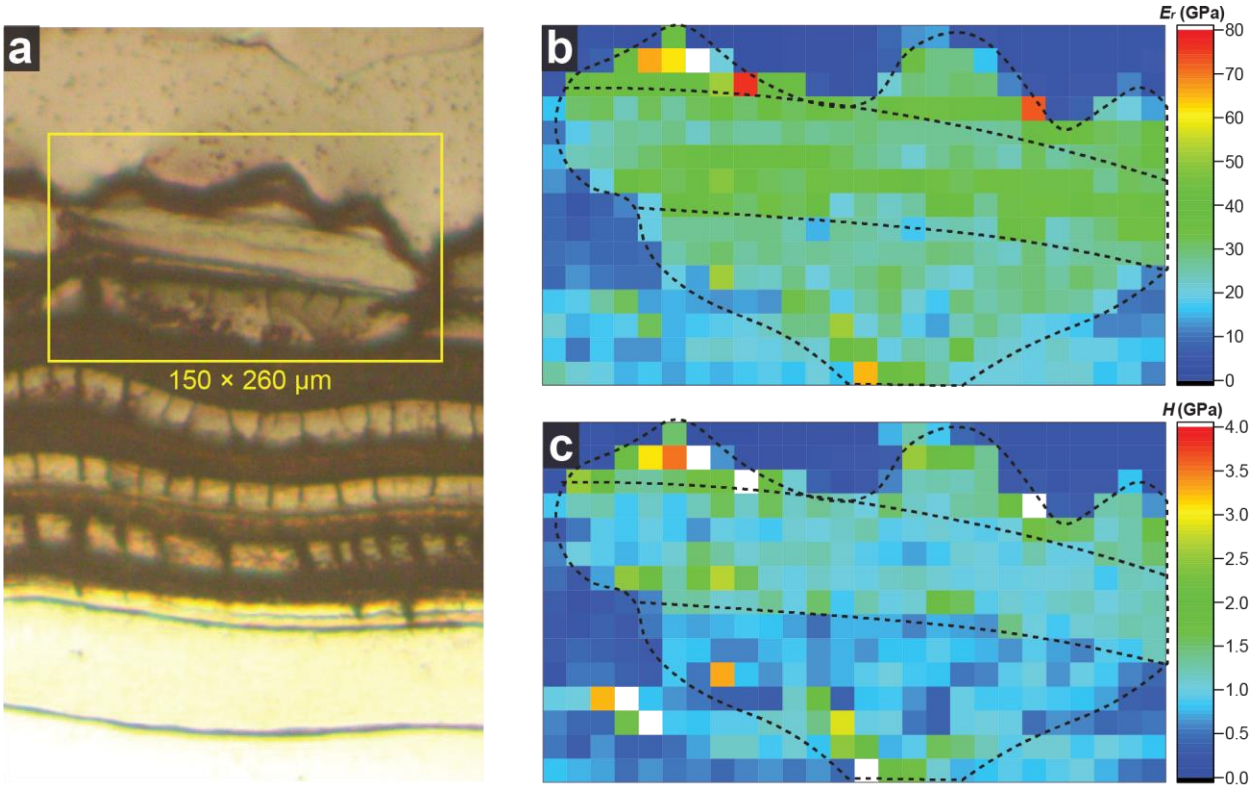

Fig. 6-7. Nanoindentation area mapping analysis of radii sectional structure in R2, include **(a**) optical image of polished sample with testing area in yellow box, **(b)** reduced modulus Er and **(c)** hardness H in GPa.

6.3 3D Modeling Analysis of Rostral Field and Focus Field Structure

6.3.1. The Constant Variables Calculations of the FE Simulations Models

We estimated Young's modulus in various regions of the rostral field and focus field based on the reduced modulus result from area mapping and the indenter modulus, which will be utilized to construct a 3D model.

By calculating the average slope (Fig. 6-8) of the stress and strain curves for the intact and acid-demineralized fish scale samples, we can deduce that Young's modulus E is approximately 492 MPa for the intact fish scale and 184 MPa for the acid-demineralized fish scale. Therefore, based on Young's modulus E of the composite is given by the 'rule of mixtures', when tensile stress applied parallel to the fiber direction[51]:

$$E_{fish\ scale} = V_{collagen}E_{collagen} + V_{mineral}E_{mineral} \quad [1]$$

Where $V_{collagen}$ is the relative volume friction of the collagen fibers and it is around 0.4 based on the volume ratio from SEM and optical images, and $V_{mineral}$ equals to $1 - V_{collagen}$ which is around 0.6.

Using equation 1, we determined that Young's modulus of external mineral layer that is mainly consist of hydroxyapatite (HA) is around 697 MPa, whereas Young's modulus of collagen fibers in internal layer is 184 MPa. In addition, by analyzing the peak value of the stress and strain curves of acid demineralized scales in Fig. 6-8, we found that the failure stress (yield stress) of collagen is around 20 MPa. The Poisson ratios of HA and collagen are approximately 0.3[48,49] based on the literature review.

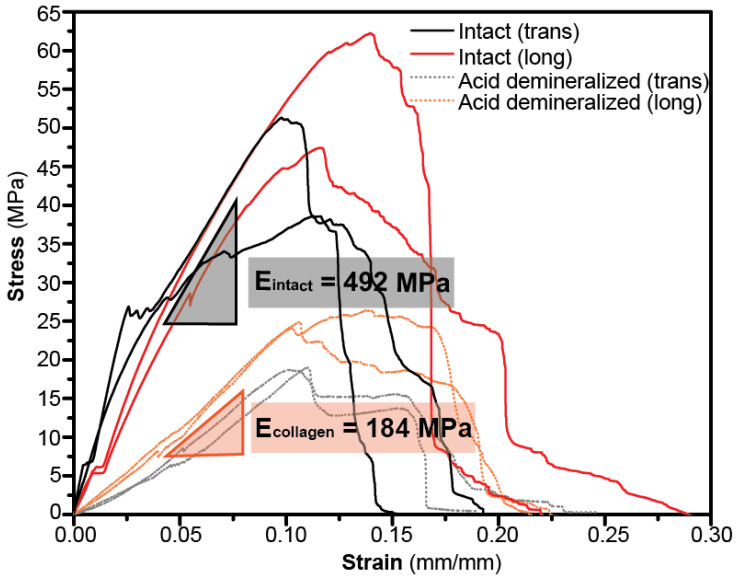

Fig. 6-8. Stress and strain curves of intact and acid demineralization scales.

According to the structure characteristics of SEM and optical images of the fish scale from the rostral and focus fields, we designed the real scale FE simulation models (F0, R1, and R2) with three specific external surfaces and different multilayer structures, as well as 3 comparative models (C0, C1 and C2) with rectangular shapes and corresponding multilayer structures. Fig. 6-9 and 10 indicated the dimensions of the real scale models and the comparative models. The upper model in these figures is developed designed based on the cross-sectional structure of the edge of the rostral field, the middle model is designed based on the structure of region between rostral and focus field, and the bottom model is designed based on focus field. The white color represents the mineral substance (HA), and the green color shows the collagen

fibers with their predicted material properties that been calculated above. Comparative models and real scale models have identical area ratios based on the SEM and optical images of cross-sectional structures of fish scale. Thereafter, we conducted a three-point bending test with 100 N of force on both three real scale simulation models and three rectangular shapes of the corresponding multilayer structures.

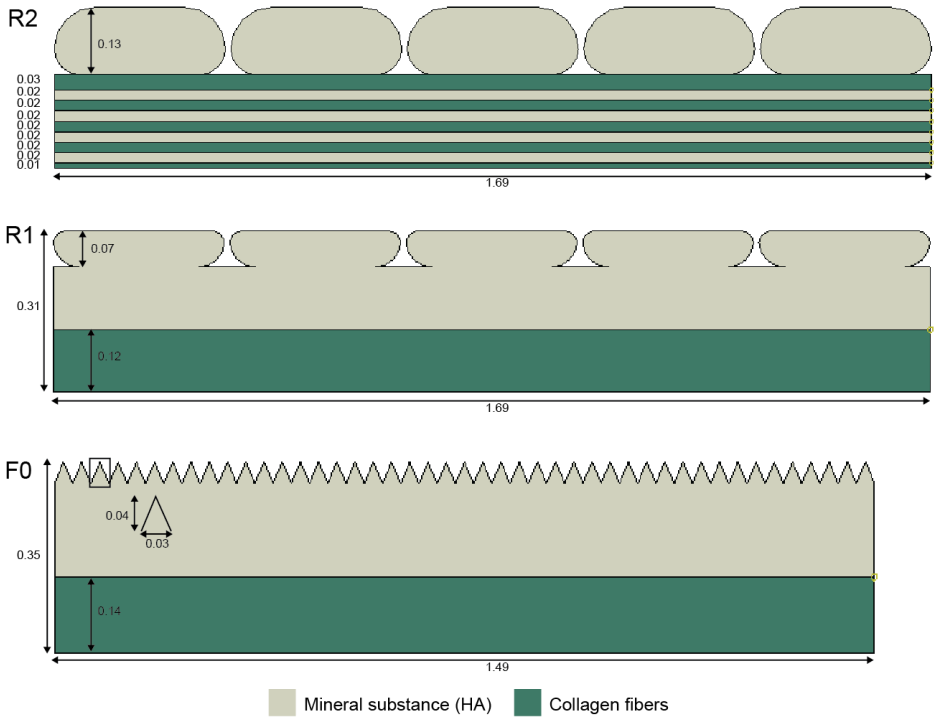

Fig. 6-9. The detailed dimension of the real scale FE simulation models. The upper model **R2** is designed based on the cross-sectional structure of the edge of the rostral field, the middle one **R1** is designed based on the cross-sectional structure of region between rostral and focus fields, and the bottom **F0** is designed based on the cross-sectional structure of focus field.

Fig. 6-10. The detailed dimension of the rectangular comparative FE simulation models. The upper model **C2** is designed based on the cross-sectional structure of **R2** model, the middle one **C1** is designed based on the cross-sectional structure of **R1** model, and the bottom **C0** is designed based on the cross-sectional structure of **F0** model.

6.3.2. Results of the Three-point Bending Analysis of the FE Simulation Models

The 8-node linear brick, decreased integration, and hourglass control elements (C3D8R) were used in finite element beam simulations. Due to the symmetry, we designed and simulated half of each model for the three-point bending test with a 100 N force. The top or bottom edge of the beam was loaded with 100 N at zero coordinates, and the other side of the model was fixed to the top or bottom edge (Fig. 6-11). Additionally, we fixed the transversely oriented area of the loading side to ensure that the model's deformation and displacement occurred exclusively in the direction of the load.

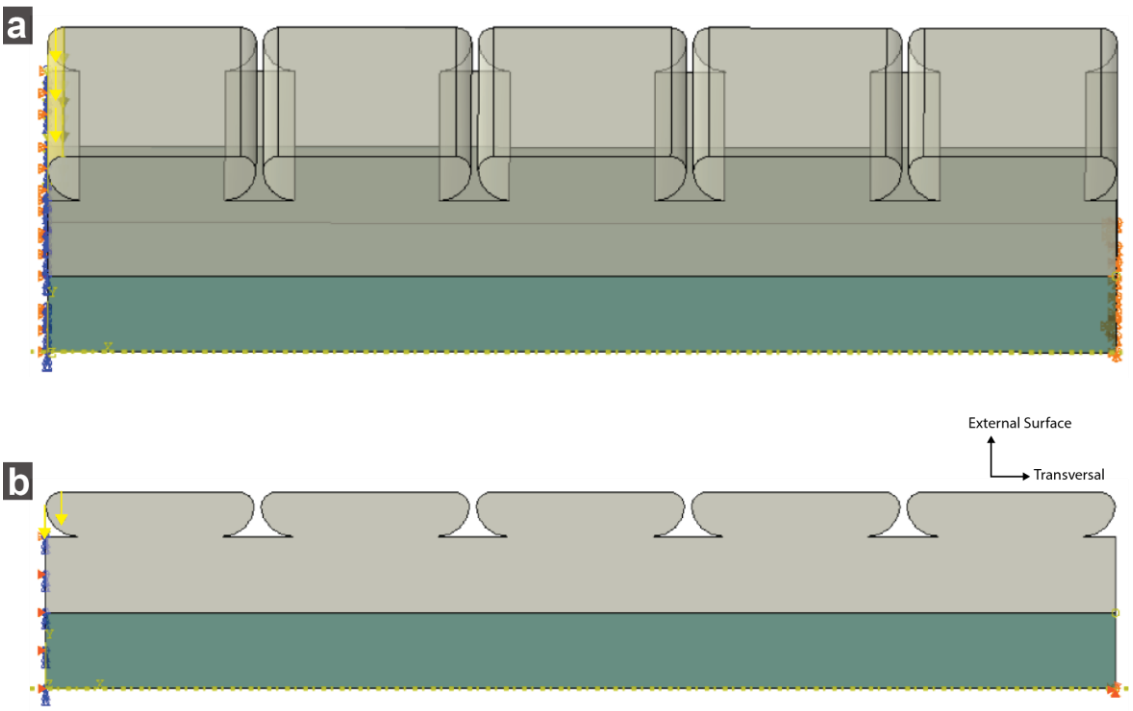

Fig. 6-11. Example of R1 simulation model design with loading and fixing boundaries for three-point bending test with upward-to-downward loading force (concave direction). (a) Overall 3D diagram of the R1 model, and **(b)** the cross-sectional diagram of R1 model with applied force (yellow arrow), the transversally fixed area (orange triangle on the left), and the fixed edge (orange triangles at the right conner).

The results of the von Mises stress and cross-section deformation of the three-point bending tests of the real scale models and rectangular comparative models in the rostral and focus with 100 N applied loading from up to down (concave direction) are depicted in Fig. 6-12 and 13, respectively. Based on Fig. 6-12, we can confirm that the real scale simulation models R2 has the maximum stress (12.24 MPa) and the largest deformation displacement that around 0.092 mm (Fig. 6-14) when compared to the real scale models R1 and F0. It is reasonable considering that the R2 is located at the anterior edge of the fish scale which is the area that the multi-scales overlap and are covered. In addition, the rectangular comparative models displayed much smaller deformation displacements compared with that of the real scale models in Fig. 6-14. At the edges of the scale, it would be desirable to have less stiffness and more flexibility. And based on Fig. 6-12 and 13, there is no discernible difference between three comparative rectangular FE simulation models. However, if we compare the von Mises stress at these rectangular comparative models, the von Mises stress of comparative models with the similar multi-layers structure as real scale models from largest to smallest as follows: comparison model (C0) at F0 region, comparison model (C2) at R2 region, and comparison model (C1) at R1

region. With equivalent thickness and volume fractions of HA and collagen, these results also indicated that the unique mineralized-unmineralized collagen-based composite structure (R2) had superior structural properties than the unformed doubt layer structure.

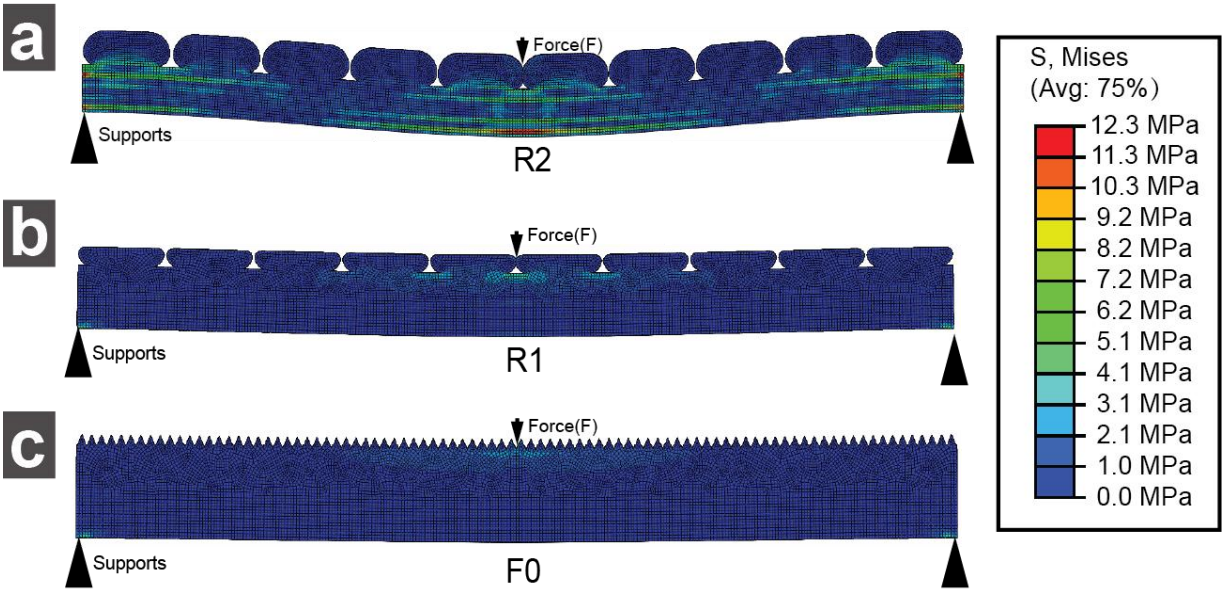

Fig. 6-12. The von Mises stress for three real scale FE simulation models of the 3-point bending test of 100 N force from up to down (concave direction). (a) R2, **(b)** R1 and **(c)** F0.

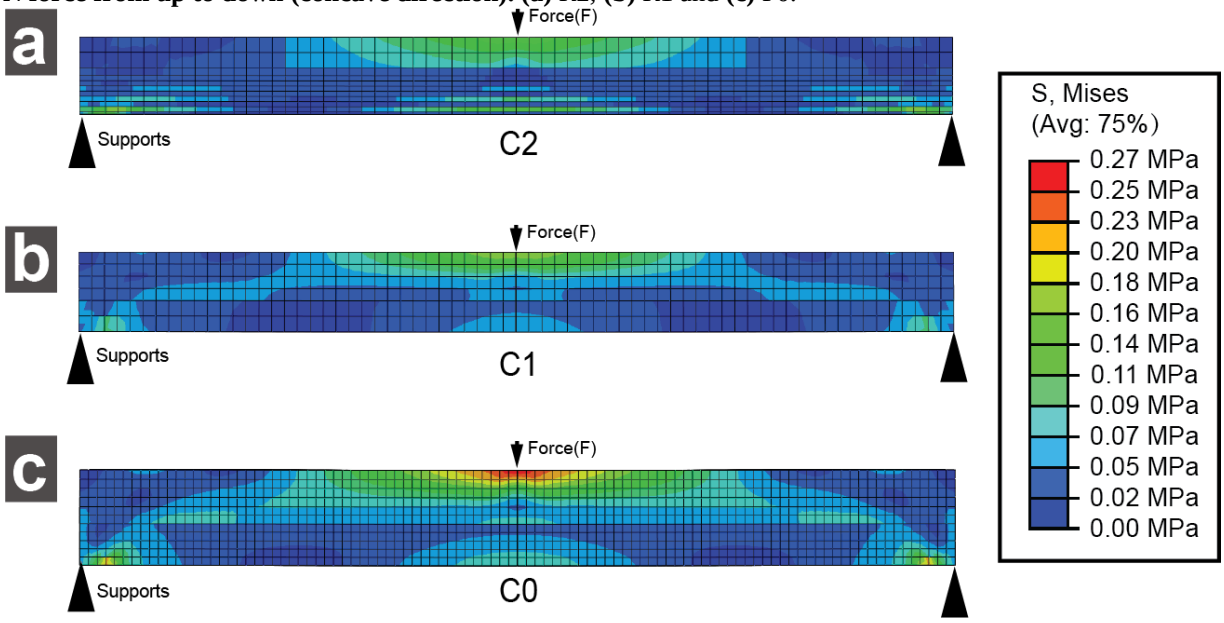

Fig. 6-13. The von Mises stress for rectangular comparative FE simulation models of the 3-point bending test of 100 N force from up to down (concave direction). (a) C2, **(b)** C1 and **(c)** C0.

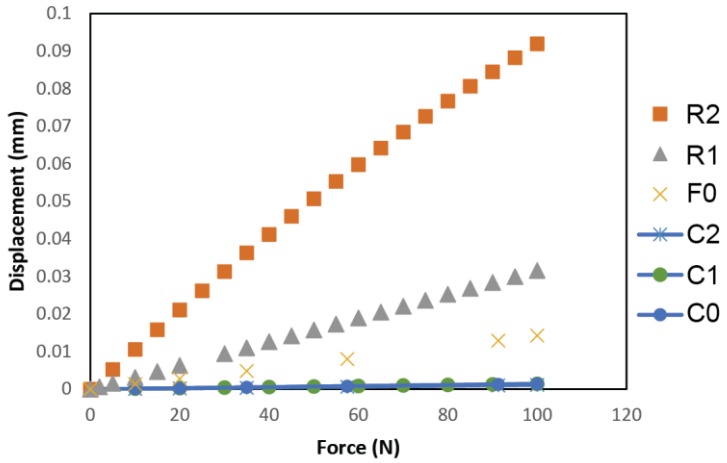

Fig. 6-14. The force vs. displacement curves of real scale FE simulation models and rectangular comparative models of the 3-point bending testing from up to down (concave direction).

Von Mises stresses and cross-section deformation of three-point bending tests of real scale simulation models and rectangular comparison models with the applied force from down to up (concave direction) lead to the similar distributions as the stresses and deformation of these models with the force from up to down (convex direction). However, in Fig. 6-15, the von Mises stress of the real scale simulation model R1 has the highest stress (0.71 MPa). Overall, the von Mises stresses and displacements of six models from convex direction are smaller than that of the stresses and displacements from concave direction. We concluded that the scale structures are more deformable in the convex direction than in the concave direction. Comparing the stress results and the force and displacement curves of the fish scale structure in different fields, the scale structure near the focus field (F0) has less deformation and higher stiff, while the fish scale structure near the edge of the rostral field (R2) has more flexible deformation capability. And the assumption for that is since R2 is placed near the anterior end of the scales, where several scales overlap and are covered, and so does not necessitate a high level of rigidity but rather requires greater flexibility. In addition, the anterior end of the fish scale is more flexible because it is the area of the scale closest to the fish's body and is therefore the area that is most likely to flex and bend in response to changes in the environment. The flexibility of the anterior end of the scale allows the fish to move through the water more easily and efficiently.

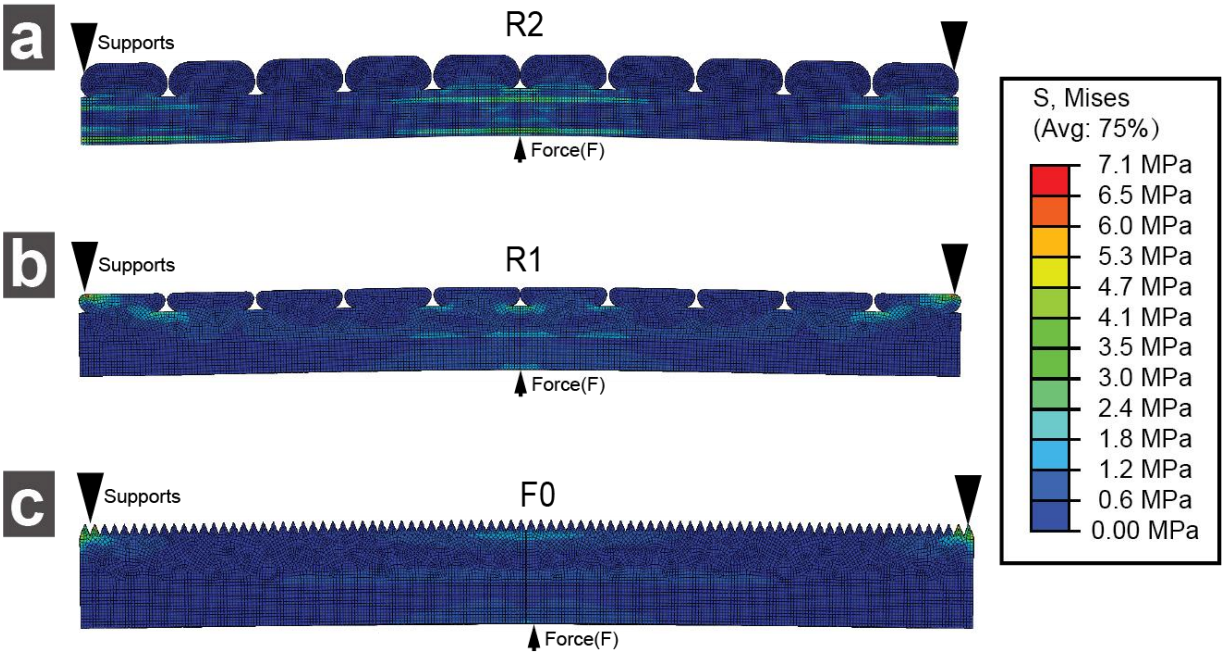

Fig. 6-15. The von Mises stress for three real scale FE simulation models of the 3-point bending test of 100 N force from down to up (convex direction). (a) R2, **(b)** R1 and **(c)** F0.

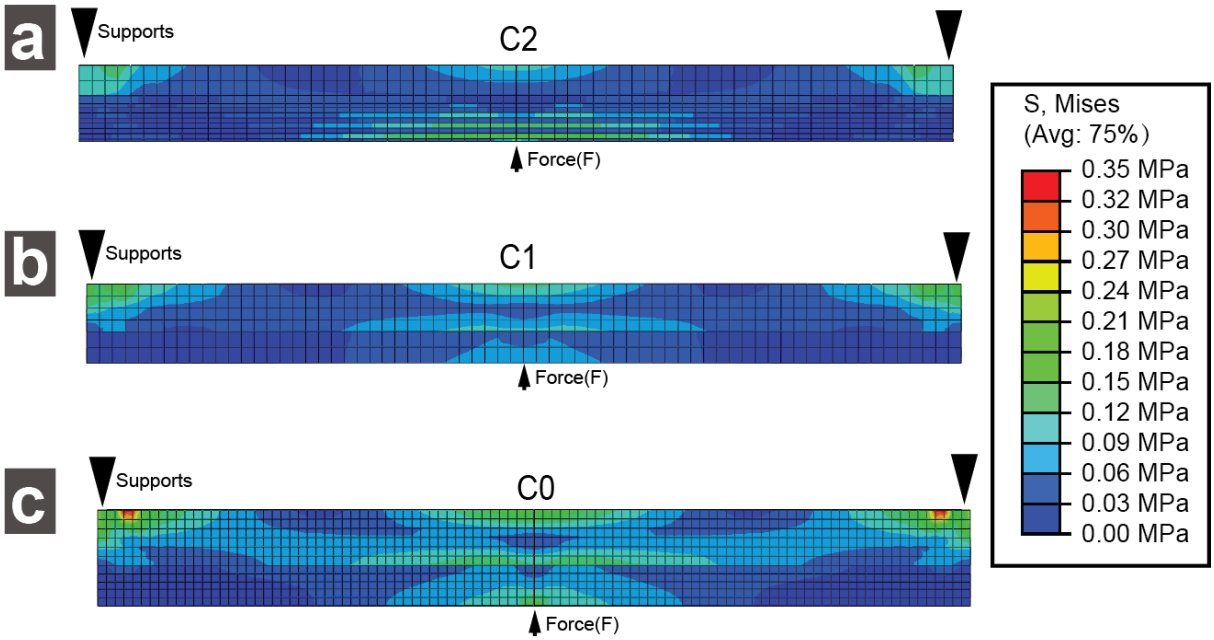

Fig. 6-16. The von Mises stress for rectangular comparative FE simulation models of the 3-point bending test of 100 N force from down to up (convex direction). (a) C2, **(b)** C1 and **(c)** C0.

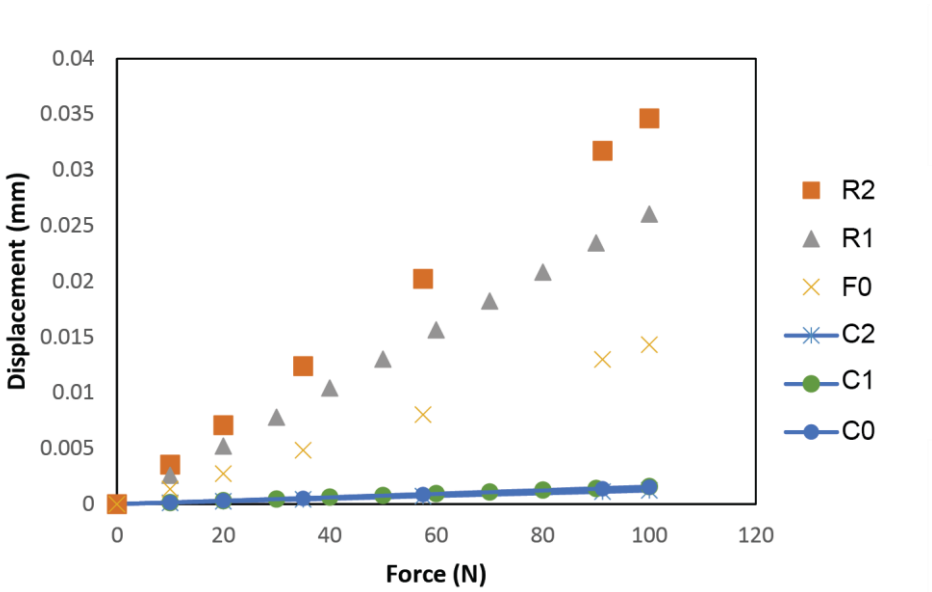

Fig. 6-17. The force vs. displacement curves of real scale FE simulation models and rectangular comparative models of the 3-point bending testing from down to up (convex direction).

Chapter 7. Conclusion

Fish scales can be conceived of as cross-plywood laminar flow composites containing collagen fibers. On the surface of fish scales, these collagen-based composites are typically slightly mineralized (mostly with hydroxyapatite) in order to prevent penetration and provide further protection. Due to their overlapping structure, fish scales serve as a valuable model for the development of fiber composite materials and flexible armor systems. In this thesis, we are able to quantify the distribution of mineral phases within individual fish scales using empirical and computational approaches, and to analyze the mechanical effects resulting from this distribution. We selected the scales of black drum fish as the modeling system for our investigation. First, a comprehensive investigation of the exterior surface morphology of individual scales identified several unique structural regions, including the focal field (centre), the lateral field (dorsal and ventral), the rostral field (anterior), and the caudal field (posterior). The conventional two-layer structure consists of a mineralized outer layer and a collagen-based inner layer in the focus region. The highly mineralized outer layer contributes to hardness, according to nanoindentation experiments. In addition, macroscopic tensile studies demonstrated that mechanical removal of mineralized layers did not reduce strength values, however acid-treated demineralized scales exhibited a reduction in mechanical properties. Through tensile testing of demineralization and intact fish scales, we can investigate that Young's modulus of external mineral layer that is mainly consist of hydroxyapatite (HA) is around 697 MPa and that of internal layer collagen fiber is approximately 184 MPa.

Moreover, we discovered a previously unreported mineral distribution pattern in the rostral fields, where the outer mineral phase is separated into long strips (approximately 300 mm in width) and the inner cross-laminated plywood structure is intersecting with one layer of mineral layer and one layer of collagen layer. Within the scales, mineral deposition appears to be closely correlated with collagen orientation, resulting in a unique composite structure of mineralized and non-mineralized collagen. On the analysis of the characterization of fish scales in different fields within a single scale, we developed three real scale finite element simulation models from rostral and focus fields and incorporated a rectangular multilayer structure as a control group to conduct three-point bending tests in different directions with the loading force of 100 N. We were able to identify that the model that was designed based on the edge of rostral

field is more flexible and less stiff, particularly when tension is at the bottom and compression is at the top. This unique structure indicates that the scale structure at the edge of the rostral field provides further flexibility within an individual scale, implying that the flexibility is more important at the anterior end of scales where the multi-scales overlap and are covered. And since the anterior end of the fish scale is the area of the scale closest to the fish body and is therefore the area that is most likely to flex and bend in response to changes in the environment.

Finally, for the recommendations for future works, firstly, mechanical characteristics and properties of mineralized phases and structures of various fields, such as lateral field and caudal field, within a single scale can be further investigated using more precise simulations and studies. The structural characteristics of multilayer structure at anterior end of the fish scale can also be further investigated to understand the mechanism of how it provides puncture resistance and energy absorption. Studying the relationship between the number and arrangement of multilayer layers and the puncture performance could help to further optimize its structure and improve puncture resistance. And investigating how the material composition and mechanical properties of each layer affect the overall puncture performance can also help to enhance the protective ability of this structure.

References

1. Wegst, U. G. K., Bai, H., Saiz, E., Tomsia, A. P. & Ritchie, R. O. Bioinspired structural materials. *Nat. Mater.* **14**, 23–36 (2015).

2. Black Drum (Pogonias cromis). *Texas Parks and Wildlife*.

3. Sire, J. Y. & Huysseune, A. Formation of dermal skeletal and dental tissues in fish: A comparative and evolutionary approach. *Biol. Rev. Camb. Philos. Soc.* **78**, 219–249 (2003).

4. Suzanne Currie, D. H. E. *The Physiology of Fishes*. (CRC Press, 2020).

5. Chen, I. H. *et al.* Armadillo armor: Mechanical testing and micro-structural evaluation. *J. Mech. Behav. Biomed. Mater.* **4**, 713–722 (2011).

6. Schönbörner, A. A., Boivin, G. & Baud, C. A. The mineralization processes in Teleost fish scales. *Cell Tissue Res.* **202**, 203–212 (1979).

7. Schönbörner, A. A., Meunier, F. J. & Castanet, J. The fine structure of calcified Mandl's corpuscles in teleost fish scales. *Tissue Cell* **13**, 589–597 (1981).

8. Rawat, P., Zhu, D., Rahman, Z. & Barthelat, F. Structural and mechanical properties of fish scales for the bio-inspired design of flexible body armors : A review. *Acta Biomater.* (2020) doi:10.1016/j.actbio.2020.12.003.

9. Onozato, H. & Watabe, N. Studies on fish scale formation and resorption. *Cell Tissue Res.* **201**, (1979).

10. Quan, H., Yang, W., Schaible, E., Ritchie, R. O. & Meyers, M. A. Novel Defense Mechanisms in the Armor of the Scales of the "Living Fossil" Coelacanth Fish. *Adv. Funct. Mater.* **28**, 1–13 (2018).

11. Yang, W. *et al.* Natural flexible dermal armor. *Adv. Mater.* **25**, 31–48 (2013).

12. Goodrich, S. & Es, F. By EDWIN. *Scales Fish, Living Extinct, aid their 'importan'ce Classif.* (1907).

13. Zhu, D. *et al.* Structure and mechanical performance of a 'modern' fish scale. *Adv. Eng. Mater.* **14**, 185–194 (2012).

14. Zylberberg, L. & Nicolas, G. Ultrastructure of scales in a teleost (Carassius auratus L.) after use of rapid freeze-fixation and freeze-substitution. *Cell Tissue Res.* **223**, 349–367 (1982).

15. Chen, P. Y. *et al.* Predation versus protection: Fish teeth and scales evaluated by nanoindentation. *J. Mater. Res.* **27**, 100–112 (2012).

16. Murcia, S. *et al.* The natural armors of fish: A comparison of the lamination pattern and structure of scales. *J. Mech. Behav. Biomed. Mater.* **73**, 17–27 (2017).

17. Allison, P. G. *et al.* Mechanical properties and structure of the biological multilayered material system, Atractosteus spatula scales. *Acta Biomater.* **9**, 5289–5296 (2013).

18. Bruet, B. J. F., Song, J., Boyce, M. C. & Ortiz, C. Materials design principles of ancient fisharmour. *Nat. Mater.* **7**, 748–756 (2008).

19. Daget, J., Gayet, M., Meunier, F. J. & Sire, J. Y. Major discoveries on the dermal skeleton of fossil and recent polypteriforms: A review. *Fish Fish.* **2**, 113–124 (2001).

20. Studart, A. R. Towards high-performance bioinspired composites. *Adv. Mater.* **24**, 5024–5044 (2012).

21. Burgert, I. & Fratzl, P. Actuation Systems in Plants as Prototypes for Bioinspired Devices Linked references are available on JSTOR for this article : Actuation systems in plants as prototypes for bioinspired devices. *Philos. Trans. Math. Phys. Eng. Sci.* **367**, 1541–1557 (2009).

22. Wegst, U. G. K. & Ashby, M. F. The mechanical efficiency of natural materials. *Philos. Mag.* **84**, 2167–2186 (2004).

23. Ikoma, T., Kobayashi, H., Tanaka, J., Walsh, D. & Mann, S. Microstructure, mechanical, and biomimetic properties of fish scales from Pagrus major. *J. Struct. Biol.* **142**, 327–333 (2003).

24. Marino Cugno Garrano, A. *et al.* On the mechanical behavior of scales from Cyprinus carpio. *J. Mech. Behav. Biomed. Mater.* **7**, 17–29 (2012).

25. Yang, W. *et al.* Protective role of Arapaima gigas fish scales: Structure and mechanical behavior. *Acta Biomater.* **10**, 3599–3614 (2014).

26. Lin, Y. S., Wei, C. T., Olevsky, E. A. & Meyers, M. A. Mechanical properties and the laminate structure of Arapaima gigas scales. *J. Mech. Behav. Biomed. Mater.* **4**, 1145–1156 (2011).

27. Torres, F. G., Troncoso, O. P., Nakamatsu, J., Grande, C. J. & Gómez, C. M. Characterization of the nanocomposite laminate structure occurring in fish scales from Arapaima Gigas. *Mater. Sci. Eng. C* **28**, 1276–1283 (2008).

28. Lin, Y. S., Wei, C. T., Olevsky, E. A. & Meyers, M. A. Mechanical properties and the laminate structure of Arapaima gigas scales. *J. Mech. Behav. Biomed. Mater.* **4**, 1145–1156 (2011).

29. Gil-Duran, S., Arola, D. & Ossa, E. A. Effect of chemical composition and microstructure on the mechanical behavior of fish scales from Megalops Atlanticus. *J. Mech. Behav. Biomed. Mater.* **56**, 134–145 (2016).

30. Zhu, D., Barthelat, F. & Vernerey, F. Intricate Multiscale Mechanical Behaviors of Natural Fish-Scale Composites. in *Handbook of Micromechanics and Nanomechanics* vol. 3 975–994 (2013).

31. Yang, W. *et al.* Structure and fracture resistance of alligator gar (Atractosteus spatula) armored fish scales. *Acta Biomater.* **9**, 5876–5889 (2013).

32. Sherman, V. R., Quan, H., Yang, W., Ritchie, R. O. & Meyers, M. A. A comparative study of piscine defense: The scales of Arapaima gigas, Latimeria chalumnae and Atractosteus spatula. *J. Mech. Behav. Biomed. Mater.* **73**, 1–16 (2017).

33. Browning, A., Ortiz, C. & Boyce, M. C. Mechanics of composite elasmoid fish scale assemblies and their bioinspired analogues. *J. Mech. Behav. Biomed. Mater.* **19**, 75–86 (2013).

34. Khayer Dastjerdi, A. & Barthelat, F. Teleost fish scales amongst the toughest collagenous materials. *J. Mech. Behav. Biomed. Mater.* **52**, 95–107 (2015).

35. Rudykh, S., Ortiz, C. & Boyce, M. C. Flexibility and protection by design: Imbricated hybrid microstructures of bio-inspired armor. *Soft Matter* **11**, 2547–2554 (2015).

36. Vernerey, F. J. & Barthelat, F. On the mechanics of fishscale structures. *Int. J. Solids Struct.* **47**, 2268–2275 (2010).

37. Zolotovsky, K. *et al.* Fish-inspired flexible protective material systems with anisotropic bending stiffness. *Commun. Mater.* **2**, 1–10 (2021).

38. Yaseen, A. A., Waqar, T., Khan, M. A. A., Asad, M. & Djavanroodi, F. Fish scales and their biomimetic applications. *Front. Mater.* **8**, 1–16 (2021).

39. Meyers, M. A., Lin, Y. S., Olevsky, E. A. & Chen, P. Y. Battle in the Amazon: Arapaima versus piranha. *Adv. Eng. Mater.* **14**, 279–288 (2012).

40. Naleway, S. E., Taylor, J. R. A., Porter, M. M., Meyers, M. A. & McKittrick, J. Structure and mechanical properties of selected protective systems in marine organisms. *Mater. Sci. Eng. C* **59**, 1143–1167 (2016).

41. Quan, H. *et al.* Structure and Mechanical Adaptability of a Modern Elasmoid Fish Scale from the Common Carp. *Matter* (2020) doi:10.1016/j.matt.2020.05.011.

42. Zimmermann, E. A. *et al.* Mechanical adaptability of the Bouligand-type structure in natural dermal armour. *Nat. Commun.* **4**, 1–7 (2013).

43. Giraud, M. M., Castanet, J., Meunier, F. J. & Bouligand, Y. The fibrous structure of coelacanth scales: A twisted 'Plywood'. *Tissue Cell* **10**, 671–686 (1978).

44. J. Meunier, F. 'Twisted plywood' structure and mineralization in the scales of a primitive living fish Amia calva. *Tissue Cell* **13**, 165–171 (1981).

45. Zhang, F., Wang, A., Li, Z., He, S. & Shao, L. Preparation and Characterisation of Collagen from Freshwater Fish Scales. *Food Nutr. Sci.* **02**, 818–823 (2011).

46. Hossain, M. S., Ebrahimi, H. & Ghosh, R. Fish scale inspired structures - A review of materials, manufacturing and models. *Bioinspiration and Biomimetics* **17**, (2022).

47. Chen, Q. & Pugno, N. M. Bio-mimetic mechanisms of natural hierarchical materials: A review. *J. Mech. Behav. Biomed. Mater.* **19**, 3–33 (2013).

48. Joon B. Park, J. D. B. *Principles and Applications. Biomaterials*. (2003).

49. Proestaki, M., Ogren, A., Burkel, B. & Notbohm, J. Modulus of Fibrous Collagen at the Length Scale of a Cell. *Exp. Mech.* **59**, 1323–1334 (2019).

50. Deng, Z. *et al.* Acta Biomaterialia Black Drum Fish Teeth : Built for Crushing Mollusk Shells. **137**, 147–161 (2022).

51. Roberts, R. J. *The anatomy and physiology of teleosts.* (W.B. Saunders, 2001).

52. Fang, Z., Wang, Y., Feng, Q., Kienzle, A. & Müller, W. E. G. Hierarchical structure and cytocompatibility of fish scales from Carassius auratus. *Mater. Sci. Eng. C* **43**, 145–152 (2014).